STAGNATION POINT FLOW OF NON-NEWTONIAN NANOFLUIDS WITH ACTIVE AND PASSIVE CONTROLS OF NANOPARTICLES

NADHIRAH BT ABDUL HALIM

FACULTY OF SCIENCE
UNIVERSITY OF MALAYA
KUALA LUMPUR

2019

STAGNATION POINT FLOW OF NON-NEWTONIAN NANOFLUIDS WITH ACTIVE AND PASSIVE CONTROLS OF NANOPARTICLES

NADHIRAH BT ABDUL HALIM

THESIS SUBMITTED IN FULFILMENT OF THE
REQUIREMENTS FOR THE DEGREE OF DOCTOR OF
PHILOSOPHY

INSTITUTE OF MATHEMATICAL SCIENCES
FACULTY OF SCIENCE
UNIVERSITY OF MALAYA
KUALA LUMPUR

2019

UNIVERSITI MALAYA

ORIGINAL LITERARY WORK DECLARATION

Name of Candidate : **NADHIRAH BT ABDUL HALIM**

Registration/Matric No.: **SHB130011**

Name of Degree : **DOCTOR OF PHILOSOPHY**

Title of Project Paper/Research Report/Dissertation/Thesis ("this Work"):

STAGNATION POINT FLOW OF NON-NEWTONIAN NANOFLUIDS WITH ACTIVE AND PASSIVE CONTROLS OF NANOPARTICLES

Field of Study : **APPLIED MATHEMATICS**

I do solemnly and sincerely declare that:

(1) I am the sole author/writer of this Work;
(2) This work is original;
(3) Any use of any work in which copyright exists was done by way of fair dealing and for permitted purposes and any excerpt or extract from, or reference to or reproduction of any copyright work has been disclosed expressly and sufficiently and the title of the Work and its authorship have been acknowledged in this Work;
(4) I do not have any actual knowledge nor do I ought reasonably to know that the making of this work constitutes an infringement of any copyright work;
(5) I hereby assign all and every rights in the copyright to this Work to the University of Malaya ("UM"), who henceforth shall be owner of the copyright in this Work and that any reproduction or use in any form or by any means whatsoever is prohibited without the written consent of UM having been first had and obtained;
(6) I am fully aware that if in the course of making this Work I have infringed any copyright whether intentionally or otherwise, I may be subject to legal action or any other action as may be determined by UM.

Candidate's Signature Date:

Subscribed and solemnly declared before,

Witness's Signature Date:

Name:
Designation:

STAGNATION POINT FLOW OF NON-NEWTONIAN NANOFLUIDS WITH ACTIVE AND PASSIVE CONTROLS OF NANOPARTICLES

ABSTRACT

In this thesis, newly upgraded non-Newtonian nanofluids models near a stagnation point are proposed under the influence of active and passive controls of the nanoparticles. These boundary layer fluid flows considered Maxwell, Williamson, second-grade, Carreau and Powell-Eyring non-Newtonian fluids. The flows are represented by the conventional partial differential equations in fluid dynamics added with unique expression of stress tensor in the momentum equation which satisfy the continuity equation for conservation of mass. The Buongiorno's model is used as a base model in this analysis as it takes into consideration the effect of Brownian motion and thermophoresis of the nanoparticles in the energy and mass transport equations of the flows. All these equations are reduced into a set of simpler partial differential equations via boundary layer approximation. The governing equations are later converted to a set of nonlinear ordinary differential equations by using similarity transformation. Shooting technique is employed to reduce these resulting equations into a set of boundary value problem in the form of nonlinear first order ordinary differential equations subject to the specific initial and boundary conditions which reflect the effect of active and passive controls of the nanoparticles in two different occasions. The bvp4c function, developed based on finite difference method by MATLAB is utilized to further solve the newly upgraded Maxwell, Williamson, Carreau and Powell-Eyring models while the BVPh 2.0 package in Mathematica is employed to solve the newly upgraded second grade nanofluids flow model. The effects of active and passive controls of the nanoparticles are compared graphically and tabularly. The influences of other considered parameters towards the flow profiles are also presented while the numerical values of skin friction coefficient, Nusselt number and Sherwood number are listed. The stagnation parameter increases the heat transfer of all the non-Newtonian nanofluids flows studied. Furthermore, the heat transfer rate of the boundary layer flows under passive control of nanoparticles is consistently higher in magnitude as compared to the ones under active control of nanoparticles.

Keywords: stagnation point, boundary layer, active and passive, nanofluid, non-Newtonian fluid

ALIRAN TITIK GENANGAN BENDALIR NANO BUKAN NEWTON DI BAWAH KAWALAN PARTIKEL NANO AKTIF DAN PASIF

ABSTRAK

Dalam tesis ini, model bendalir nano bukan Newton berhampiran titik genangan yang baru dinaik taraf diajukan di bawah pengaruh kawalan partikel nano aktif dan pasif. Aliran bendalir lapisan sempadan ini mempertimbangkan bendalir bukan Newton Maxwell, Williamson, gred kedua, Carreau dan Powell-Eyring. Aliran-aliran ini diwakili oleh persamaan pembezaan separa konvensional dalam dinamik bendalir yang ditambah ungkapan unik tensor tegasan ke dalam persamaan momentum yang mematuhi persamaan keselanjaran bagi pengabadian jisim. Model Buongiorno digunakan sebagai model asal dalam analisis ini kerana ia mempertimbangkan kesan gerakan Brownian dan thermophoresis partikel nano dalam persamaan tenaga dan pengangkutan jisim bagi aliran. Kesemua persamaan ini diturunkan kepada satu set persamaan pembezaan separa yang ringkas dengan menggunakan penghampiran lapisan sempadan. Persamaan menakluk itu kemudiannya ditukarkan kepada satu set persamaan pembezaan biasa tak linear dengan menggunakan transformasi keserupaan. Teknik meluru digunakan untuk menurunkan persamaan yang terhasil kepada satu set permasalahan nilai sempadan dalam bentuk persamaan pembezaan biasa peringkat pertama tak linear yang tertakluk kepada syarat permulaan dan sempadan yang khusus yang mencerminkan kesan kawalan partikel nano aktif dan pasif dalam dua keadaan yang berlainan. Fungsi bvp4c yang dibangunkan berasaskan kaedah beza terhingga oleh MATLAB diguna pakai untuk menyelesaikan model Maxwell, Williamson, Carreau dan Powell-Eyring manakala pakej BVPh 2.0 dalam Mathematica digunakan untuk menyelesaikan model aliran bendalir nano peringkat kedua yang baru dinaik taraf. Kesan kawalan partikel nano aktif dan pasif dibandingkan secara grafik dan penjadualan.

Pengaruh parameter lain yang dipertimbangkan terhadap profil aliran juga dibentangkan manakala nilai berangka pekali geseran kulit, nombor Nusselt dan nombor Sherwood disenaraikan. Parameter genangan meningkatkan pemindahan haba semua aliran bendalir nano bukan Newton yang dikaji. Selain itu, kadar pemindahan haba aliran lapisan sempadan di bawah kawalan partikel nano pasif adalah secara konsisten bermagnitud lebih tinggi berbanding dengan yang berada di bawah kawalan partikel nano aktif.

Kata kunci: titik genangan, lapisan sempadan, aktif dan pasif, bendalir nano, bendalir bukan Newton

ACKNOWLEDGEMENTS

Alhamdulillah. Allahuakbar. All praises to Allah for the strength and wisdom that is given to me to successfully complete this thesis.

I would like to express my biggest gratitude to my supervisor, Dr. Noor Fadiya bt Mohd Noor for her many suggestions and constant support throughout my whole Ph.D journey. I am also thankful to Prof. Dr. Sivasankaran and En. Md. Abu Omar Awang for their guidance through the early years of chaos and confusion.

Of course, I am grateful to my parents, Abdul Halim b Abdul Rashid and Salbiah bt Jais, for their patience, love and dua'. Without them this work would never have come into existence smoothly.

Not forgetting, Huda Zuhrah bt Ab. Halim and Nur Raihan bt Jalil, my two fellow postgraduate friends for being the best support team throughout my study.

Also, to Ministry of Higher Education of Malaysia for the financial assistance through MyPhD programme under MyBrain15.

Last but not least, to all the people around me. Thank you.

University of Malaya, Kuala Lumpur Nadhirah bt Abdul Halim

18 September 2018

TABLE OF CONTENTS

LIST OF FIGURES

LIST OF TABLES

LIST OF ABBREVIATIONS

CNTs	carbon nanotubes
HAM	homotopy analysis method
MHD	magnetohydrodynamic
ODE	ordinary differential equation
PDE	partial differential equation
PEHF	prescribed exponential order heat flux
PEST	prescribed exponential surface temperature
RK4	Runge-Kutta 4th order
UCM	upper-convected Maxwell

LIST OF SYMBOLS

A	unsteadiness parameter
A_1	first Rivlin-Erickson tensor
A_2	second Rivlin-Erickson tensor
B	uniform magnetic field
$B(t)$	time dependent magnetic field
B_0	initial strength of magnetic field
C	nanoparticle volume fraction/concentration
C_j	arbitrary constants
C_w	nanoparticle volume concentration near the wall surface for actively controlled mass flux
C_∞	nanoparticle volume concentration outside the boundary layer region
Cf_x	local skin friction
D_B	Brownian diffusion coefficient (m^2/s)
D_T	thermophoretic diffusion coefficient (m^2/s)
Gr_x	Grashoff number
I	identity vector
K	elasticity parameter
Le	Lewis number
M	magnetic parameter
N	buoyancy force ratio
N_c	heat capacity ratio
N_{bt}	the diffusivity ratio
Nb	Brownian motion parameter

Nt	thermophoresis parameter
Nu_x	local Nusselt number
P	pressure (Pa)
Pr	Prandtl number
Rd	thermal radiation parameter
Re_x	Reynolds number
S	stretching/shrinking parameter
Sc	Schmidt number
Sh_x	local Sherwood number
T	temperature (K)
T_w	temperature near the wall surface (K)
T_∞	temperature outside the boundary layer region (K)
U_{slip}	hydrodynamic slip velocity
V	fluid velocity (m/s)
V_e	fluid velocity at the free stream region (m/s)
V_o	fluid velocity at the stagnation point (m/s)
We	Weissenberg number
è	fluid parameter (m/s)
$\mathbb{L}$	linear operator
$\mathbb{T}$	Cauchy stress tensor (Pa)

a	positive constant
b	positive constant
c	positive constant
c_0^{ϕ}	convergence control parameter
c_0^{θ}	convergence control parameter
c_0^{f}	convergence control parameter
c_p	specific heat (J/(kgK))
d_{ij}	symmetric of the velocity gradient tensor
$f(\eta)$	velocity function
g	acceleration due to gravity (m^2/s)
k	HAM iteration
k_*	Rosseland mean absorption coefficient
k_1	relaxation time of the UCM fluid
m	order of approximation
n	power law index
q_m	wall mass flux
q_r	radiative heat flux (W/m^2)
q_w	wall heat flux (W/m^2)
r	stagnation parameter
t	time (s)
u	velocity component in $x-$direction (m/s)
u_e	free stream velocity / velocity outside the boundary layer region (m/s)
u_w	stretching velocity / velocity near the wall surface (m/s)
v	velocity component in $y-$direction (m/s)

z	elevation
z_e	elevation at the far upstream
z_o	elevation at the stagnation point

Greek letter

α	slip coefficient
α_1	material modulli
α_2	material modulli
$\mathring{\alpha}$	thermal diffusivity (m^2/s)
α_w	dimensional slip coefficient
β	fluid parameter
β_C	nanoparticle volumentric coefficient (m^2/s)
β_T	thermal expansion coefficient (m^2/s)
δ	fluid parameter
ϵ	fluid parameter
ϵ_k^f	average squared residual error
ϵ_k^ϕ	average squared residual error
ϵ_k^θ	average squared residual error
Γ	material constant
γ	buoyancy parameter
κ	thermal conductivity (W K/m)
λ	fluid parameter
μ	dynamic viscosity (Pa s)
μ_∞	maximum effective viscosity
μ_o	minimum effective viscosity

ν	kinematic viscosity (m^2/s)
ω	material fluid parameter
Π	second invariant strain tensor
ψ	stream function
ρ	fluid density (kg/m^3)
$(\rho c)_f$	heat capacity of nanofluid
$(\rho c)_p$	heat capacity of nanoparticles
σ	electrical conductivity
σ^*	Stefan-boltzmann constant
τ	effective heat capacity ratio
τ_{ij}	extra stress tensor (Pa)
τ_w	wall shear stress (Pa)
τ_{xy}	viscous stress (Pa)
$\theta(\eta)$	temperature function
$\phi(\eta)$	nanoparticle volume fraction function
Υ	time constant
Υ_x	local time constant

Superscript

$'$	differentiation with respect to η

Subscript

w	condition near the wall surface
∞	condition outside the boundary layer region

CHAPTER 1: INTRODUCTION

1.1 Preliminary

This chapter consists of preliminary of research, problem statement, the motivation that encourages us to pursue this topic, the objectives of the study that we hope to achieve and our contributions towards the scientific knowledge in this field. Lastly, the structure of the thesis will be described in detail.

In general, matter can be divided into solids and fluids. Solids have definite shape and volume while fluids have no fixed shape and deform continuously under applied shear stress. Fluids can roughly be divided into Newtonian and non-Newtonian fluids. The most common fluids among us such as water and air are Newtonian. Under constant temperature, their viscosity will remain constant regardless of the amount of shear stress applied on them. However, the fluids commonly used in our daily life such as ketchup, toothpaste, paint and shampoo are mostly non-Newtonian. The viscosity of non-Newtonian fluids are dependent on the shear stress that is applied on them. Heat transfer fluids are important in many industrial sectors including power generation, chemical production, transportation and microelectronics to name a few. Most conventional heat transfer fluids such as water, ethylene glycol and oil, have limited capabilities in terms of thermal properties which may impose several restrictions in thermal applications. The concept of nanofluids is introduced as a new class of heat transfer fluids with expected higher thermal conductivity as compared to conventional heat transfer fluids. They are engineered by suspending nanoparticles made of metals, oxides, carbides or carbon nanotubes in a base fluid. Meanwhile, stagnation-point flow over a stretching surface is a classic problem in fluid mechanics. The flow is seen whenever a fluid is impinged on a solid surface where its velocity reduced to zero and its pressure and heat mass transfer reached its highest point. The stagnation point flow rises in many applications and has a very important role in industrial processes such as cable coating, glass fibre production, glass blowing and designing of rockets and ships.

1.2 Problem Statement and Motivation

Nanofluids are base fluids with suspended nanoparticles in it. The use of nanofluids in a wide range of applications appears promising. Its application of interest in particular is as the next-generation heat transfer fluids. Heat transfer fluids are used in a cooling and heating system for vehicles, buildings and electronic appliances. It is also used in fuel, brake fluid, power reactors and many other applications. From a recent review (Raja et al., 2016), it is found that the convective heat transfer behaviour of nanofluids is evidently more superior than the conventional fluids with both numerical and experimental studies supporting the fact. The larger relative surface area of nanoparticles should significantly improve heat transfer capabilities as well the stability of suspensions and abrasion-related properties (C. Y. Wang, 2008). With the recent trend of miniaturization in modern science and technology, successful employment of nanofluids will be very beneficial towards component miniaturization by enabling a smaller and lighter design of heat exchanger system. Despite all the recent advances, development of this field still faces some huge challenges. Some difficulties that need to be overcome includes nanoparticle aggregation, stability of the nanofluids and erosion of oxide nanoparticles in pipes. Suspended nanoparticles can also alter the fluid flow and heat transfer characteristics of the base fluid. To conquer this problem, it is important to conduct more experiments and studies to explore and to understand the underlying physics of the nanofluids under various systems before wide applications for nanofluids can be found. However, these experiments are very costly with production of nanofluids using expensive materials and equipments. The next best approach that is much more affordable is by utilizing numerical modelling of nanofluids to stimulate the flow and to assess the thermal performance of the system.

There have been many attempts in developing convective transport models for nanofluids. Most of the earlier proposed model can be classified into two main groups; single-phase model and two-phase model. The single-phase model main assumption is that nanofluid is considered as a homogenous liquid. Due to its superfine size, the nanoparticles are assumed to be easily dispersed in the base fluid and are in thermal balance without any slip between molecules. Using this model for nanofluid will simplifies the simulation and it has the lowest computational cost but it comes with some limitations. The model may underestimate the heat transfer rate obtained as this model is strongly dependent on adopted thermophysical properties (Safaei et al., 2016). Therefore, selecting suitable thermophysical properties are of much importance for this model. In two-phase model, a classic theory of solid liquid mixture is applied for nanofluids. Nanoparticles and base fluids are considered as two separate phases with different temperature and velocity (Safaei et al., 2016). It took into account other slip mechanisms to provide more appropriate results. It seems to be more appropriate to use this model for nanofluid simulation, although it does come with a much higher computational cost.

Over the years, a lot of new mechanism and unconventional models has been proposed but there is yet a general formulation that can be used for all nanofluids. A review of the latest works on mathematical modelling for nanofluids simulation has been done by Safaei et al. (2016). The Buongiorno (2006) model is a non-homogenous two-component equilibrium model. It was developed not to explain the effect of nanoparticles on their thermophysical properties but to focus on explaining the further heat advancement that is observed in convective situations. It is an alternative model that eliminates the shortcomings of the homogenous and dispersion models. The model described the effect of the nanoparticle/base-fluid relative velocity more mechanistically than in the dispersion models. The results predicted with this model are in promising accordance with results from previous studies. It took into consideration the effects of the Brownian motion and thermophoresis. A common boundary condition used to study nanofluid boundary layer flow is to assume a constant nanoparticle volume fraction near the wall surface. That is to say, there exist a normal mass flux of nanoparticles at the surface. However, in practical, there is no justification on how the concentration of nanoparticles can be controlled actively at the surface. Nield and Kuznetsov (2009) in their paper shares an idea that they had in which if one could control the temperature at the boundary, one could also control the nanoparticle volume fraction in the same way. Again, the thoughts are difficult to apply in practice hence no indication is given on how it could be done. But recently, they revisited the problem and proposed a new condition (Kuznetsov & Nield, 2013). In order to make the model physically more realistic, the boundary condition they proposed now assumed that, the nanoparticle volume fraction on the surface is being controlled passively via temperature gradient which resulted in a zero mass flux of nanoparticles at the boundary. Thus, combined with the Buongiorno model, it is hoped that the nanofluid boundary layer flow can be represented more realistically and hence providing a more accurate results on the flow characteristics. Previously, researchers on nanofluid only have the option to apply the active boundary condition for their model. Even though the active boundary condition is still used and valid till now (Noor et al., 2015; Mabood & Khan, 2016; Othman et al., 2017; Saif et al., 2017), there are an increasing works on nanofluids that used the newly introduced passive control boundary condition (Rahman et al., 2014; Mustafa et al., 2015; Haq et al., 2015; Dhanai et al., 2015). There are also many authors that published a revised model of their work to incorporate the passive control boundary conditions (Kuznetsov & Nield, 2014; Nield & Kuznetsov, 2014a; Hayat, Shafiq, et al., 2016; Ishfaq et al., 2016; M. Khan, 2016; Waqas et al., 2017; Jahan et al., 2017). Because of this trend, it motivates us to study both boundary conditions of active and passive control of nanoparticles, in order to capture their effects and differences towards the boundary layer flow characteristic.

Stagnation-point flow is a classic problem in fluid dynamics. It describes the flow around the stagnation region and it exists on all solid bodies moving in a fluid. The stagnation region encounters the highest pressure, heat and mass transfer rate. This flow has many benefits and it arises in many applications. One of the more widely known application of this flow is in aerodynamics where it has a definite role especially in designing rockets, aircrafts, submarines and oil ships. It is also important in analytical chemistry where isolated microfluidic stagnation point flows are used for characterizing emulsions and polymers (Brimmo & Qasaimeh, 2017). Admittedly, there are already an abundance of literatures available on stagnation-point flow of boundary layers. However, with the recently introduced boundary condition for nanoparticles, it opens up new research opportunity as well as new perspective on this well-known flow. Hence, it is important to study this particular flow, knowing that it will contributes to the knowledge in this field.

As mention earlier, nanofluids are expected to be very beneficial as heat transfer fluid in various industries and applications. There are many industrial fluids that show non-Newtonian behaviour (Bush, 1989) such as those encountered in chemical and plastic processing industry as well as in applications such as lubrication and biomedical flows. As such, the simulation of non-Newtonian nanofluids flow is of importance to industry. There are many different non-Newtonian fluids, each with different viscosity. For a particular application, viscosity can play a vital role in the selection of the nanofluid as higher viscosity may incur a penalty in pressure drop, and thus gives rise in pumping power (Sharma et al., 2016). Since the flow behaviours are so diverse, there is no unique mathematical relationship that can explain all the rheological attributes of these flows. Thus, there are various non-Newtonian fluid models proposed as researchers try to capture the different characteristic of the non-Newtonian fluids. Different fluid model might have different characteristic that can be highlighted, hence explained the various type of fluid model used in this study.

In short, the aim of the present work is to analyze the stagnation boundary layer flow of several non-Newtonian nanofluid model under active and passive control of nanoparticles over a stretching surface with Buongiorno's model as the basis.

1.3 Scope of Research

The goal of this work is to provide a better understanding of the stagnation-point flow of non-Newtonian nanofluids. The non-Newtonian fluids included in the study are Maxwell, Williamson, second grade, Carreau and Powell-Eyring fluids. The study of each model emphasizes on the flow characteristics under the active and passive control environments. It is hoped that this work can help to discover more flow characteristic and heat transfer enhancement properties of the extended non-Newtonian nanofluid models in this study.

1.4 Research Questions and Objectives

The research questions for this study are listed as follows:

1. Does stagnation flow show similar characteristics in different non-Newtonian fluids?
2. What are the implications of applying active and passive controls of nanoparticles in the boundary condition towards the flow characteristic? Will there be any difference between the two boundary conditions?
3. How can different stream and boundary condition affect the stagnation flow of the nanofluids?
4. How can non-Newtonian stagnation point flows with active and passive controls of nanoparticles be solved?

5. Can the results obtained be interpreted to discuss specific characteristics of the non-Newtonian model considered?

The following research objectives are maneuvered to answer the above research questions:

- Objective 1: To develop extended models of some non-Newtonian boundary layer nanofluid flows. The specific extension for each model are as follow:
    + To extend the Maxwell nanofluid model with stagnation point flow and hydrodynamic slip velocity.
    + To extend the Williamson nanofluid model with stagnation point flow over a stretching/shrinking surface.
    + To extend second-grade nanofluid model with stagnation point flow.
    + To extend Carreau nanofluid model with unsteady stagnation point flow.
    + To extend mixed convection Powell-Eyring model with stagnation point flow.
- Objective 2: To study the effects of active and passive controls of nanoparticles towards the fluid profiles and its heat and mass transfer rate.
    + To include both active and passive boundary conditions of nanoparticles in each model.
    + To study the boundary layer flow behaviour under active and passive controls of the nanoparticles.
- Objective 3: To study the effects of various stream and boundary conditions towards the boundary layer flow. The specific conditions for each model are as follow:
    + To study the effect of slip velocity in Maxwell nanofluid model.
    + To study the flow characteristic over both stretching and shrinking surface in Williamson nanofluid model.

  - + To study the second-grade nanofluid model using an augmented boundary condition.
  - + To study an unsteady MHD flow with thermal radiation effect in Carreau nanofluid model.
  - + To study the effect of buoyancy force in Powell-Eyring nanofluid model

- Objective 4: To find the approximate solutions for the extended non-Newtonian nanofluids model
  - + To utilize the MATLAB *bvp*4*c* package and Mathematica *BVPh*2.0 to solve the models.
  - + To develop programme codes unique to each model to be used together with the *bvp*4*c* and *BVPh*2.0 package.

- Objective 5: To analyze the results obtained pertaining to the specific non-Newtonian boundary layer problems
  - + To use descriptive analysis to quantitatively describes the numerical data obtained.
  - + To provide physical interpretation for the flow profiles when necessary.
  - + To understand the effect of each parameter on the boundary layer flow.

1.5 Contribution to Scientific Knowledge

This thesis considers the stagnation-point flow of some non-Newtonian nanofluids under active and passive controls of nanoparticles. The study of stagnation-point flow over a stretching surface is such a classic problem in fluid dynamics that it has become quite saturated over the years. However, with the introduction of nanofluid in 1995 (Choi & Eastman, 1995), combined with the recently proposed boundary conditions for nanoparticle near the wall (Kuznetsov & Nield, 2013), it opens up a new research interest in this particular field. This research contributes by extending some existing models of some non-Newtonian nanofluids to study the stagnation-point flow under various stream and boundary conditions. The specific extension of each model is as follows:

- **Maxwell nanofluid**

  The model presented in Chapter 4 is among the earliest to consider stagnation-point flow of Maxwell nanofluid past a stretching surface. It also considers the effect of hydrodynamic velocity slip. Another model that is published around the same time is by Ramesh et al. (2016) who considered stagnation-point flow of Maxwell nanofluid with suction. However, the model is only studied under active control of nanoparticles.

- **Williamson nanofluid**

  Nadeem et al. (2013) claimed to be the first ones to develop a two-dimensional boundary layer equations for the Williamson fluid past a stretching sheet. Later, Nadeem and Hussain (2014a) extended the model to study the flow and heat transfer of Williamson nanofluid over a stretching sheet. They consider an active control of nanoparticles for their boundary condition. Not many works have been done on stagnation-point flow of Williamson nanofluid yet. One available is by Gorla and Gireesha (2016) who investigated the stagnation flow of Williamson nanofluid under a convective boundary condition over a stretching and shrinking surface using active control of nanoparticles. The model presented in Chapter 5 considered a stagnation-point flow of a Williamson nanofluid over a stretching and shrinking surface which is simpler than the earlier model proposed by Gorla and Gireesha (2016) but without the convective boundary condition.

- **Second-grade nanofluid**

  Mustafa et al. (2014) are among the first few to examine the second-grade nanofluid flow, followed by Goyal and Bhargava (2014) and Bhargava and Goyal (2014). They have considered active control of nanoparticles for the boundary condition. The model in Chapter 6 considered the stagnation-point flow of second grade nanofluid using an augmented boundary condition. The literature on stagnation-point flow of second grade nanofluid is still very scarce. Few literatures that are available include the work done by Farooq et al. (2016) who studied stagnation flow of MHD second grade nanofluid with convective boundary condition under passive control of nanoparticles and a recent work by Saif et al. (2017) who investigated the mixed convection stagnation flow of second grade nanofluid over non-linear stretched surface with variable thickness under active control of nanoparticles.

- **Carreau nanofluid**

The model presented in Chapter 7 considered an unsteady stagnation point flow of Carreau nanofluid over a stretching surface. There is no work done on unsteady stagnation point flow of Carreau nanofluid under both active and passive controls yet. There are researches available on unsteady Carreau nanofluid, for example the study by M. Khan, Azam, and Alshomrani (2017a) and M. Khan, Azam, and Munir (2017), who both considered a Falkner-Skan flow of MHD Carreau nanofluid over a wedge. M. Khan and Azam (2017) investigated the unsteady flow of MHD Carreau nanofluid while M. Khan, Azam, and Alshomrani (2017b) examined the effect of velocity slip and thermal radiation towards unsteady Carreau nanofluid under convective boundary condition.

- **Powell-Eyring nanofluid**

The mixed convection flow of Powell-Eyring nanofluid flow has been studied by Malik et al. (2015) who considered the effect of magnetic field and active control of boundary condition. The model presented in Chapter 8 is on stagnation-point flow of mixed convection Powell-Eyring nanofluid over a vertical stretching surface. No work has been published yet on this particular type of flow of mixed convection Powell-Eyring nanofluid.

This research also contributes by considering the study of boundary condition of both active and passive controls of nanoparticles. Most available literatures in this field only consider either one of the conditions. Some authors published a revised model of their work to incorporate the passive control of nanoparticles. By considering both boundary conditions, this research can provide a better insight on the effects the boundary conditions have towards the boundary layer flow, heat and mass transfer characteristics.

1.6 Outline of Thesis

The thesis is organized as follows:

Chapter 1 is an introductory chapter. It contains problem statement, research motivation, scope and objectives of the research. This chapter also outlines the whole thesis arrangement. Chapter 2 is mainly about literature reviews and the mathematical formulation. The literature reviews are subdivided into three main topic that is stagnation point flow, nanofluids and non-Newtonian fluid. The characteristic of the stagnation point flow is briefly explained, the basic concept of nanofluids are introduced and classification of non-Newtonian fluids is given. Recent works on these topics are also compiled and arranged. Chapter 3 covers the mathematical formulation and methodology. The governing equations of a boundary layer flow and the unique constitutive equations for non-Newtonian fluids are given. Different stream conditions are discussed and its mathematical term are presented. All initial and boundary conditions used throughout the thesis are also explained. To solve the governing equations, similarity transformation is applied, and the non-dimensional variables used are provided for both steady and unsteady cases. Important dimensionless number are also listed. Lastly, a methodology section that includes work flow charts and information on the mathematical package used to solve the models.

In the subsequent chapters, the model and analysis of each particular non-Newtonian nanofluid under both active and passive controls of nanoparticles are described in detail. They include a short literature review on each particular fluid, the problem formulation, similarity transformation, numerical method, results and discussion as well as each chapters' summary.

Chapter 4 is on stagnation-point flow of a Maxwell nanofluid model. A hydrodynamic slip velocity is added to the initial condition as a component of the stretching velocity. To validate the accuracy of the computation, the present results are compared with published work of others that used different numerical methods that is HAM, finite difference method and also, RK4. Brownian motion and thermophoresis parameter are defined and used to study the effect nanoparticles had onto the flow.

Chapter 5 is on stagnation-point flow of a Williamson nanofluid model. The flow is studied over a stretching and shrinking surface. Compared to the other four models, this model defined a parameter for heat capacity ratio of nanoparticles over nanofluid and also a parameter for diffusivity ratio of Brownian diffusivity over thermophoretic diffusivity. Numeric validations are made by comparing present results with results obtained by others that used Keller-Box method and HAM. The effect of stretching surface and shrinking surface had towards the flow physical quantities can be investigate using this model.

Chapter 6 is on stagnation-point flow of a second grade nanofluid model. This model incorporated the augmented boundary condition to compensate the paucity of existing boundary conditions. Due to the nature of this model, a HAM based analytical tool are needed to solve the problem posed. Convergence analysis are done to make sure of the accuracy and convergence of the numerical.

Chapter 7 is on stagnation-point flow of a Carreau nanofluid model. The model is a time dependent model that took into consideration the effect of both magnetic and thermal radiation. This is the only model in the thesis that considered an unsteady boundary layer flow. Result comparison are made with other existing literature to validate the numerical calculation accuracy.

Chapter 8 is on mixed convection stagnation-point flow of a Powell-Eyring nanofluid model. It is a flow resulting from buoyancy forces that arises from temperature and concentration gradient of comparable magnitude. Effects of opposing and assisting flows can be observed through the variation of buoyancy parameter.

All governing PDEs for the models in Chapter 4 to Chapter 8 are reduced into a system of ODEs by using similarity transformation. The resulting systems of ODEs are then solved using $bvp4c$ function in MATLAB software except for the second grade nanofluid model in Chapter 6 that is solved using $BVPH2.0$; a Mathematica package software based on HAM. All obtained results are then tabulated and shown graphically to exhibit the impact of different parameters towards the flow, heat and mass transfer characteristics.

Lastly, in Chapter 9, we summarized the conclusion of all of our research and discussed some improvements that can be made on current research and possible future research.

CHAPTER 2: LITERATURE REVIEW

2.1 Introduction

This chapter consists of study background of the research focusing on the three main topic that is boundary layer stagnation point flow, nanofluids and also non-Newtonian fluid.

Boundary layer is a narrow region adjacent to solid surface where confined modifying effect appears. For flowing fluids, it is a region with steep gradient of shearing stress. The description of the boundary layer concept was first introduced by a German scientist, Ludwig Prandtl in 1904. He presented the boundary layer equations for steady two dimensional flows, assuming that the non-slip condition at the surface and that frictional effects were experienced only in a thin region near the surface (Anderson, 2005). The concept of boundary layer has allowed prediction of skin friction drag, heat transfer from the wall and separation of the boundary layer that enable proper design of airplanes, ships and other equipments (Tulapurkara, 2005). His work provided the key in the analysis and understanding of fluid dynamics which has now developed rapidly and applied in almost all branches of engineering.

Boundary layers are of vital importance for transport phenomena. There is a specific boundary layer with different properties for each transport phenomena. The boundary layers can be classified as viscous boundary layer (for the velocity or momentum), thermal boundary layer (for temperature or energy) and mass boundary layer (for the chemical concentrations) (Hauke, 2008).

2.2 Stagnation-point Flow

One class of flows which has thoroughly been studied in literature is the stagnation-point flow. The plane stagnation point flow is also known as Hiemenz flow, referring to the first person who discovered that the stagnation point flow can be analyzed exactly by the

Navier-Stokes equations. Weidman and Putkaradze (2003) characterized these flows as inviscid or viscous, steady or unsteady, two-dimensional or three-dimensional, symmetric or asymmetric, normal or oblique, homogeneous or two-fluid, and forward or reverse.

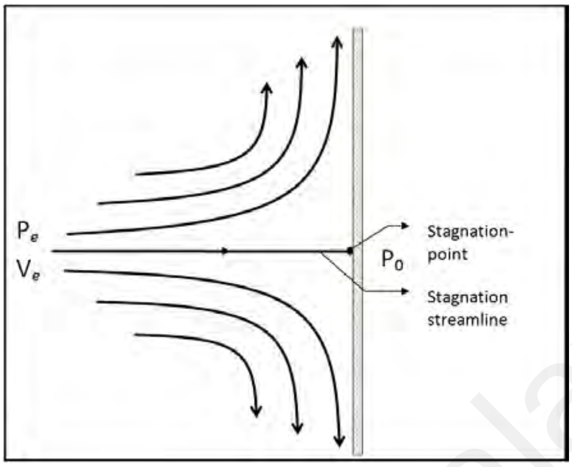

Figure 2.1: A stagnation-point flow.

Consider a steady flow impinging on a perpendicular plate (Fig. 2.1). There is one streamline that divides the flow in half. Along it, the fluid moves towards the plate and come to rest at the point where it meets the plate i.e it stagnates. The point it comes to rest is called the stagnation point and the dividing streamline is called stagnation streamline. The Bernoulli's equation states that in a steady inviscid and incompressible flow, the total pressure along a streamline is constant:

$$P + \frac{1}{2}\rho V^2 + \rho g z = constant \tag{2.1}$$

Here, P is the static pressure, $\frac{1}{2}\rho V^2$ is the dynamic pressure and $\rho g z$ is the hydrostatic pressure. Then, assuming that the elevation effects are negligible, the Bernoulli's equation along the stagnation streamline is given as (Smits, 2018):

$$P_e + \frac{1}{2}\rho V_e^2 + \rho g z_e = P_o + \frac{1}{2}\rho V_o^2 + \rho g z_o \tag{2.2}$$

where ρ is the fluid density, V is the fluid velocity, z is the elevation and g is the gravitational acceleration. The points "e" and "o" represent the far upstream and stagnation point respectively. Since the velocity at the stagnation point is zero ($V_o = 0$) and $z_e = z_o$, it became (Smits, 2018):

$$P_e + \frac{1}{2}\rho V_e^2 = P_o \tag{2.3}$$

From the above equation, it can be seen that the pressure at a stagnation point is the sum of static pressure and dynamic pressure, making it the point with the highest pressure in the flow field.

The stagnation point flow over a stretching surface is a classic problem in fluid mechanics. This flow arises in many applications and it has a definite role especially in transportation industries on designing of rockets, aircraft, submarines and oil ships as well as in the process of polymer extrusion, paper production, insulating materials, glass drawing, continuous casting, fine fibre mats and many others. A large number of analytical and numerical studies explaining various aspects of the boundary layer stagnation point flow over a stretching/shrinking surface have been done.

Study on a stagnation point flow of a nanofluid has also garnered interest from many investigators. Mustafa et al. (2011) are one of the first few who investigate the stagnation-point flow of a nanofluid. They take into account the combined effects of heat and mass transfer in the presence of Brownian motion and thermophoresis. Then, Bachok et al. (2012) investigated the boundary layer of an unsteady two-dimensional stagnation-point flow of a nanofluid. Alsaedi et al. (2012) further conducted an analysis to examine the stagnation point flow of nanofluid near a permeable stretched surface with a convective boundary condition. Some studies include the pioneering article on the stagnation point flow of CNTs over a stretching sheet by Akbar et al. (2014). Water is used as the base fluid encompassing single- and multi-wall CNTs to discuss flow under the influence of slip velocity and convective boundary condition. U. Khan et al. (2014) presented the effects of thermo-diffusion on stagnation point flow of a nanofluid towards a stretching surface with applied magnetic field. Hayat, Asad, et al. (2015) studied the stagnation point flow of Jeffrey fluid over a convectively heated stretching sheet. They took into account the combined effects of thermal radiation and magnetic field. Their result showed that for a sufficiently large Biot number, the analysis for constant wall temperature case can be recovered and that the velocity ratio has a dual behavior on the momentum boundary layer and the skin friction coefficient. Sajid et al. (2015) investigated the steady mixed convection stagnation point flow of a MHD Oldroyd-B fluid over a stretching sheet. They found that the magnitude of heat transfer at the wall increases by increasing the Archimedes number. Dinarvand et al. (2015) investigated the development of double-diffusive mixed convective boundary layer flow of a nanofluid near stagnation point region over a vertical surface. The model is solved numerically using Keller-box method and a comprehensive study of the boundary layer behavior is illustrated through the sensitivity analysis model. Hamid et al. (2015) dealt with a stagnation point boundary layer flow towards a permeable stretching/shrinking sheet in a nanofluid where the flow and the sheet are not aligned. Their research showed that the non-alignment function can ruin the symmetry of the flows which are prominent in the shrinking sheet. However, the fluid suction can reduce the impact of the non-alignment function while increasing the velocity profiles and the shear stress at the surface. W. A. Khan et al. (2016) investigated non-aligned MHD stagnation point flow of nanofluids with radiation. They found that the non-alignment of the re-attachment point on the sheet surface decreases with an increase in the magnetic field intensity. Ramesh et al. (2016) have carried out an analysis to study the stagnation point flow of Maxwell fluid towards a permeable stretching sheet in the presence of nanoparticles. Their study showed increasing trend of velocity and decreasing temperature and concentration profile when the Maxwell parameter is increased. Farooq et al. (2016) addressed the MHD stagnation point flow of a viscoelastic nanofluid towards a stretching surface with non-linear radiative effects. The obtained result shows that the skin friction increases with increasing magnetic parameter. A. U. Khan et al. (2016) analyzed the slip effects on the oscillatory oblique stagnation point flow of MHD nanofluid using three different nanoparticles namely copper (Cu), alumina (Al_2O_3) and titania (TiO_2). Most recently, Dinarvand et al. (2017) applied the Tiwari-Das nanofluid model in investigating the steady axisymmetric mixed convective stagnation-point flow of a nanofluid over a vertical permeable circular cylinder in the presence of transverse magnetic field. Their computation shows that the curvature parameter has a strong additive effect on the skin friction coefficient and local Nusselt number.

A stagnation flow in pure forced convection usually refers to the rather symmetric flow in the neighbourhood of a stagnation point line. However, a mixed convection stagnation flow will no longer be symmetrical towards the stagnation line (Ramachandran et al., 1988). Ishak et al. (2007) studied the mixed convection of the stagnation-point flow of an incompressible viscous fluid towards a stretching vertical sheet. Their study shows that dual solution exists for the opposing flow while a unique solution is available for assisting flow. Later, they investigated the effects that stagnation mixed convection flow had when a constant magnetic field is applied normal to the vertical plate (Ishak et al., 2010). With applied suction and injection on the surface, their results show that dual solution actually exists for both assisting and opposing flows. Suction as well as magnetic field increases the range of buoyancy parameter for which the solution exists. Hayat et al. (2010) applied the homotopy analysis method (HAM) in their study on the influence of thermal radiation on the MHD stagnation point flow with mixed convection. Both thermal radiation and magnetic parameter are found to improve the heat transfer rate of the fluid in assisting flow as well as opposing flow. Aman et al. (2011) considered a boundary slip in the mixed convection stagnation-point flow on a vertical surface. In their study, velocity slip helps to improve the heat transfer rate while the thermal slip worsens it. Abbas et al. (2010) discussed the stagnation point flow of a Maxwell fluid on a stretching vertical surface with mixed convection. They found that increasing the fluid relaxation time represented by the Deborah number will increase the heat transfer rate in opposing flow but decreases it in assisting flow. Hayat et al. (2012) studied the stagnation-point flow of Casson fluid with mixed convection under convective boundary conditions. Their result shows that the Biot number has a qualitatively similar effect towards velocity and temperature profiles.

Nowadays, there are a lot of literatures on mixed convection stagnation point flow of nanofluid available. Some of them include work from Makinde et al. (2013) who studied the influence of buoyancy force and magnetic field had on stagnation point flow towards a convectively heated surface. Here, the buoyancy force helps to improve the heat transfer rate of the fluid. Noor et al. (2015) investigated the mixed convection boundary layer flow of a micropolar nanofluid near a stagnation point along a vertical stretching sheet with slip effects. Their investigation showed that the presence of slip velocity between the base fluid and the nanoparticles has significant impact on the heat transfer enhancement of the stagnation flow. Pal and Mandal (2015) researched on the effects of thermal radiation, heat generation and viscous dissipation towards a mixed convection flow over a stretching/shrinking surface that is embedded in nanofluids. Hsiao (2016) investigated the stagnation point flow of a nanofluid with electrical magnetohydrodynamic (EMHD) and slip boundary effect on a stretching surface. Abbasi et al. (2016) analyzed the mixed convection flow of Jeffrey nanofluid while taking into consideration the effects of thermal radiation and double stratifications. Their result shows that thermal radiation increases the fluid temperature, but thermal stratification lowers the temperature. Just recently, Othman et al. (2017) worked on a mixed convection stagnation point flow of a nanofluid past a vertical stretching/shrinking surface.

2.3 Nanofluids

The term nanofluids was first coined by Dr. Stephen Choi in 1995 (Choi & Eastman, 1995). Nanofluids are colloidal mixtures of nanometre-sized particles (1 - 100nm) in a base fluid. The nanoparticles can be metallic, oxide, carbide, and carbonic among others while the base fluid may be liquids such as water, refrigerant, ethylene glycol, mineral oil or even a mixture of different types of liquids. Dispersion of a small amount of solid nanoparticles in a base fluid may alter the thermo-physical properties of fluids. Various experiments have shown that nanofluids shows a remarkable improvement in the thermal conductivity for heat transfer process. Besides the enhanced thermal conductivity, nanofluids also have special qualities which includes ultra fast heat transfer ability, decreased pumping power, enhanced stability over other colloids, superior lubrication, decreased friction coefficient and decreased erosion and clogging in microchannels (Solangi et al., 2015). This uncommon features makes the use of nanofluids significant for various applications such as in microelectronics, thermal engineering, nuclear reactors, solar thermal, transportation, biomedicine, medical and military applications.

It has been 20 years since the term nanofluid first introduced and extensive theoretical and experimental research have been made to study the nanofluid properties. However, the research in nanofluids are still growing with more and better models incorporating nanoparticles being proposed over the years. In 2006, Buongiorno (2006) proposed a transport model for the nanofluids that took into consideration the effect of Brownian diffusion and thermophoresis. His model quickly become one of the most used in nanofluid modelling. In 2009, Nield and Kuznetsov (2009) made an assumption that one could control the value of the nanoparticle fraction at the boundary the same way one could control the temperature. However, no indication is given on how it could be done in practice. Recently, they revised the problem by replacing the boundary condition with a more physically realistic set that accounts for the effect of both Brownian and thermophoresis parameters (Kuznetsov & Nield, 2013). It is now assumed that there is no normal nanoparticle mass flux at the plate and that the particle fraction value there adjusts accordingly. Since then, more models are presented by taking into consideration the zero normal flux of nanoparticles at the wall. Nield and Kuznetsov themselves have revised a few of their existing models on the corresponding problems in the onset of convection in a horizontal nanofluid layer of finite depth (Nield & Kuznetsov, 2014a), in natural convective boundary layer flow of a nanofluid (Kuznetsov & Nield, 2014) and in a thermal instability analysis of a nanofluid-saturated porous layer (Nield & Kuznetsov, 2014b).

The new boundary condition was also employed by others such as Rahman et al. (2014) where they investigated the forced convective flow and heat transfer characteristics of a nanofluid over an exponentially permeable stretching/shrinking surface in the presence of partial slip at the interface. They identified the critical suction and stretching/shrinking parameters that determine the existence of the dual solutions. Mustafa et al. (2015) explored the boundary layer flow due to convectively heated non-linear stretching sheet. Their results show that influence of Brownian motion on the temperature and nanoparticle volume fraction is negligible. Haq et al. (2015) discussed the combined effects of both thermal radiation and thermal slip on MHD boundary layer stagnation-point flow of nanofluid. It is found that both slip parameter and Hartmann number enhance the temperature profile. Dhanai et al. (2015) investigated the combined effects of magnetic field, mass transfer parameter and viscous dissipation on steady boundary layer nanofluid flow induced by a power law stretching/shrinking sheet.

Some of the recent studies on nanofluid involved the study done by Garoosi et al. (2016a, 2016b) on heat transfer performance of nanofluids in a heat exchanger. Amani et al. (2017) investigated the effect of heterogeneous distribution of nanoparticles using a two-phase mixture model for nanofluid turbulent flow and heat transfer. They observed that an increase in the Peclet number caused heterogeneity in the distribution of the properties and the effect of nanofluid concentration on Nusselt number is more noticeable in lower Reynolds number. Sheikholeslami and Sadoughi (2017) investigated a magnetohydrodynamic (MHD) nanofluid convective flow in a porous cavity while taking into accounts the various shapes of nanoparticles. G. Wang and Zhang (2017) calculated the thermal and power efficiencies of nanofluid flows around cylinder and developed a nanofluid-flowrate assessment criterion for nanofluid applications. They found out that the nanoparticle density plays a more significant role than the thermal conductivity in determining the thermal performances.

2.4 Non-Newtonian Fluid

Rheological analysis of nanofluids shows that they can exhibit either or both Newtonian and non-Newtonian behaviours. The behaviour depends on various factors such as nanoparticle shape, nanoparticle size, nanoparticle concentration, nanoparticle structure, surfactants, shear rate range and even magnetic field (Sharma et al., 2016). Viscosity of nanofluids can play a vital role in selection of the nanofluid for a particular applications. Non-Newtonian fluids are marking their important presence with their complex and yet interesting characteristics. They are multi-component and chemically complex, and they display shear-dependence of viscosity, thixotropy and elasticity in different degrees (Pearson & Tardy, 2002). These fluids are characterized by their viscosity behaviour. Considerable efforts have been directed towards understanding the characteristics of these so-called rheological fluids because of their growing use in various manufacturing and processing industries.

Due to their flow diversities, it is no surprise that there is no unique single mathematical relationship that can explain all the rheological attributes related to these non-Newtonian fluids. As a result, a variety of non-Newtonian fluid models have been proposed. One of the earliest models that gained much acceptance is the power-law model in which the shear stress varies according to a power function of the strain rate (Xu et al., 2006). Schowalter (1960) and Acrivos et al. (1960) were the first to perform the theoretical analysis of a steady boundary layer flow of incompressible power-law fluids in 1960. Since then, more and better models have been proposed to suit different types of non-Newtonian behavior such as Jeffrey fluid, Bingham fluid, Oldroyd-B fluid and Casson fluid, to name a few.

These non-Newtonian fluids may be grouped into three general classes (Chhabra, 2010):

- **Generalized Newtonian fluids**

  The rate of shear of this particular fluid at any point is determined only by the value of shear stress at that point at that instant. Also known as a purely viscous or time-independent fluid.

- **Time-dependent fluids**

  The relation between shear stress and shear rate of this fluid depends upon the duration of shearing and their kinematic history. There are two types of the fluids, thixotropy and rheopexy.

- **Viscoplastic fluids**

  The fluid exhibits characteristics of both ideal fluid and elastic solid. It shows partial elastic recovery after deformation.

The above classifications are quite arbitrary as most real materials often display a combination of two or even all these types of features under appropriate circumstances. The fluids from the time-independent group can further be subdivided into three types:

- **Shear-thinning / pseudoplastic**

  This fluid is characterized by an apparent viscosity that decreases with increasing shear rate. At a very low or very high shear rates, most of this shear-thinning fluid will exhibit Newtonian behaviour.

  Example: power-law model, Carreau model, Ellis fluid model

- **Shear thickening / dilatant**

  The fluid is similar to pseudoplastic fluid in which they show no yield stress but the apparent viscosity increases with increasing shear rate. Dilatant fluids are typically multi-phase fluids.

  Example: Oobleck

- **Viscoplastic**

  This fluid is characterized by the existence of a yield stress which must be exceeded before the fluid will deform or flow. When external stress is applied, the fluid will behave like an elastic solid or it may exhibit Newtonian behavior or shear-thinning characteristics, depending on the magnitude of the stress applied against the fluids yield stress.

  Example: Bingham plastic model, Herschel-Bulkley model, Casson model

In this thesis, five different non-Newtonian fluid has been considered which is Maxwell, Williamson, second-grade, Carreau and Powell-Eyring.

2.4.1 Maxwell fluid

Maxwell model is the simplest subclass of rate-type fluid that can predict the relaxation time effects. Investigations involving Maxwell fluid are plenty (Shehzad et al., 2013; Awais et al., 2014; Abbasbandy et al., 2014; Nadeem, Haq, & Khan, 2014; Ramesh et al., 2016). Some recent ones include the study by Hussain et al. (2016) on the impact of double stratification and magnetic field in mixed convective radiative flow of Maxwell nanofluid. Their study showed that the thermal stratification parameter and concentration stratification parameter caused a reduction in temperature and nanoparticle concentration. N. Khan et al. (2016) investigated the heat and mass transfer on MHD mixed convection axisymmetric chemically reactive flow of a Maxwell fluid driven by exothermal and isothermal stretching disks. Sadeghy et al. (2006) opted to study the stagnation-point flow of viscoelastic fluids by relying on a more realistic constitutive equation. They proposed that upper-convected Maxwell UCM model is the best candidate to study the effects of fluid elasticity on the characteristics of its boundary layer in stagnation-point flow. Currently, there are not many literature available on stagnation-point flow of Maxwell nanofluid. One available work is done by Ramesh et al. (2016) who studied the stagnation point flow of Maxwell nanofluid with suction.

2.4.2 Williamson fluid

One of the most encountered non-Newtonian fluids is pseudoplastic fluids. The study of the boundary layer flow of pseudoplastic fluids has garnered much interest due to its wide range of applications in industry that includes extrusion of polymer sheets, solutions and melts of high molecular weight polymers and emulsion coated sheets like photographic films. Many models have been proposed to explain the behavior of this type of fluid such as the power law model, Carreau model, Cross model and Ellis model but little attention has been paid to the Williamson fluid model. The flow of pseudoplastic materials has been discussed by Williamson (1929). He proposed a model to describe the flow of pseudoplastic fluids and experimentally verified the results. A fluid has both minimum and maximum effective viscosities depending upon the molecular structure of the fluid. In the Williamson fluid model, both the minimum and maximum viscosities are considered to ensure better results for pseudoplastic fluids. Articles on Williamson fluid model are available (Nadeem & Akram, 2010; Akbar et al., 2012; Ellahi et al., 2013; N. A. Khan et al., 2014; Zehra et al., 2015; Eldabe et al., 2016), but most of them describe the peristaltic flows of the Williamson fluid. Nadeem et al. (2013) are the first ones to develop the two-dimensional boundary layer equations for the flow of Williamson fluid past a stretching sheet. The problem is solved analytically using HAM. Their results show that both velocity profile and skin friction decrease with increasing Williamson parameter. Nadeem and Hussain (2014b) considered the flow of Williamson fluid over an exponentially stretching sheet. They explored the effects of heat transfer by considering two cases of boundary temperature; the PEST and the PEHF. They also examined the two dimensional flow of Williamson nanofluid over a stretching sheet (Nadeem & Hussain, 2014a). They found out that the parameters Le, N_{bt}, N_c and Pr have strong impacts on heat transfer very close to the wall and are almost negligible slightly away from the wall. Literature on stagnation point flow of Williamson fluid over stretching/shrinking surface is still very scarce. One available is by Gorla and Gireesha (2016) who investigated the stagnation flow of Williamson nanofluid under a convective boundary condition over a stretching and shrinking surface using active control of nanoparticles.

2.4.3 Second grade fluid

One of the simplest model of differential type fluids is known as second grade fluid. This fluid model is capable in exploring the shear thinning and shear thickening effects. It can also describe the normal stress effects especially in steady flows. However, its equation of motion is an order higher than the standard Navier-Stokes equation. This renders towards the boundary condition insufficiency in determining the complete solution. In order to overcome the difficulty caused by the paucity existing of boundary conditions, Garg and Rajagopal (1990) suggested to augment them on the basis of physically reasonable assumptions. This is possible in the case of flows with unbounded domains by using the fact that the solution has to be bounded or the solution has a certain smoothness at infinity. Their study of the stagnation flow of second grade fluid with augmented boundary conditions shows good agreement with other study that used perturbation approach. Labropulu and Li (2008) examined the steady two dimensional stagnation point flow of a second grade fluid with slip. The numerical solutions are obtained using a quasi-linearization technique. Gorder and Vajravelu (2010) established the existence and uniqueness results over the semi-infinite interval for a hydromagnetic stagnation point flow of a second grade fluid over a stretching sheet. Hassan and Siddiqui (2012) proposed a modified approach to exact solutions of a general form of a non-Newtonian second grade fluid. Mehmood et al. (2013) worked on non-orthogonal stagnation point flow of a micropolar second grade fluid towards a stretching surface with heat transfer. Hayat and his fellow researchers (Hayat et al., 2007, 2011; Hayat, Qasim, et al., 2014) discussed the flow of a second grade fluid under different conditions over the years including the MHD flow in a porous channel, a convective boundary condition as well as an unsteady stagnation point flow with variable free stream.

It is found that the literature on second grade nanofluid in general is still very scarce. Ramzan and Bilal (2015) studied the series solution of time dependent MHD second grade incompressible nanofluid towards a stretching sheet while taking into account the effects of mixed convection and thermal radiation. Hayat with his co-authors (Hayat, Muhammad, et al., 2015; Hayat, Aziz, et al., 2016; Hayat, Shafiq, et al., 2016) investigated second grade nanofluid covering different environments including a three dimensional boundary layer flow past a stretching surface with thermal radiation and heat source/sink, a magnetohydrodynamics flow over a nonlinear stretching sheet and impact of melting phenomenon in the Falkner-Skan wedge flow. Saif et al. (2017) presented a research on the flow of second grade nanofluid towards a nonlinear stretching surface near a stagnation point that is subjected to variable surface thickness. They studied the simultaneous effects of melting heat and mixed convection towards the flow. Most recently, Sithole et al. (2018) addressed the matter of entropy generation in a magnetohydrodynamic flow of a second grade nanofluid over a heated stretching surface. They also took into consideration the effect of nonlinear thermal radiation and viscous dissipation. The model is then solved using the spectral local linearization method. Their finding shows that entropy generation is improved when higher values of magnetic parameters and Reynolds number are used.

2.4.4 Carreau fluid

One of the various models of non-Newtonian fluids available is called the Carreau fluid model from the class of generalized Newtonian fluids. This model gains a wider acceptance in chemical engineering and technological process for its ability to depict both the shear thinning and shear thickening properties. Research on Carreau fluid involves one done by Nadeem, Riaz, et al. (2014) who presented an analytical series solution for the unsteady peristaltic flow of Carreau fluid in a gap between two eccentric tubes. M. Khan, Hussain, and Azam (2016) investigated the heat transfer and squeezed flow of Carreau fluid over a sensor surface with variable thermal conductivity and found out that increasing the values of squeezed flow parameter will enhance the velocity and temperature profile. Raju et al. (2017) analyzed the MHD unsteady Carreau nanofluid over a cone filled with different alloy nanoparticles. Their result shows that the viscous variation parameter enables to enhance the heat transfer rate.

However, amongst the abundance of research done on Carreau fluids, there is a shortage of literature available on the flow of Carreau fluids past a stretching/shrinking sheet. It is not until recently that researchers begin to study this flow on Carreau fluids. Hayat, Asad, et al. (2014) are the first few that considered a 2-D boundary layer flow of Carreau fluid above a stretching sheet with convective boundary condition. Their result shows that material parameter increases the fluid velocity while decreases the temperature field. Sulochana et al. (2016) investigated the transpiration effect on stagnation-point flow of a Carreau nanofluid. They found out that the non-Newtonian parameter effectively increases the heat and mass transfer rate. Recently, Waqas et al. (2017) explored the MHD flow of Carreau nanoliquid by exponentially convected stretchable surface. Their results show that large Hartman number will retards the flow for both shear thinning and thickening cases. Zaib et al. (2018) studied the effect of nonlinear thermal radiation on stagnation-point flow of Carreau nanofluid over a nonlinear stretching surface while also taking into account the activation energy and binary chemical reaction. Currently, M. Khan and his fellow researchers (M. Khan & Hashim, 2015; M. Khan, Hashim, & Alshomrani, 2016; M. Khan, Hussain, & Azam, 2016; M. Khan & Azam, 2016; M. Khan, 2016) are ones of the most active contributors into the literature of Carreau fluid over stretching/shrinking sheet. Their recent works on unsteady flow of Carreau nanofluid involved a magnetohydrodynamic flow (M. Khan & Azam, 2017), a slip flow (M. Khan, Azam, & Alshomrani, 2017b), a Falkner-Skan flow (M. Khan, Azam, & Alshomrani, 2017a) and MHD Falkner-Skan flow (M. Khan, Azam, & Munir, 2017).

2.4.5 Powell-Eyring fluid

Among the abundance of non-Newtonian fluids available, the Powell-Eyring fluid holds some advantages over the others especially in chemical engineering. This particular fluid model is derived from the kinetic theory of liquids. Furthermore, the model can properly exhibit Newtonian behaviour at low and high shear rates. Bhatti et al. (2016) investigated the entropy generation of an Eyring-Powell nanofluid through a permeable stretching surface and found that the entropy profile enhances all the physical parameters involved. Hayat and his fellow researchers presented a few works on Powell-Eyring nanofluid which include radiative flow with convective boundary conditions (Hayat, Hussain, et al., 2017), effectiveness of magnetic nanoparticles in radiative flow (Hayat, Khan, et al., 2017) and MHD nonlinear stretching flow (Hayat, Sajjad, et al., 2017). Rahimi et al. (2017) applied collocation method towards a boundary layer flow of Eyring-Powell nanofluid over a linear stretching surface. Qayyum et al. (2017) described the nonlinear convective flow of Powell-Eyring nanofluid with enforced Newtonian heat and mass condition near the surface. Upadhay et al. (2017) addressed the heat and mass transfer flow of an unsteady Eyring-Powell dusty nanofluid by imposing a Cattaneo-Christove heat flux model. And recently, I. Khan et al. (2018) explored the flow of MHD mixed convection of Eyring-Powell nanofluid over an inclined surface with exponentially varying viscosity.

CHAPTER 3: MATHEMATICAL FORMULATION AND METHODOLOGY

3.1 Introduction

This chapter presented the governing equations and their boundary conditions. Specific terminologies and parameters that are used throughout the thesis will also be explained briefly. The methodology used for this study is presented including some information on the numerical tools used to solve the models.

3.2 Mathematical Formulation

3.2.1 Boundary Layer Flow

The fluid flow in physical domain is driven by various properties. In order to develop a mathematical model that can present the fluid characteristics, those properties have to be defined precisely as to provide transition between physical and numerical domain. In order to predict the evolution of a fluid field, a system of non-linear transport equations needs to be solved. The Navier-Stokes equation is a partial differential equation that is widely used to describes the flow of incompressible fluids. The equation is expressed based on the principle of conservation of mass, momentum and energy and can be extended with thermodynamical equations of state.

Following the discovery of nanofluid as the next possible heat transfer fluid, Buongiorno (2006) worked to develop an explanation for the observed abnormal convective heat transfer in nanofluids. The absolute velocity of the nanoparticles are viewed as the sum of the base fluid velocity and a relative (slip) velocity. He considered seven possible mechanisms that the nanoparticles can develop slip velocity with against the base fluid: inertia, Brownian diffusion, thermophoresis, diffusiophoresis, Magnus effect, fluid drainage and gravity settling. Out of the seven, he concluded that the only two important nanoparticle/base-fluid slip mechanisms are Brownian diffusion and thermophoresis. Brownian motion is the random motion of nanoparticles within the base fluid that happens due to continuous collisions between nanoparticles and molecules of the base fluid while thermophoresis is a phenomenon where particles diffuse under the effect of a temperature gradient.

Buongiorno (2006) then proceed to develop a transport model for the nanofluids by treating the nanofluid as a two-component mixture (base fluid + nanoparticles). Consider a steady boundary-layer flow of a nanofluid past a stretching surface which coincides with the plane $y = 0$ (Fig. 3.1). T and C represents the fluid temperature and the nanoparticle volume concentration. Temperature at the surface of the wall is defined as T_w while the ambient temperature and nanoparticle volume concentration are denoted by T_∞ and C_∞ respectively. Using the model of Buongiornos' and abiding the conservation of total mass, momentum, thermal energy and nanoparticles, Nield and Kuznetsov (2010) makes the standard boundary layer approximation based on scale analysis and wrote down the continuity, momentum, energy and nanoparticle volume fraction equation as below:

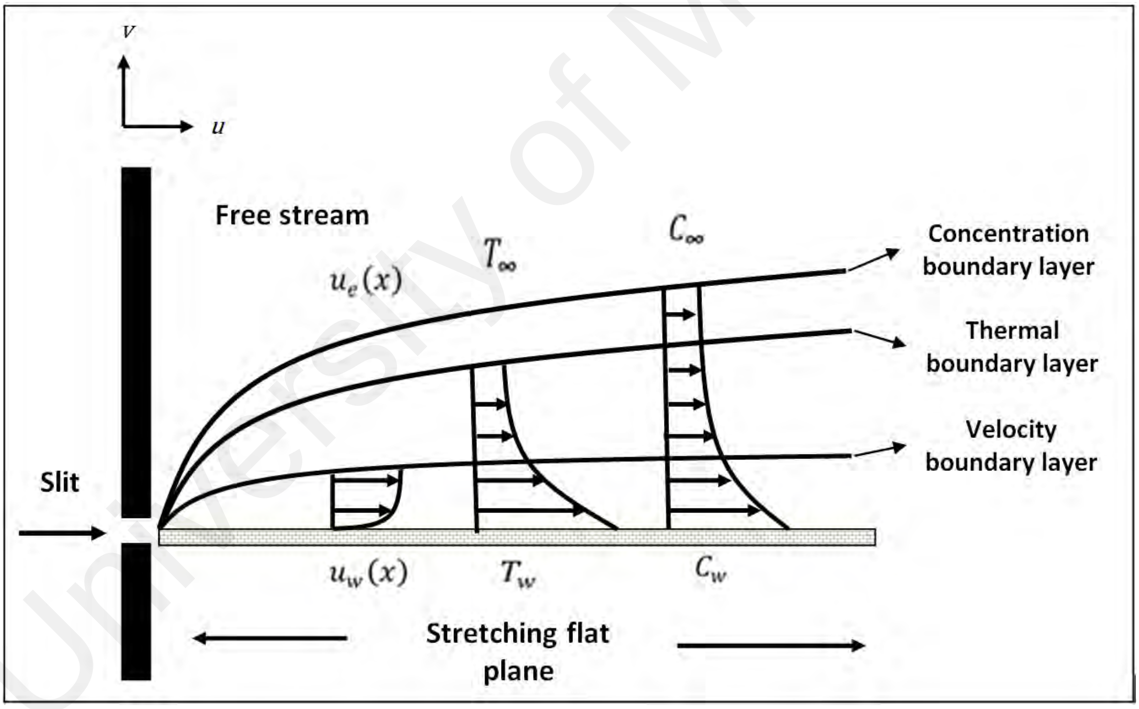

Figure 3.1: A boundary layer flow over a stretching flat plane.

3.2.1.1 Continuity equation

The continuity equation for nanofluid is written as:

$$\nabla.\boldsymbol{v} = 0 \tag{3.1}$$

where $\boldsymbol{v}$ is the nanofluid velocity. This equation is identical to the continuity equation for a pure incompressible fluid. In Cartesian coordinates:

$$\frac{\partial u}{\partial x} + \frac{\partial v}{\partial y} = 0, \tag{3.2}$$

where u, v are the velocity components in the x, y directions respectively.

3.2.1.2 Momentum equation

The nanofluid momentum equation is given as (Buongiorno, 2006; Bachok, Ishak, & Pop, 2010):

$$\rho\left(\frac{\partial \boldsymbol{v}}{\partial t} + \boldsymbol{v}.\nabla\boldsymbol{v}\right) = -\nabla P + \mu\nabla^2\boldsymbol{v} \tag{3.3}$$

where ρ is the density of the base fluid, t is time, P is pressure and μ is the dynamic viscosity. This equation is identical to the momentum equation for a pure fluid. In Cartesian coordinates:

$$u\frac{\partial u}{\partial x} + v\frac{\partial u}{\partial y} = \nu\left(\frac{\partial^2 u}{\partial x^2} + \frac{\partial^2 u}{\partial y^2}\right). \tag{3.4}$$

where ν is the kinematic viscosity.

3.2.1.3 Energy equation

The nanofluid energy equation is given as (Buongiorno, 2006; Bachok et al., 2010):

$$\rho c\left[\frac{\partial T}{\partial t}+\boldsymbol{v}.\nabla T\right]=\kappa\nabla^2 T+(\rho c)_p\left[D_B\nabla C.\nabla T+\left(\frac{D_T}{T_\infty}\right)\nabla T.\nabla T\right] \tag{3.5}$$

where T is the nanofluid temperature, κ is the thermal conductivity, $(\rho c)_p$ is the effective heat capacity of the nanoparticle material, D_B is the Brownian diffusion coefficient and D_T is the thermophoretic diffusion coefficient. The equation states that heat in nanofluid can be transported via convection, conduction and also by nanoparticle diffusion. The last two terms on the right-hand side represent the contribution associated with nanoparticle motion relative to the fluid. In Cartesian coordinates:

$$\begin{aligned}u\frac{\partial T}{\partial x}+v\frac{\partial T}{\partial y}=\mathring{\alpha}\left(\frac{\partial^2 T}{\partial x^2}+\frac{\partial^2 T}{\partial y^2}\right)+\tau D_B\left(\frac{\partial C}{\partial x}\frac{\partial T}{\partial x}+\frac{\partial C}{\partial y}\frac{\partial T}{\partial y}\right)\\+\frac{\tau D_T}{T_\infty}\left[\left(\frac{\partial T}{\partial x}\right)^2+\left(\frac{\partial T}{\partial y}\right)^2\right],\end{aligned} \tag{3.6}$$

where $\mathring{\alpha}$ is the thermal diffusivity of the fluid and τ is the ratio of effective heat capacity between the nanoparticles material and the fluid.

3.2.1.4 Mass transport equation

The nanoparticle continuity equation is given as (Buongiorno, 2006; Bachok et al., 2010):

$$\frac{\partial c}{\partial t}+\boldsymbol{v}.\nabla C=\nabla.\left[D_B\nabla C+\frac{D_T}{T_\infty}\nabla T\right] \tag{3.7}$$

where C is the nanoparticle volume concentration. The equation states that the nanoparticles can move homogenously within the fluid but also possesed a slip velocity relative to the fluid due to Brownian diffusion and thermophoresis. In Cartesian coordinates:

$$u\frac{\partial C}{\partial x}+v\frac{\partial C}{\partial y}=D_B\frac{\partial^2 C}{\partial y^2}+\frac{D_T}{T_\infty}\frac{\partial^2 T}{\partial y^2}. \tag{3.8}$$

3.2.2 Constitutive Equations for Non-Newtonian Fluids

The non-Newtonian fluids are characterized by their viscosity behaviors. These are represented by the constitutive equation that relates the stress to motion of the continuum. Different non-Newtonian fluids models can be distinguished via the momentum equation of each fluid.

3.2.2.1 Maxwell fluid

Maxwell fluid is a subclass of a rate-type fluid. The shear viscosity of a UCM fluid model is a constant which enables it to focus on the fluid elasticity effects towards the boundary layer characteristic. The model can predict the relaxation time effects. For an UCM model, the constitutive equation can be written as (Sadeghy, Najafi, & Saffaripour, 2005):

$$\tau_{ij}+k_1\frac{\delta}{\delta t}\tau_{ij}=2\mu_o d_{ij} \tag{3.9}$$

where μ_o is the zero-shear rate viscosity, k_1 is the relaxation time of the fluid and d_{ij} is the symmetric part of the velocity gradient tensor; that is:

$$d_{ij}=\frac{1}{2}\left(\frac{\partial u_i}{\partial x_j}+\frac{\partial u_j}{\partial x_i}\right). \tag{3.10}$$

Using the above equations, the momentum equation for UCM can be written as:

$$u\frac{\partial u}{\partial x}+v\frac{\partial u}{\partial y}=\nu\frac{\partial^2 u}{\partial y^2}-k_1\left(u^2\frac{\partial^2 u}{\partial x^2}+v^2\frac{\partial^2 u}{\partial y^2}+2uv\frac{\partial^2 u}{\partial x\partial y}\right) \tag{3.11}$$

where ν is the kinematic viscosity.

3.2.2.2 Williamson fluid

Depending on the molecular structure of the fluid, a real fluid has both minimum and maximum effective viscosities. Williamson fluid model takes into consideration of both viscosities. The constitutive equations of the Williamson fluid model are given as (Nadeem et al., 2013):

$$\begin{aligned} \mathbb{T} &= -P\boldsymbol{I} + \tau_{ij}, \\ \tau_{ij} &= \left[\mu_\infty + \frac{(\mu_o - \mu_\infty)}{1 - \Upsilon\dot{\gamma}}\right]\boldsymbol{A_1}, \end{aligned} \tag{3.12}$$

where $\mathbb{T}$ is the Cauchy stress tensor, P is the pressure, $\boldsymbol{I}$ is the identity vector, τ_{ij} is the extra stress tensor, μ_o is the limiting viscosity at zero shear rate, μ_∞ is the limiting viscosity at infinite shear rate, $\Upsilon > 0$ is the time constant, A_1 is the first Rivlin-Erickson tensor and $\dot{\gamma}$ is defined as:

$$\dot{\gamma} = \sqrt{\frac{1}{2}\Pi}, \qquad \Pi = \text{trace}(A_1^2). \tag{3.13}$$

Here Π is the second invariant of strain-rate tensor. Consider the case when $\mu_\infty = 0$ and $\Upsilon\dot{\gamma} < 1$, then we have:

$$\tau_{ij} = \mu_o\left[1 + \Upsilon\dot{\gamma}\right]A_1. \tag{3.14}$$

By using the above equations, the momentum equation for Williamson fluid can be written as follows:

$$u\frac{\partial u}{\partial x} + v\frac{\partial u}{\partial y} = \nu\frac{\partial^2 u}{\partial y^2} + \sqrt{2}\nu\Upsilon_x\frac{\partial u}{\partial y}\frac{\partial^2 u}{\partial y^2} \tag{3.15}$$

where ν is the kinematic viscosity and Υ_x is a local time constant.

3.2.2.3 Second grade fluid

Second grade fluid model is an example of a differential type fluids model that can be used to study the effect of shear thinning and shear thickening. Additionally, it is used to describe the normal stress effects especially in steady flows (Hayat et al., 2011). The constitutive equation for the Cauchy stress tensor $\mathbb{T}$ that describes the second-grade fluids is given by (Bariş, 2002):

$$\mathbb{T} = -PI + \mu \boldsymbol{A_1} + \alpha_1 \boldsymbol{A_2} + \alpha_2 \boldsymbol{A_1^2}, \tag{3.16}$$

where P is the pressure, I is the identity tensor, μ is the coefficient of viscosity, α_1, α_2 are the material modulli which also referred as the normal stress modulli and A_1, A_2 are the kinematical tensor of Rivlin-Ericksen defined as:

$$\begin{aligned} A_1 &= (\nabla v) + (\nabla v)^T, \\ A_2 &= \frac{dA_1}{dt} + (\nabla v) A_1 + (\nabla v)^T A_1. \end{aligned} \tag{3.17}$$

where v is the velocity vector and ∇ is the gradient operator. For a fluid modelled by (3.16) to be compatible with thermodynamics, it has to be characterized with following restrictions:

$$\mu \geq 0, \qquad \alpha_1 \geq 0, \qquad \alpha_1 + \alpha_2 = 0. \tag{3.18}$$

By using the above equations, the momentum equation for second-grade fluid can be written as follows:

$$u\frac{\partial u}{\partial x} + v\frac{\partial u}{\partial y} = \nu\frac{\partial^2 u}{\partial y^2} + \frac{\omega}{\rho}\left[u\frac{\partial^3 u}{\partial x \partial y^2} + \frac{\partial u}{\partial x}\frac{\partial^2 u}{\partial y^2} + v\frac{\partial^3 u}{\partial y^3} + \frac{\partial u}{\partial y}\frac{\partial^2 v}{\partial y^2}\right] \tag{3.19}$$

where ω is the material fluid parameter and ρ is the density.

3.2.2.4 Carreau fluid

Carreau rheological model is from the class of generalized Newtonian fluids. The model can predict the viscosity for low and high shear rates. The constitutive equation for a Carreau fluid is (Hayat, Asad, et al., 2014):

$$\tau_{ij} = \left[\mu_\infty + (\mu_o - \mu_\infty)(1 + (\Gamma\dot{\gamma})^2)^{\frac{n-1}{2}}\right]\dot{\gamma}, \tag{3.20}$$

where τ_{ij} is the extra stress tensor, μ_∞ is the infinity shear rate viscosity, μ_o is the zero shear rate viscosity, Γ is the material constant, n is the dimensionless power law index and $\dot{\gamma}$ is defined as

$$\dot{\gamma} = \sqrt{\frac{1}{2}\sum_i\sum_j \dot{\gamma}_{ij}\dot{\gamma}_{ji}} = \sqrt{\frac{1}{2}\Pi} \tag{3.21}$$

Here Π is the second invariant of strain-rate tensor. Consider the constitutive equation when $\mu_\infty = 0$, so (3.20) becomes:

$$\tau_{ij} = \left[\mu_o\left(1 + \Gamma\dot{\gamma})^2\right)^{\frac{n-1}{2}}\right]\dot{\gamma}. \tag{3.22}$$

By using (3.22), the momentum equation for Carreau fluid is as follows:

$$u\frac{\partial u}{\partial x} + v\frac{\partial u}{\partial y} = \nu\frac{\partial^2 u}{\partial y^2}\left[1 + \Gamma^2\left(\frac{\partial u}{\partial y}\right)^2\right]^{\frac{n-1}{2}} + \nu(n-1)\Gamma^2\frac{\partial^2 u}{\partial y^2}\left(\frac{\partial u}{\partial y}\right)^2\left[1 + \Gamma^2\left(\frac{\partial u}{\partial y}\right)^2\right]^{\frac{n-3}{2}} \tag{3.23}$$

where ν is the kinematic viscosity.

3.2.2.5 Powell-Eyring fluid

Powell-Eyring model is derived from kinetic theory of liquids. It reduced to Newtonian behaviour for low and high shear rates and is able to describes the shear thinning properties of fluids. A constitutive equation for a Powell-Eyring fluid is given by (Hayat, Farooq, Alsaedi, & Iqbal, 2013):

$$\tau_{ij} = \mu\frac{\partial u_i}{\partial x_j} + \frac{1}{\beta}\sinh^{-1}\left(\frac{1}{\grave{e}}\frac{\partial u_i}{\partial x_j}\right), \tag{3.24}$$

where μ is the viscosity coefficient, β and $\grave{e}$ are the fluid parameter for Powell-Eyring. Using

$$\sinh^{-1}\left(\frac{1}{\grave{e}}\frac{\partial u_i}{\partial x_j}\right) \cong \frac{1}{\grave{e}}\frac{\partial u_i}{\partial x_j} - \frac{1}{6}\left(\frac{1}{\grave{e}}\frac{\partial u_i}{\partial x_j}\right)^3, \qquad \left|\frac{1}{\grave{e}}\frac{\partial u_i}{\partial x_j}\right| \ll 1, \tag{3.25}$$

the momentum equation for Powell-Eyring can be written as:

$$u\frac{\partial u}{\partial x} + v\frac{\partial u}{\partial y} = \left(v + \frac{1}{\rho\beta\grave{e}}\right)\frac{\partial^2 u}{\partial y^2} - \frac{1}{2\rho\beta\grave{e}^3}\left(\frac{\partial u}{\partial y}\right)^2\frac{\partial^2 u}{\partial y^2} \tag{3.26}$$

where v is the kinematic viscosity and ρ is the density.

3.2.3 Stream Condition

A flow has many different properties such as density, viscosity, heat capacity, thermal conductivity and diffusion coefficients to name a few. Depending on the model and problem posed, the properties can be specified accordingly.

3.2.3.1 Classification of fluid flow

Fluid flow can be classified according to the following criteria (Hauke, 2008):

- **Stationary and non-stationary**

The flow is stationary when the fluid variables in the Eularian description do not depend on time. That is

$$\frac{\partial \cdot}{\partial t} = 0. \tag{3.27}$$

For a large, fixed control volume, it is possible that inflow and outflow conditions do not change with time. If the fluid properties inside the control volume are also independent of time, the flow is called a steady flow. When this is not the case, the flow is transient or unsteady. This is the situation when the flow is evolving from the initial state towards stationary solution. There are cases when the long-term solution is not steady but it repeats itself in time. This flow is called periodic.

- **Compressible and incompressible flow**

Incompressible flow assumed constant density. It satisfies

$$\nabla . \boldsymbol{v} = \text{div } \boldsymbol{v} = 0. \tag{3.28}$$

Compressible flows depends on the Mach number, Ma which is the ratio of local fluid velocity and local propagation speed of sound. The flow can be classified as subsonic, transonic or supersonic.

- **Dimensionality of flow field**

The dimensionality of a flow field is governed by the number of space dimensions needed to define the flow field completely. In one-dimensional flow, the flow variables can only vary in one direction. For example, a spherically symmetric flow. In a two-dimensional flow, the flow variables vary along the flow direction as well as across it. A plane flow is a two-dimensional flow with respect to Cartesian or polar coordinates. In three-dimensional flow, the flow variables will vary in all three directions.

- **Viscous and ideal flow**

  Flows where friction is taken into account are termed viscous flows. This friction between the layers of fluid that provides resistance to the motion is caused by a fluid property called viscosity, μ. When this fluid property is neglected ($\mu = 0$), the fluid motion will be frictionless and it is called ideal flows. For this type of fluid, the rest of the diffusion coefficients like thermal conductivity and mass diffusivity will also be neglected.

- **Laminar and turbulent**

  The flow is laminar when the motion of the fluid particles is well-organized, predictable and deterministic. A flow is called turbulent when it has random component and its flow is the sum of an average motion plus chaotic fluctuations due to the non-linearities of the transport equations.

3.2.3.2 Stagnation point flow

The structure of a boundary layer formed in a stagnation-point flow of an incompressible viscous fluid towards a stretching surface is found to depend on the ratio of the velocity of the stretching surface to the inviscid flow in the neighbourhood of the stagnation point (Mahapatra & Gupta, 2002).

The stagnation flow is represented by the term:

$$u_e \frac{du_e}{dx} \tag{3.29}$$

in the fluid momentum equation where u_e is the velocity distribution for the free stream, far away from the surface. The term signifies the fluid flow towards the vertical plate surface by the free stream normally (Hsiao, 2016).

3.2.3.3 Magnetohydrodynamic (MHD)

MHD flow past a flat surface has many applications in industry such as polymer technology and metallurgy where hydromagnetic techniques are used. In the case where the final product actually depends on the rate of cooling, an electrically conducting fluid subject to magnetic is very important. It can control the cooling rate thus helps in achieving the desired standard of the final product. The MHD term is represented by the term:

$$\frac{\sigma B^2}{\rho}u \tag{3.30}$$

where σ is the electrical conductivity, B is the uniform magnetic field and ρ is the fluid density. In an unsteady boundary layer flow, a time dependent magnetic field $B(t) = B_o/\sqrt{1 - bt}$ will be applied normally to the surface where B_o is the initial strength of magnetic field and b is a positive constant.

3.2.3.4 Thermal radiation

Thermal radiation is important in some applications because of the manner in which radiant emission depends on temperature. Radiation is intensified at high absolute temperature. The thermal radiation term is represented by the term:

$$\frac{1}{\rho c_p}\frac{\partial q_r}{\partial y} \tag{3.31}$$

where q_r is the radiative heat flux defined by Rosseland approximation (Haq et al., 2015):

$$q_r = -\frac{4\sigma^*}{4k^*}\frac{\partial T^4}{\partial y}, \tag{3.32}$$

where σ^* is the Stefan-Boltzmann constant and k^* is the Rosseland mean absorption coefficient. By describing T^4 as a linear function of temperature and expanding it in

Taylors series about the free stream temperature T_∞, we have $T^4 \cong 4T_\infty^3 T - 3T_\infty^4$. The radiative heat flux can now be expressed as

$$q_r = -\frac{16\sigma^*}{3k^*} T_\infty^3 \frac{\partial T}{\partial y} \tag{3.33}$$

3.2.3.5 Mixed convection

Mixed convection flow occurs when effects from forced convection and natural convection mechanism contributes significantly to heat transfer. According to Chen, Sparrow, and Mucoglu (1977), buoyancy forces that arise from temperature difference will instigate a longitudinal pressure gradient which changes the flow field and hence the heat transfer rate from the surface as well. The mixed convection term is represented by the term:

$$g\left[\beta_T(T - T_\infty) + \beta_C(C - C_\infty)\right] \tag{3.34}$$

where g is the acceleration due to gravity, β_T is the thermal expansion coefficient and β_C is the nanoparticle volumetric coefficient.

3.2.4 Initial and Boundary Conditions

When solving a mathematical model, initial and boundary conditions are a required component. For fluid flow model, appropriate initial conditions and boundary conditions are needed as they direct the motion of the flow. The initial conditions provide the initial state from which the flow evolves. The boundary conditions are values of flow properties or fluxes that must be provided on the surface of the control volume. Different types of boundary condition can be applied using different variables. There are many types of boundary conditions such as the boundary conditions for flow inlets and outlets that permit the flow to enter and exit the solution domain, wall boundaries condition that is used to bound fluid and solid regions, axis boundaries, porous media conditions and many others.

3.2.4.1 Velocity

For viscous flow, the velocity $\boldsymbol{v}$ of the fluid in contact with a wall equals the wall velocity $\boldsymbol{v}_w$. This is called the *no-slip* boundary condition (Smits, 2018). In this thesis, a steady boundary layer flow over a linearly stretching surface is considered.

$$\text{At} \quad y = 0: \qquad u = u_w(x) = cx, \qquad v = 0 \tag{3.35a}$$

$$\text{As} \quad y \to \infty: \qquad u = u_e(x) = ax. \tag{3.35b}$$

For the case where an unsteady boundary layer flow is studied, the velocity boundary condition is given as (Freidoonimehr, Rashidi, & Mahmud, 2015):

$$\text{At} \quad y = 0: \qquad u = u_w(x,t) = \frac{cx}{1-bt}, \qquad v = 0 \tag{3.36a}$$

$$\text{As} \quad y \to \infty: \qquad u = u_e(x,t) = \frac{ax}{1-bt} \tag{3.36b}$$

Here, u_w is the fluid velocity near the wall or the stretching surface velocity and u_e is the velocity outside the boundary layer or the free stream velocity. Flow of an incompressible viscous fluid over a stretching surface has an important bearing on technological processes. In processes like melt-spinning in extrusion of polymer, metals casting, fibres spinning and glass blowing, there are flows due to at least one stretching surface. In all these cases, the quality of final product depends on the rate of heat transfer at the stretching surface (Mahapatra & Gupta, 2002).

- **Stretching/shrinking surface**

Velocity boundary condition for a linearly stretching/shrinking surface is given as:

$$\text{At} \quad y = 0 : \qquad u = Su_w(x) = Scx \qquad , v = 0 \tag{3.37}$$

Here, S is the stretching parameter that determines the surface condition. For $S < 0$, it will be a shrinking surface and for $S > 0$, it will be a stretching surface (Pal, Mandal, & Vajravelu, 2014).

- **Slip boundary condition**

In general, the widely accepted boundary condition for a fluid over a solid surface is the no-slip condition. However, there is a large class of polymeric materials that slip or stick-slip on solid boundaries (Hayat, Khan, & Ayub, 2005). The slip velocity highly depends on the shear stress. The constitutive equations for slip developed are mostly depend mostly on shear stress but some do take into consideration the effect of normal stress too (Rao & Rajagopal, 1999). There is no one fixed term for the velocity slip. In this thesis, the hydrodynamic velocity slip is imposed on the Maxwell model and the term is as follows:

$$U_{slip} = \alpha_w \left[(1 + k_1 c) \frac{\partial u}{\partial y} \right], \tag{3.38}$$

where α_w is the dimensional slip coefficient and k_1 is the relaxation time of Maxwell fluid. The velocity boundary condition near the wall will then become:

$$\text{At} \quad y = 0 : \qquad u = u_w(x) = cx + U_{slip}, \qquad v = 0 \tag{3.39}$$

3.2.4.2 Temperature

For a steady boundary layer flow of an incompressible fluid, temperature T at the wall equals to the wall temperature T_w (Smits, 2018).

$$\text{At} \quad y = 0: \qquad T = T_w \tag{3.40}$$

In unsteady flow, the wall temperature boundary condition is given as (Freidoonimehr et al., 2015):

$$\text{At} \quad y = 0: \qquad T = T_w(x,t) = T_\infty + \frac{cx}{(1-bt)^2} \tag{3.41}$$

As the flow moves further away from the wall, the temperature will reach a uniform value:

$$\text{As} \quad y \to \infty: \qquad T = T_\infty \tag{3.42}$$

3.2.4.3 Nanoparticle volume concentration

- **Active control of nanoparticles**

  In most nanofluid literature, the nanoparticle volume fraction is assumed to be constant at the surface (actively controlled). Therefore, there exist a normal mass flux of nanoparticles at the surface with independent Sherwood number. However, there is no justification on how the concentration of nanoparticles can be controlled actively at the surface (Zargartalebi, Ghalambaz, Noghrehabadi, & Chamkha, 2015). The condition is represented as follows:

$$\text{At} \quad y = 0: \qquad C = C_w. \tag{3.43}$$

- **Passive control of nanoparticles**

  A new condition was introduced by Kuznetsov and Nield (2013) which stated that there is a zero normal mass flux of nanoparticles at the boundary. It started with the idea that one could control the value of nanoparticle volume fraction at the boundary in the same way as the temperature there could be controlled (Nield & Kuznetsov, 2009). However, the thoughts are difficult to apply in practice. Thus, in order to make the model physically more realistic, the boundary conditions are defined as follows:

  $$\text{At} \quad y = 0: \qquad D_B \frac{\partial C}{\partial y} + \frac{D_T}{T_\infty} \frac{\partial T}{\partial y} = 0 \tag{3.44}$$

  It is now assumed that the nanoparticle volume fraction is being controlled passively on the surface via temperature gradient. The condition may result in negative values of nanoparticles volume fraction at the surface when the thermophoresis effect is more dominant than the Brownian effect. Accordingly, as negative volume fraction of nanoparticles is physically not valid, it represents zero volume fraction of nanoparticles i.e zero mass flux near the surface (Zargartalebi et al., 2015).

As the flow moves further away from the wall, the nanoparticle volume concentration will reach a uniform value:

$$\text{As} \quad y \to \infty: \qquad C = C_\infty \tag{3.45}$$

3.2.4.4 Augmented boundary condition

The viscoelastic model is capable in exploring the shear thinning and shear thickening effects. It can also describe the normal stress effects especially in steady flows. However, its equation of motion is an order higher than the standard Navier-Stokes equation. This renders towards the boundary condition insufficiency in determining the complete solution. In order to overcome the difficulty caused by the paucity of the existing of boundary conditions, Garg and Rajagopal (1991) suggested to augment them on the basis of physically reasonable assumptions. This is possible in the case of flows with unbounded domains by using the fact that the solution must be bounded or the solution has a certain smoothness at infinity. The augmented condition is as follows:

$$\text{As} \quad y \to \infty : \qquad \frac{\partial u}{\partial y} \to 0 \tag{3.46}$$

3.2.5 Similarity Transformation

In certain flow problems, similarity transform may be applied to reduce the partial differential equations (PDEs) of Navier-Stokes equations to a set of nonlinear ordinary differential equations (ODEs). The most common one used in fluid mechanics is the scaling transformation. Prandtl found a similarity transformation for the two-dimensional incompressible laminar fluid flow by employing ad hoc methods (Pakdemirli & Yurusoy, 1998). Similarity transform reduces the number of independent variables of PDE and is only possible for problems with certain physical symmetries (C. Y. Wang, 2008). The similarity solutions describe fundamental physically significant problems and also serve as accuracy standards for full numerical solutions. The simplified ODEs made the original PDEs easier to be solved and reduce the computing time in the numerical analysis.

3.2.5.1 Non-dimensional variables

For a two-dimensional flow of an incompressible fluid, the velocity can be expressed in terms of another scalar function ψ, called the stream function that satisfies the continuity

Eqn. (3.2):

$$u = \frac{\partial \psi}{\partial y} \qquad \text{and} \qquad v = -\frac{\partial \psi}{\partial x} \tag{3.47}$$

To transform the partial differential equations (PDEs) into ordinary differential equations (ODEs), a set of non-dimensional variables are introduced:

- **Variables for a steady flow**:

$$\begin{aligned} &\text{The similarity variable:} && \eta = y\sqrt{\frac{c}{\nu}}, \\ &\text{The stream function:} && \psi = \sqrt{c\nu}\,x f(\eta), \\ &\text{The temperature function:} && \theta(\eta) = \frac{T - T_\infty}{T_w - T_\infty}, \\ &\text{The nanoparticle volume fraction function:} && \\ &\text{For passive control of } \phi : && \phi(\eta) = \frac{C - C_\infty}{C_\infty}, \\ &\text{For active control of } \phi : && \phi(\eta) = \frac{C - C_\infty}{C_w - C_\infty}. \end{aligned} \tag{3.48}$$

- **Variables for an unsteady flow**:

$$\begin{aligned} &\text{The similarity variable:} && \eta = \sqrt{\frac{c}{\nu(1 - bt)}}y, \\ &\text{The stream function:} && \psi = \sqrt{\frac{c\nu}{1 - bt}}x f(\eta), \\ &\text{The temperature function:} && \theta(\eta) = \frac{T - T_\infty}{T_w - T_\infty}, \\ &\text{The nanoparticle volume fraction function:} && \\ &\text{For passive control of } \phi : && \phi(\eta) = \frac{C - C_\infty}{C_\infty}, \\ &\text{For active control of } \phi : && \phi(\eta) = \frac{C - C_\infty}{C_w - C_\infty}. \end{aligned} \tag{3.49}$$

3.2.5.2 Dimensionless number

- **Dynamic viscosity,** μ

Dynamic viscosity is the proportionality constant between the viscous stress τ_{xy} and the velocity gradient.

$$\tau_{xy} = \mu \frac{du}{dy} \tag{3.50}$$

Its dimensions are $[\mu] = ML^{-1}T^{-1}$ and its units in the SI is PA s or kg/(ms).

- **Kinematic viscosity,** ν

The kinematic viscosity is the ratio

$$\nu = \frac{\mu}{\rho} \tag{3.51}$$

where μ is the dynamic viscosity and ρ is the density. Its dimensions are $[\nu] = L^2/T$.

- **Thermal conductivity,** κ

Thermal conductivity is the proportionality coefficient between the heat flux and the temperature gradient.

$$q_y = -\kappa \frac{\partial T}{\partial y} \tag{3.52}$$

Its units in the SI are $[\kappa] = W/(mK)$.

- **Thermal diffusivity,** $\mathring{\alpha}$

Its the ratio

$$\mathring{\alpha} = \frac{\kappa}{\rho c_p} \tag{3.53}$$

where κ is the thermal conductivity, ρ the fluid density and c_p the specific heat at constant pressure. Its dimensions are $[\mathring{\alpha}] = L^2/T$

- **Reynolds number,** *Re*

The Reynolds number comes from dividing the convective term by the viscous term, representing the ratio of inertial to viscous forces. In the study, the local Reynolds number is defined as:

$$Re = \frac{u_w(x)\cdot x}{\nu} \tag{3.54}$$

where $u_w(x)$ is the velocity function near the wall and ν is the kinematic viscosity. If $Re << 1$, the viscous forces (friction) are dominant and when $Re >> 1$, convection (inertial) forces are dominant.

- **Prandtl number,** Pr

Prandtl number is a ratio of viscous diffusion over thermal diffusion. It is defined as:

$$\mathrm{Pr} = \frac{\nu}{\mathring{\alpha}} \tag{3.55}$$

The number indicates the importance of momentum transport by diffusion as compared to heat transport by diffusion.

- **Lewis number,** *Le*

Lewis number is a ratio of thermal diffusion over mass diffusion. It is defined as:

$$Le = \frac{\mathring{\alpha}}{D_B} \tag{3.56}$$

where $\mathring{\alpha}$ is the thermal diffusivity and D_B is the Brownian diffusion coefficient.

- **Schmidt number,** *Sc*

Schmidt number is a ratio of viscous diffusion over mass diffusion. It is defined as:

$$Sc = \frac{\nu}{D_B} \tag{3.57}$$

where ν is the kinematic diffusivity and D_B is the Brownian diffusion coefficient.

- **Brownian motion parameter,** Nb

The Brownian motion parameter is given as:

$$
\begin{aligned}
\text{For passive control of } \phi: \qquad & Nb = \frac{\tau D_B C_\infty}{\nu}, \\
\text{For active control of } \phi: \qquad & Nb = \frac{\tau D_B \left(C_w - C_\infty\right)}{\nu}.
\end{aligned}
\tag{3.58}
$$

where $\tau = (\rho c)_p/(\rho c)_f$ is the effective heat capacity ratio of nanoparticles and the nanofluid and D_B is the diffusion coefficient.

- **Thermophoresis parameter,** Nt

The thermophoresis parameter is given as:

$$
Nt = \frac{\tau D_T \left(T_w - T_\infty\right)}{\nu T_\infty}. \tag{3.59}
$$

where $\tau = (\rho c)_p/(\rho_c)_f$ is the effective heat capacity ratio of nanoparticles and the nanofluid and D_T is the thermophoretic diffusion coefficient.

- **Heat capacity ratio,** N_c (Nadeem & Hussain, 2014a):

The heat capacity ratio is given as:

$$
N_c = \frac{(\rho c)_p}{(\rho c)_f} \left(C_w - C_\infty\right) = \frac{\text{nanoparticles heat capacity}}{\text{nanofluid heat capacity}}, \tag{3.60}
$$

- **Diffusivity ratio,** N_{bt} (Nadeem & Hussain, 2014a):

The diffusivity ratio is given as:

$$
N_{bt} = \frac{D_B T_\infty \left(C_w - C_\infty\right)}{D_T \left(T_w - T_\infty\right)} = \frac{\text{Brownian diffusivity}}{\text{Thermophoretic diffusivity}} \tag{3.61}
$$

- **Skin friction coefficient,** Cf_x

The local skin friction coefficient is given as:

$$Cf_x = \frac{\tau_w}{\rho u_w^2(x)}, \tag{3.62}$$

where ρ is the density and $u_w(x)$ is the velocity function near the wall. The wall shear stress, τ_w differs with each fluid and are defined accordingly with the specific fluid properties:

+ Maxwell fluid (Nadeem, Haq, & Khan, 2014):

$$\tau_w = \mu(1+K)\left(\frac{\partial u}{\partial y}\right)_{y=0} \tag{3.63}$$

where K is the elasticity parameter.

+ Williamson fluid (Nadeem & Hussain, 2014a):

$$\tau_w = \mu\left[\frac{\partial u}{\partial y} + \frac{\Upsilon_x}{\sqrt{2}}\left(\frac{\partial u}{\partial y}\right)^2\right]_{y=0}, \tag{3.64}$$

where Υ_x is the time constant.

+ Second-grade fluid (Hayat, Shafiq, et al., 2016):

$$\tau_w = \mu\left(\frac{\partial u}{\partial y}\right) + \alpha_1\left[u\frac{\partial^2 u}{\partial x \partial y} + v\frac{\partial^2 u}{\partial y^2} + 2\frac{\partial u}{\partial x}\frac{\partial u}{\partial y}\right]_{y=0} \tag{3.65}$$

where α_1 is the material fluid parameter for second-grade fluid.

+ Carreau fluid (M. Khan, Hashim, & Alshomrani, 2016):

$$\tau_w = \mu\frac{\partial u}{\partial y}\left[1+\Gamma^2\left(\frac{\partial u}{\partial y}\right)^2\right]_{y=0}^{\frac{n-1}{2}} \tag{3.66}$$

where Γ is the material constant for Carreau fluid and n is the power law index.

+ Powell-Eyring fluid (I. Khan et al., 2018):

$$\tau_w = \left[\left(\nu + \frac{1}{\rho\beta\grave{e}} \right) \frac{\partial u}{\partial y} - \frac{1}{6\beta\grave{e}^3} \left(\frac{\partial u}{\partial y} \right)^3 \right]_{y=0} \tag{3.67}$$

where β and $\grave{c}$ is the fluid parameter for Powell-Eyring and ρ is the density.

- **Nusselt number,** Nu_x

The wall heat transfer coefficient or the local Nusselt number is given as:

$$Nu_x = \frac{q_w x}{\kappa(T_w - T_\infty)} \tag{3.68}$$

where q_w is the surface heat flux and is defined by:

$$q_w = -\kappa \left(\frac{\partial T}{\partial y} \right)_{y=0} \tag{3.69}$$

- **Sherwood number,** Sh_x

The wall mass transfer coefficient or the local Sherwood number for actively controlled nanoparticle is given as:

$$Sh_x = -\frac{q_m x}{D_B(C_w - C_\infty)}. \tag{3.70}$$

where q_m is the surface mass flux and is defined by:

$$q_m = -D_B \left(\frac{\partial C}{\partial y} \right)_{y=0} \tag{3.71}$$

Sherwood number for passively controlled nanoparticle is not defined directly due to the assumption of zero normal mass wall flux.

3.3 Methodology

All boundary flow models of the non-Newtonian fluids proposed in this thesis are made of systems of non-linear partial differential equations (PDE). Using the non-dimensional variables introduced in subsection 2.5.5.1, the PDEs are reduced into ordinary differential equations (ODEs) by applying similarity transformation. The resulting ODEs are then solved using either $bvp4c$ function in MATLAB or $BVPh2.0$ package that utilized Mathematica.

3.4 Numerical Toolbox

3.4.1 MATLAB bvp4c

The function $bvp4c$ offered in MATLAB is used to solve boundary value problems for ordinary differential equations (ODEs). The numerical method of $bvp4c$ can be viewed as an implicit Runge-Kutta formula with a continuous extension. Its algorithm is a finite difference code that implements the three-stage Lobatto IIIa formula which is a collocation method (Kierzenka & Shampine, 2001). The solution provided is of fourth-order accuracy and it is uniformly distributed in the interval $[a, b]$ while the error control and mesh selection are based on the residual of the continuous solution. In $bvp4c$, the quality of the solution is heavily dependent on the initial guess. A bad initial guess may result in inaccurate solutions, or no solutions, or solutions that makes no sense (X. Wang, 2009).

In this thesis, the models of Maxwell, Williamson, Carreau and Powell-Eyring are solved using $bvp4c$. In the initialization process, all the global parameters need to be defined accordingly following each model. A suitable finite value of $\eta \to \infty$ is chosen and the relative error tolerance is set. The transformed ODEs are rewritten as a system of first order ODEs with its corresponding boundary conditions. Most of the time, the initial guesses with all zeroes are enough for the solution to converge. However, for the cases where the solution failed to met the relative error tolerance condition, the initial guesses can be improved using shooting method. The steps are summarized in a flow chart given in Figure 3.2. Further details and information on the method used in *bvp4c* can be read in the paper by Kierzenka and Shampine (2001).

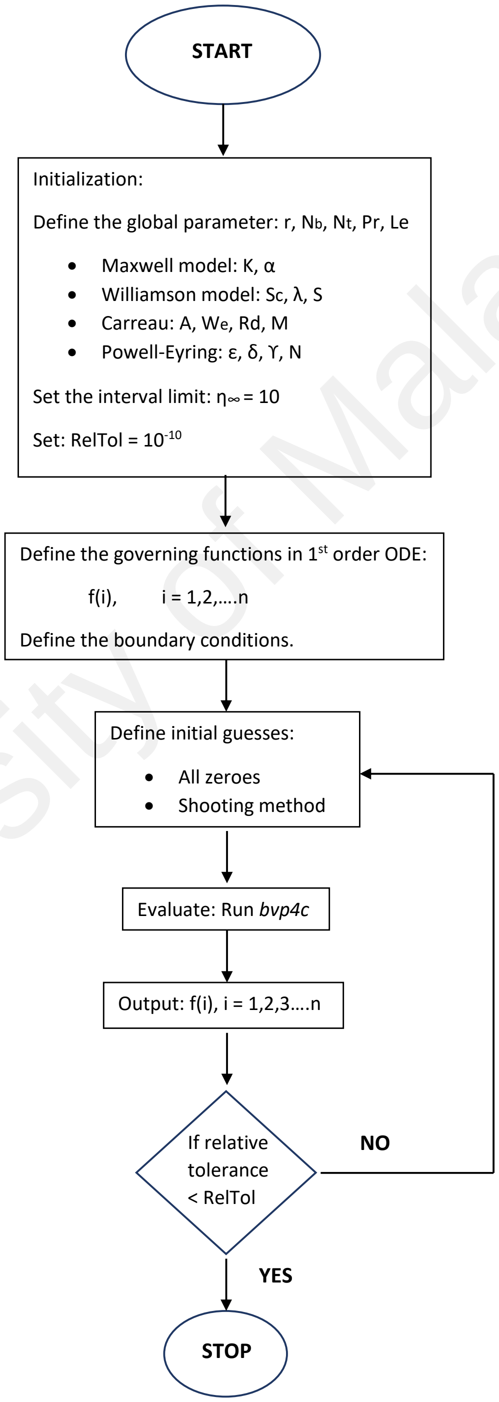

Figure 3.2: Flow chart for using MATLAB *bvp4c*.

3.4.2 Mathematica BVPh 2.0

The OHAM-based Mathematica package $BVPh2.0$ can deal with many systems of coupled ODEs defined in finite and/or semi-infinite intervals. It is an analytic tool for nonlinear boundary layer value and eigenvalue problems. Compared to $bvp4c$, it is based on the idea of "computing numerically with functions instead of numbers" (Zhao & Liao, 2013). According to Liao (2013), HAM has few advantages over the traditional non-perturbation methods:

- It is independent of any small/large physical parameters
- It provides great freedom and flexibility in choosing the equation type and solution expression of linear high-order approximation equations
- It provides a guarantee of the convergence of approximation series.

The model of second-grade nanofluid is solved using $BVPh2.0$. In the initialization step, the differential equations, boundary conditions, solution interval, initial guesses, auxiliary linear operator and the physical parameters are defined. Using $BVPh2.0$, the optimal values of the convergence-control parameters are then obtained together with the m^{-th} order of HAM approximation. Figure 3.3 shows the steps taken when using the $BVPh2.0$. The $BVPh2.0$ are available free on-line at $http://numericaltank.sjtu.edu.cn/BVPh2\_0.htm$.

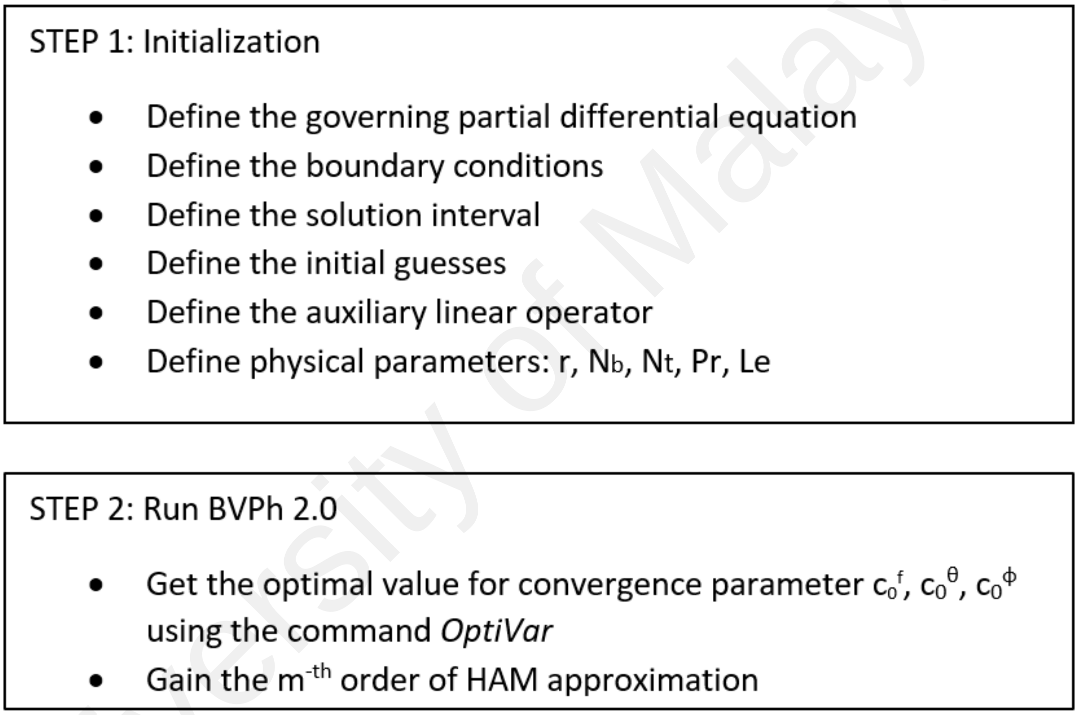

STEP 1: Initialization

- Define the governing partial differential equation
- Define the boundary conditions
- Define the solution interval
- Define the initial guesses
- Define the auxiliary linear operator
- Define physical parameters: r, N_b, N_t, Pr, Le

STEP 2: Run BVPh 2.0

- Get the optimal value for convergence parameter c_0^f, c_0^θ, c_0^ϕ using the command *OptiVar*
- Gain the m^{-th} order of HAM approximation

Figure 3.3: Flow chart for using MATHEMATICA *BVPh*2.0.

CHAPTER 4: ACTIVE AND PASSIVE CONTROLS OF NANOPARTICLES IN MAXWELL STAGNATION POINT FLOW OVER A SLIPPED STRETCHED SURFACE

4.1 Introduction

In this chapter, the model of a stagnation-point flow of Maxwell nanofluid is presented. The model included the effect of slip velocity by adding a hydrodynamic slip velocity in the initial condition and studied under active and passive control of nanoparticles. The work has been published in Meccanica (Halim, Haq, & Noor, 2017).

4.2 Problem Formulation

Consider a two-dimensional steady stagnation-point flow of an incompressible Maxwell fluid towards a horizontal linearly stretching sheet which coincides with the plane $y = 0$. The flow is assumed to be confined to $y > 0$ with the stretching velocity $u_w(x) = cx$ while the velocity external to the boundary layer flow is $u_e(x) = ax$ where a and c are positive constants. Temperature at the surface of the wall is defined as T_w. Nanoparticle volume concentration takes the value C_w at the surface for actively controlled mass flux while the ambient temperature and concentration are denoted by T_∞ and C_∞ respectively. The nanoparticle volume fraction for passively controlled mass flux is defined separately by the temperature gradient resulting with zero normal flux of nanoparticles. By mean of the above said assumptions, the problem can be formulate using the continuity equation (3.2), energy equation (3.6) and nanoparticle volume concentration equation (3.8) with the momentum equation given as:

$$u\frac{\partial u}{\partial x} + v\frac{\partial u}{\partial y} = u_e\frac{du_e}{dx} + \nu\frac{\partial^2 u}{\partial y^2} - k_1\left(u^2\frac{\partial^2 u}{\partial x^2} + v^2\frac{\partial^2 u}{\partial y^2} + 2uv\frac{\partial^2 u}{\partial x\partial y}\right), \tag{4.1}$$

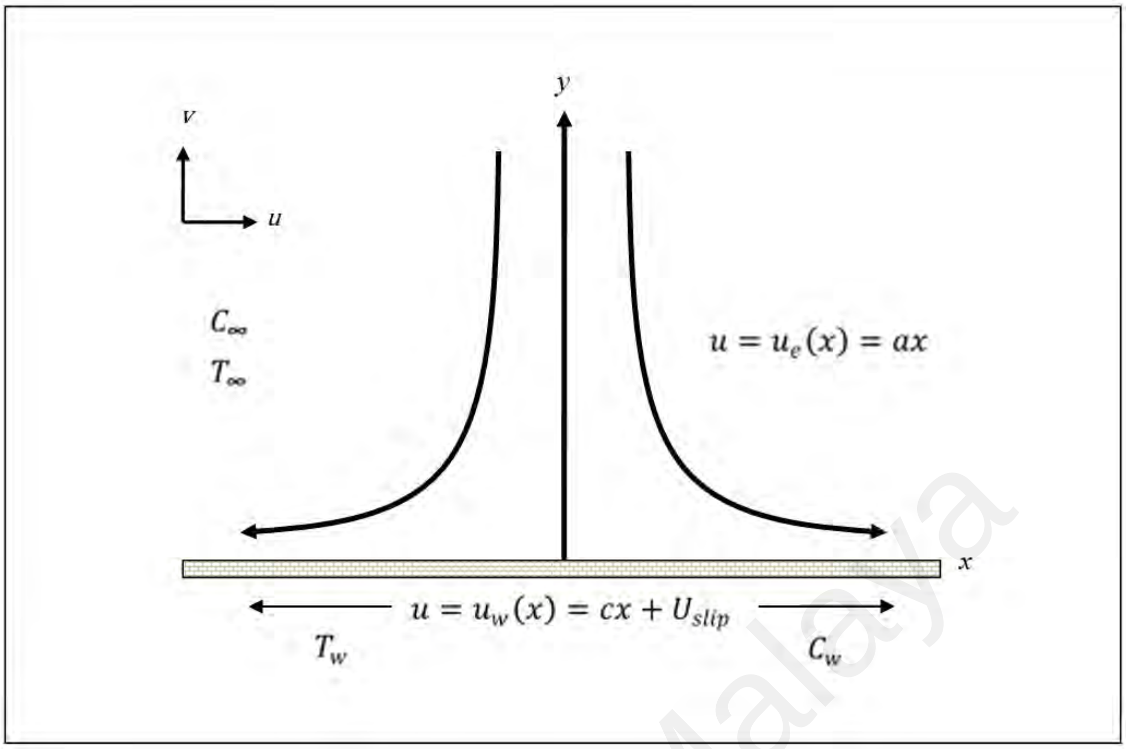

Figure 4.1: Geometry of the flow in Cartesian coordinate.

subject to velocity boundary condition (3.35b, 3.39), temperature boundary condition (3.40, 3.42) and the active and passive control of nanoparticle condition (3.43, 3.44). In the equation, u and v are the velocity components in the x, y directions respectively, ν is the kinematic viscosity and k_1 is the relaxation time of the UCM fluid. By using the set of non-dimensional variables for steady flow (3.48), the above model can then be transformed into a simplified non-linear ordinary differential equation below:

$$\begin{aligned}
&f''' - (f')^2 + ff'' + r^2 + K(2ff'f'' - f^2f''') = 0,\\
&\theta'' + \Pr\left[f\theta' + Nb\,\theta'\phi' + Nt(\theta')^2\right] = 0,\\
&\phi'' + Le\Pr f\phi' + \frac{Nt}{Nb}\theta'' = 0,
\end{aligned} \tag{4.2}$$

subject to the corresponding boundary conditions

$$
\begin{aligned}
& f(0)=0, \qquad f'(0)=1+\alpha(1+K)f''(0), \qquad \theta(0)=1, \qquad \phi(0)=1,\\
& \qquad \begin{cases} Nb\phi'(0)+Nt\,\theta'(0)=0, & \text{(passive control of } \phi)\\[2ex] \phi(0)=1, & \text{(active control of } \phi) \end{cases}\\
& f(\infty)=0, \quad f\,'(\infty)=r, \qquad \theta(\infty)=0, \qquad \phi(\infty)=0.
\end{aligned}
\tag{4.3}
$$

where primes denote differentiation with respect to η. Here, $r = a/c$ is the stagnation parameter, $K = k_1 c$ is the elasticity parameter, Pr is the Prandtl number, Le is the Lewis number and $\alpha = \alpha_w\sqrt{c/\nu}$ denotes the slip coefficient. The parameters of Brownian motion, Nb and thermophoresis, Nt are defined as in (3.58, 3.59).

The physical quantities of interest are the local skin friction coefficient (3.62), the wall heat transfer coefficient or the local Nusselt number (3.68) and the wall deposition flux or the local Sherwood number (3.70). These expressions can be reduced into the dimensionless form below:

$$
\begin{aligned}
& Cf_x Re_x^{1/2} = (1+K)f''(0),\\
& Nu_x Re_x^{-1/2} = -\theta'(0),\\
& \qquad \begin{cases} Sh_x Re_x^{-1/2} = -\phi'(0), & \text{for active control of } \phi\\[2ex] Sh_x Re_x^{-1/2} = \frac{Nt}{Nb}\theta'(0), & \text{for passive control of } \phi \end{cases}
\end{aligned}
\tag{4.4}
$$

Following the classical shooting technique, the system of nonlinear differential equations

(4.2) and (4.3) are first converted into the first-order system as below:

$$\begin{aligned} x_3' &= \frac{1}{Kx_1^2 - 1}\left[x_1x_3 + 2Kx_1x_2x_3 - x_2^2 + r^2\right], \\ x_5' &= -\Pr\left[x_1x_5 + Nb\, x_5x_7 + Nt\, x_5^2\right], \\ x_7' &= -Le\Pr x_1x_7 - \frac{Nt}{Nb}x_5', \end{aligned} \tag{4.5}$$

subject to the boundary conditions

$$\begin{aligned} & x_1(0) = 0, \qquad x_2(0) = 1 + \alpha(1+K)x_3(0), \qquad x_4(0) = 1, \\ & \begin{cases} Nbx_7(0) + Ntx_5(0) = 0, & \text{(for passive control of } \phi\text{)} \\ x_6(0) = 1, & \text{(for active control of } \phi\text{)} \end{cases} \\ & x_2(\infty) = r, \qquad x_4(\infty) = 0, \qquad x_6(\infty) = 0, \end{aligned} \tag{4.6}$$

where

$$\begin{aligned} & x_1 = f, \qquad x_2 = x_1' = f', \qquad x_3 = x_2' = f'', \\ & x_4 = \theta, \qquad x_5 = x_4' = \theta', \\ & x_6 = \phi, \qquad x_7 = x_6' = \phi'. \end{aligned} \tag{4.7}$$

Solving the above system of first order ordinary differential equations required initial guesses that could satisfy the boundary conditions. Since the values $x_3(0) = z_1$, $x_4(0) = z_2$ and $x_6(0) = z_3$ are not given initially, therefore all these missing conditions can be determined using shooting method. In this case, setting the initial values to zeroes are enough for the *bvp4c* function to solve the problem within the required error tolerance which has been set to 10^{-10}.

Table 4.1: Comparison of the numerical values for the reduced Nusselt number when $K = 0, Le = 1$ and $Nb = Nt = 0$.

Pr	r	Nu_x	
		Mustafa et al. (2011)	**Present Work**
1.0	0.1	0.602156	0.602157
	0.2	0.624467	0.624469
	0.5	0.692460	0.692449
1.5	0.1	0.776802	0.776801
	0.2	0.797122	0.797122
	0.5	0.864771	0.864794

Table 4.2: Comparison of the numerical values for the reduced Nusselt number, and the reduced Sherwood number in the absence of elasticity and stagnation parameter when $K = r = 0, \mathrm{Pr} = 10, Le = 1, Nb = 0.1$ and Nt is varied.

Nt	**Nadeem, Haq, and Khan (2014)**		**Present Work**	
	Nu_x	Sh_x	Nu_x	Sh_x
0.1	0.9524	2.1294	0.9524	2.1294
0.2	0.6932	2.2732	0.6932	2.2740
0.3	0.5201	2.5286	0.5201	2.5286
0.4	0.4026	2.7952	0.4026	2.7952
0.5	0.3211	3.0351	0.3211	3.0351

4.3 Results and Discussion

To ensure accuracy in our computation, present results are compared with the published results as presented in Table 4.1 to Table 4.3. In Table 4.1, values for reduced Nusselt number for various values of Pr and r are compared with the results published by Mustafa et al. (2011) who employed HAM. Table 4.2 shows the comparison of the numerical values for the reduced Nusselt number and the reduced Sherwood number in the absence of elasticity and stagnation parameters as obtained by Nadeem, Haq, and Khan (2014) using Runge-Kutta-Fehlberg method. Present results for the reduced Nusselt number when Pr is varied as compared with the results by W. A. Khan and Pop (2010) who used implicit finite-difference method is presented in Table 4.3. From these comparison tables, it can be verified that all present results are in good agreement with existing studies.

Analysis has been made to see the influence of various emerging parameters such

Table 4.3: Comparison of results for the reduced Nusselt number $-\theta'(0)$ when $Le = 1, Nb = Nt = K = 0, r = 1$ and Pr is varied.

Pr	**Nu_x**	
	W. A. Khan and Pop (2010)	**Present Work**
0.70	0.4539	0.4544
2.00	0.9113	0.9114
7.00	1.8954	1.8954
20.00	3.3539	3.3539
70.00	6.4621	6.4622

as stagnation parameter r, elasticity parameter K, Lewis number Le, slip parameter α, Brownian motion parameter Nb and thermophoresis parameter Nt in both active and passive control environments. The results of this analysis are presented in Fig. 4.2 to Fig. 4.10. On the other hand, the numerical values of reduced skin friction coefficient, $Re_x^{1/2}Cf_x$, reduced Nusselt number, $Re_x^{1/2}Nu_x$ and reduced Sherwood number, $Re_x^{1/2}Sh_x$ for different values of K, r, α, Le, Nb and Nt are also listed in Table 4.4 and Table 4.5 for both active and passive controls on mass transfer.

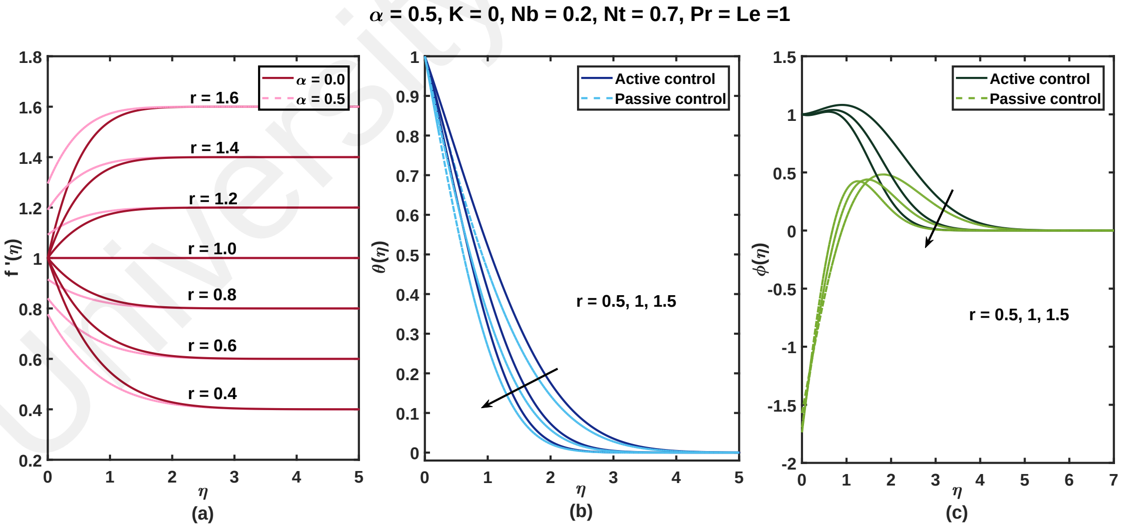

Figure 4.2: Velocity, temperature and nanoparticle volume fraction profiles for both active and passive controls when the stagnation parameter r varies with $\Pr = 1, Le = 1, K = 0, Nb = 0.2, Nt = 0.7, \alpha = 0.5$.

The effects of stagnation parameter r to the flow are depicted in Fig. 4.2. The stagnation parameter tends to increase the distributions of velocity and nanoparticle volume fraction

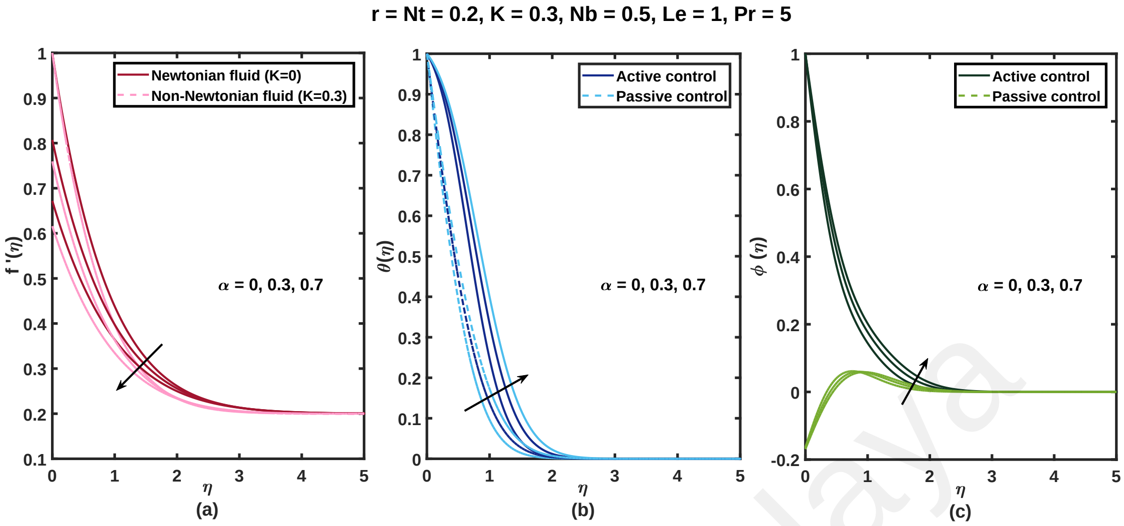

Figure 4.3: Velocity, temperature and nanoparticle volume fraction profiles for both active and passive controls when the slip parameter α varies with $\Pr = 5, Le = 1, K = 0.3, Nb = 0.5, Nt = 0.2, r = 0.2$.

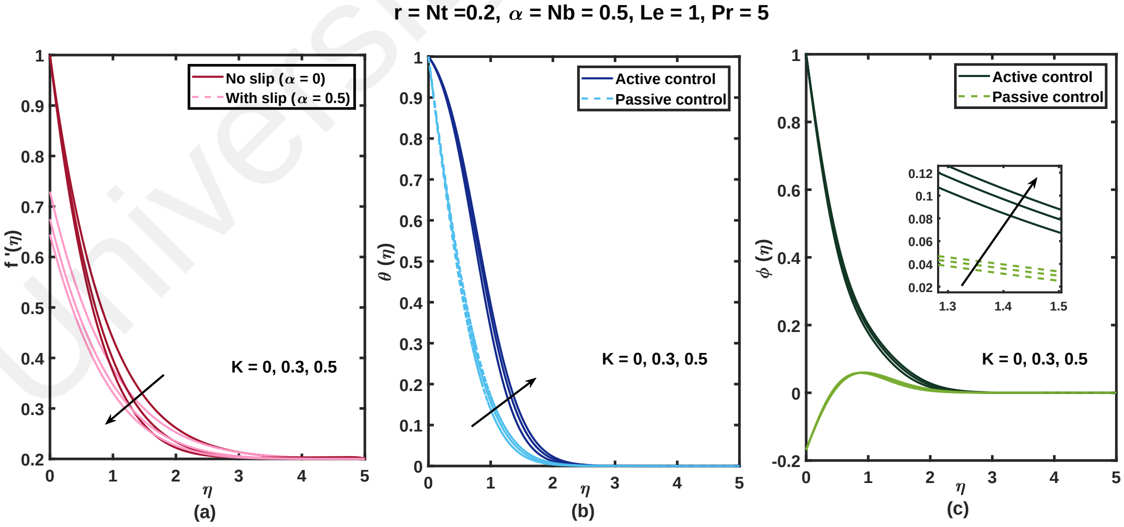

Figure 4.4: Velocity, temperature and nanoparticle volume fraction profiles for both active and passive controls when the elasticity parameter K varies with $\Pr = 5, Le = 1, \alpha = 0.5, Nb = 0.5, Nt = 0.2, r = 0.2$

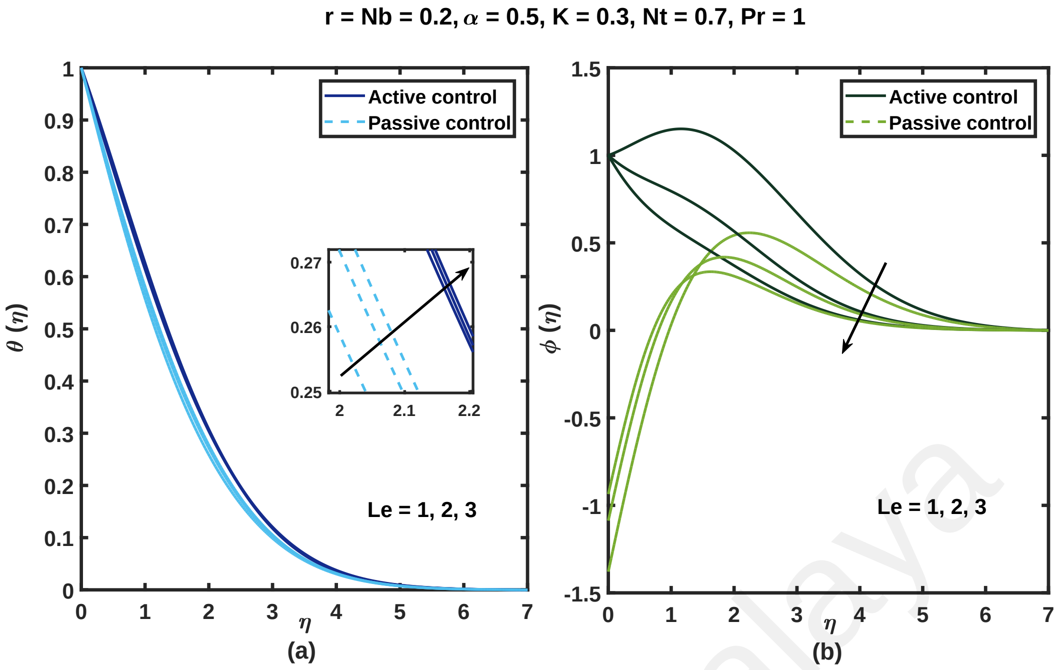

Figure 4.5: Temperature and nanoparticle volume fraction profiles for both active and passive controls when the Lewis number Le varies with $\Pr = 5, \alpha = 1, K = 0.2, Nb = 0.1, Nt = 0.7, r = 0.3$

for passive control while opposite behaviors are observed for the temperature and active controlled nanoparticle volume fraction profiles. It is also found that the presence of slip parameter α promotes acceleration for $r > 1.0$ and deceleration for $r < 1.0$ in the flow movement. Based on Fig. 4.3 and Fig. 4.4, the slip parameter α and elasticity parameter K have the same effect on velocity and temperature. Velocity is a decreasing function while temperature is an increasing function of α and K. Increasing value of both parameter α and K gives the effect of increasing friction in the fluid. Because of the friction, the velocity will decrease and subsequently temperature will arise as heat is being retained in the flow longer instead of being transported to the surroundings. As for the nanoparticle volume fraction in the active control, $\phi(\eta)$ will increase with increasing α and K.

From Fig. 4.5, it can be seen that Lewis number has an increasing effect towards temperature. However, the effect in active control is very minimal if compared relatively towards the effect in passive control. Le depends on the value of thermal diffusivity and

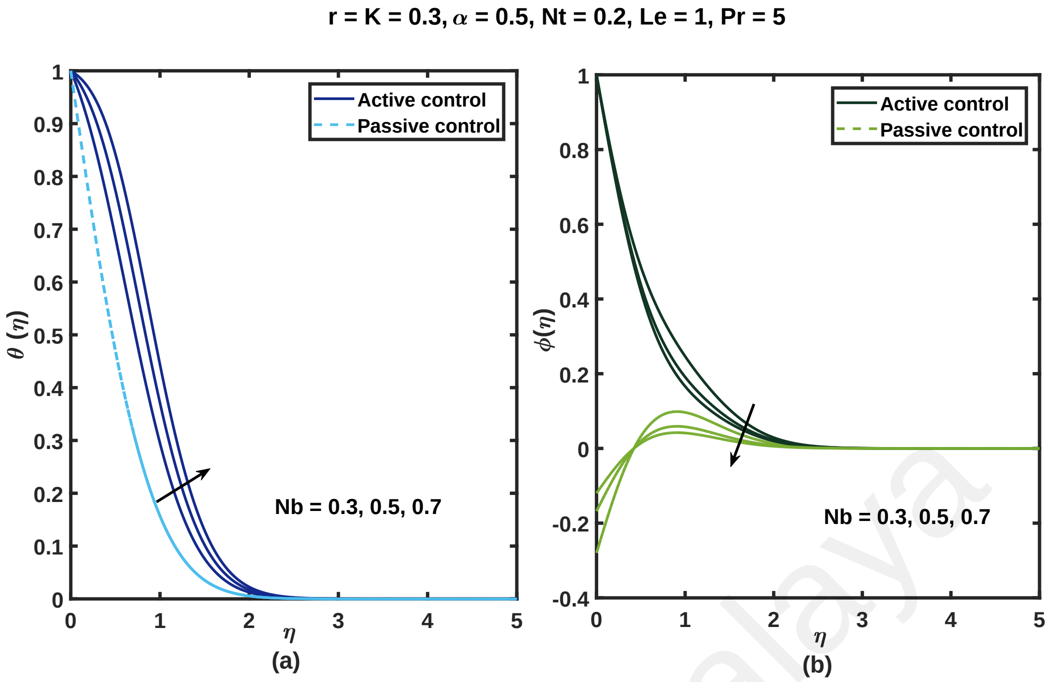

Figure 4.6: Temperature and nanoparticle volume fraction profiles for both active and passive controls when the Brownian parameter Nb varies with $\Pr = 5, \alpha = 0.5, K = 0.3, Le = 2, Nt = 0.1, r = 0.2$.

Brownian diffusion parameter. Because of the zero flux condition in passive control, value of Brownian diffusion coefficient is kept at minimum and thermal diffusivity becomes the major contributor towards value of Le. Hence, higher value of Le means higher thermal diffusivity which is a cause of increasing temperature. Nanoparticle volume fraction however, reacts in the opposite manner. Increasing Le will decrease value of $\phi(\eta)$ in active control.

In Fig. 4.6 and Fig. 4.7, influences of nanoparticles towards temperature and nanoparticle volume fraction are observed. Increasing the value of Brownian motion parameter and thermophoresis parameter will result in increasing temperature. Increasing Nb means more frequent collisions where heat absorbed from the collisions causes the temperature to rise. Frequent collisions indicate that the displacements between nanoparticles are reduced hence the decrement of volume fraction occurs. When the passive mass flux condition is applied, it can be observed that Nb has almost a negligible effect on temperature making

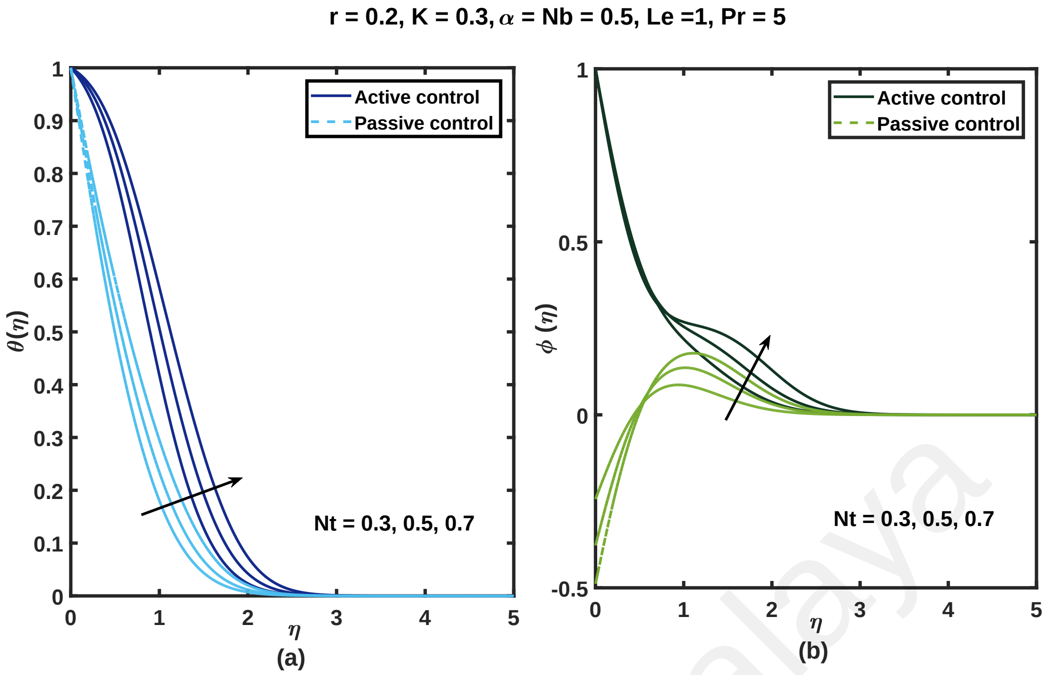

Figure 4.7: Temperature and nanoparticle volume fraction profiles for both active and passive controls when the thermophoresis parameter Nt varies with $Pr = 5, \alpha = 0.5, K = 0.3, Le = 2, Nb = 0.4, r = 0.2$.

the effect of Nt is more significant in temperature increment. Higher Nt means a higher temperature gradient and due to the increasing temperature difference, the nanoparticles are more dispersed in order to escape to a cooler environment hence increasing the nanoparticle volume fraction in the process. In passive control, $\phi(\eta)$ shows flipping behavior but in opposite manner towards Nb and Nt. For Nb, $\phi(\eta)$ increases with increasing value of Nb near the wall surface but it starts to flip to decrease as it moves away farther from the wall. The same behavior of $\phi(\eta)$ can be seen in respond to increasing r and Le in Fig. 4.2(c) and Fig. 4.5(b). As for Nt, $\phi(\eta)$ decreases near the wall before it flips to increase the same way it reacts to α in Fig. 4.4(c). It can be seen in Fig. 4.2 to Fig. 4.7 that the variable $\phi(\eta)$ overshoots and attains negative values in the neighbourhood of the surface. This behavior illustrates that the nanoparticle flux at the surface is being suppressed due to passive control of mass transfer (Ishfaq et al., 2016). Note also that the temperature for passive control model is always lower than the temperature in active control model.

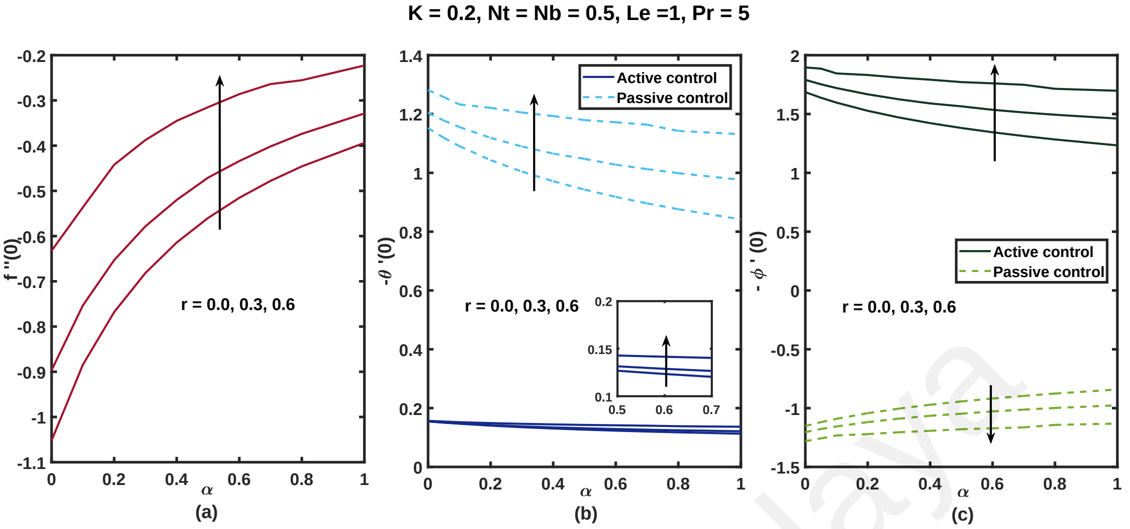

Figure 4.8: Variation of reduced skin friction coefficient, reduced Nusselt number and reduced Sherwood number profiles against slip parameter, α when the stagnation parameter, r varies with $\mathrm{Pr} = 5, K = 0.2, Le = 1, Nb = 0.5, Nt = 0.5$.

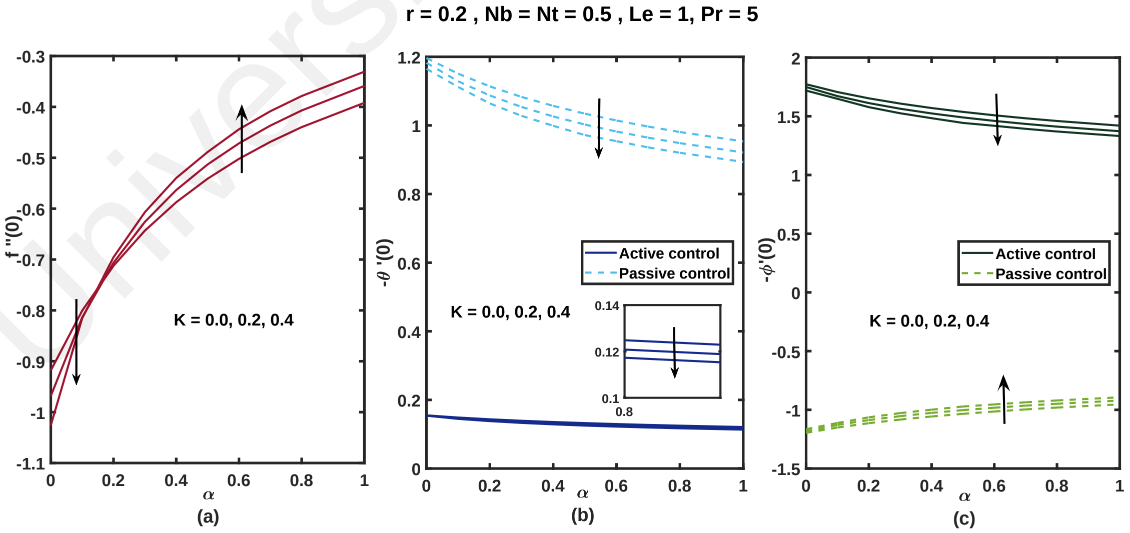

Figure 4.9: Variation of reduced skin friction coefficient, reduced Nusselt number and reduced Sherwood number profiles against slip parameter α when the elasticity parameter, K varies with $\mathrm{Pr} = 5, r = 0.2, Le = 1, Nb = 0.5, Nt = 0.5$.

Figure 4.8 and Fig. 4.9 show the influence of different values of r and K towards reduced skin friction coefficient, reduced Nusselt number $Re_x^{-1/2}Cf_x$ and reduced Sherwood number $Re_x^{-1/2}Nu_x$ with increasing value of slip velocity parameter. It is found that the reduced skin friction and reduced Nusselt number behave oppositely towards α. With increasing α, skin friction will increase while the heat flux rate will decrease. As for reduced Sherwood number, it will decrease in active control but increases in passive control. It seems that the stagnation parameter is an increasing function of $Re_x^{-1/2}Cf_x$, $Re_x^{-1/2}Nu_x$ and active control of $Re_x^{-1/2}Sh_x$. The elasticity parameter however is affected by the value of α in its outcome towards skin friction. When α is small (< 0.25), skin friction is decreasing with increasing K before it flips to increase. Meanwhile, the Nusselt number decreases when K increases suggested that the heat transfer performance of Newtonian fluid when $K = 0$ in Fig. 4.9 is better than the non-Newtonian Maxwell fluid. Furthermore, mass flux decreases in active control but increases in passive control with increasing value of K.

Figure 4.10 and Fig. 4.11 demonstrate the effects of different values of Nt towards heat and mass fluxes with increasing K and Nb. $Re_x^{-1/2}Nu_x$ is a decreasing function of both Nb and Nt. With increasing value of K, $Re_x^{-1/2}Sh_x$ is an increasing function of Nt in active control but a decreasing function of Nt in passive control. However, with increasing Nb, the reduced Sherwood number is an increasing function of Nt in both active and passive control.

Table 4.4 and Table 4.5 list the values of reduced skin friction, reduced Nusselt number and reduced Sherwood number for different parameters. It is observed that the values of $Re_x^{-1/2}Sh_x$ in passive controls are all negative. The mass is being transferred to surroundings due to the zero mass flux condition at the surface that prevents nanoparticle deposition. Increasing values of both parameter K and α will decrease the magnitude of the physical quantities. A slight fluctuation of value on the reduced Sherwood number

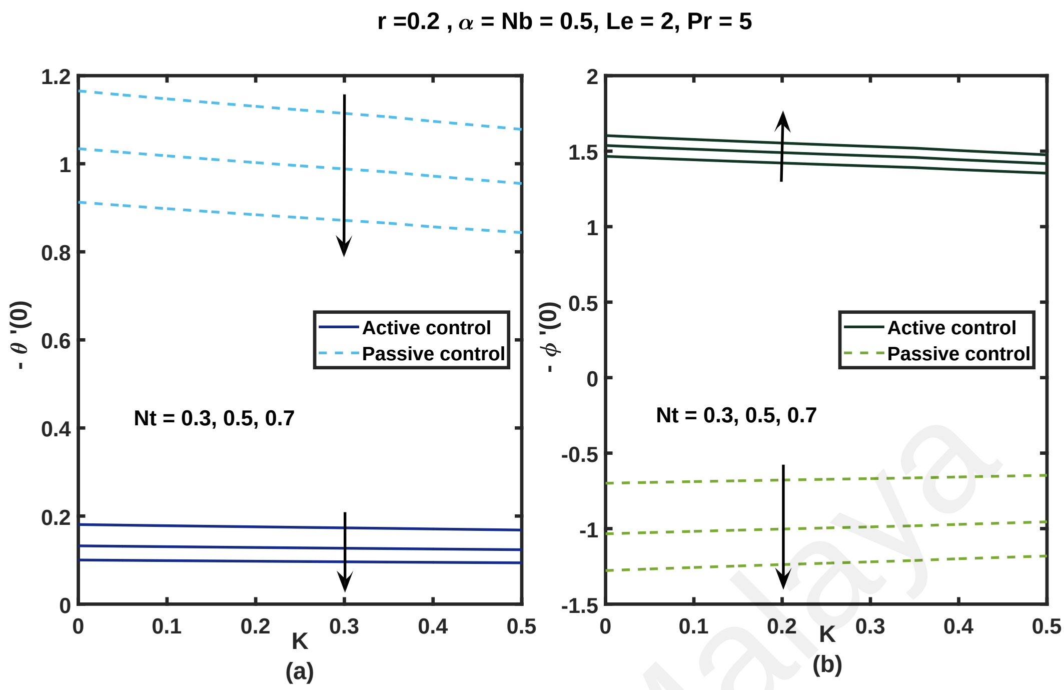

Figure 4.10: Variation of reduced Nusselt number and reduced Sherwood number profiles against elasticity parameter K when the thermophoresis parameter, Nt varies with $\Pr = 5, r = 0.2, Le = 2, Nb = 0.5, \alpha = 0.5$.

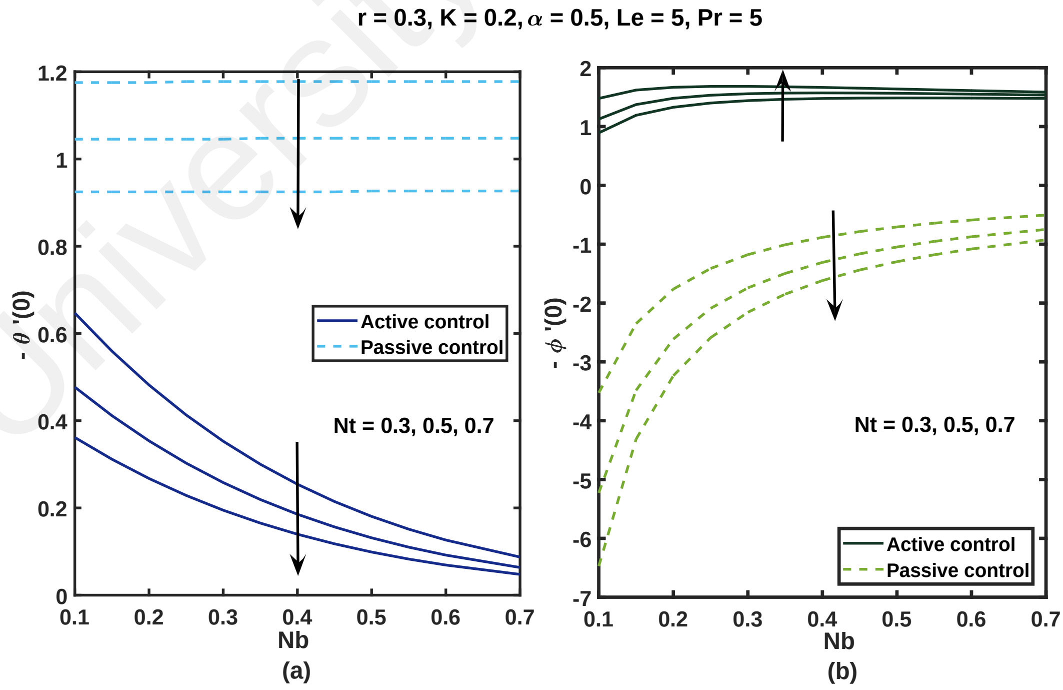

Figure 4.11: Variation of reduced Nusselt number and reduced Sherwood number profiles against Brownian parameter Nb when the thermophoresis parameter, Nt varies with $\Pr = 5, r = 0.3, Le = 5, K = 0.2, \alpha = 0.5$.

Table 4.4: Values of $f''(0), -\theta'(0)$ and $-\phi'(0)$ for both active and passive control when $\Pr = 5.0, Le = 1.0$ and $Nb = Nt = 0.5$.

K	r	α	$Re_x^{-1/2}Cf_x$	$Re_x^{-1/2}Nu_x$		$Re_x^{-1/2}Sh_x$	
				active	**passive**	**active**	**passive**
0.1	0.2	0.5	-0.52698	0.13044	1.01791	1.51306	-1.01791
0.3			-0.49839	0.12695	0.99024	1.47276	-0.99024
0.5			-0.47782	0.12357	0.95643	1.41977	-0.95643
0.3	0.05		-0.53882	0.12489	0.93625	1.37584	-0.93625
	0.1		-0.52889	0.12519	0.95067	1.40305	-0.95067
	0.2		-0.49839	0.12695	0.99024	1.47276	-0.99024
0.3	0.2	0.1	-0.81574	0.14572	1.11980	1.65935	-1.11980
		0.5	-0.49839	0.12695	0.99024	1.47276	-0.99024
		0.9	-0.36588	0.11699	0.92125	1.37304	-0.92125

Table 4.5: Values of $-\theta'(0)$ and $-\phi'(0)$ for both active and passive control when $K = 0.3, \alpha = 0.5, r = 0.2$ and $\Pr = 5.0$.

Le	Nb	Nt	$Re_x^{-1/2}Nu_x$		$Re_x^{-1/2}Sh_x$	
			active	**passive**	**active**	**passive**
0.1	0.5	0.5	0.54145	1.26549	0.01058	-1.26549
0.5			0.19732	1.10965	0.96423	-1.10965
1.0			0.12695	0.99024	1.47276	-0.99024
2.0			0.08863	0.86291	2.12723	-0.86291
1.0	0.3		0.24901	0.99024	1.45159	-1.65041
	0.5		0.12695	0.99024	1.47276	-0.99024
	0.7		0.06136	0.99024	1.44965	-0.70732
	0.9		0.02838	0.99024	1.42375	-0.55014
1.0	0.5	0.3	0.17333	1.11641	1.40432	-0.66984
		0.5	0.12695	0.99024	1.47276	-0.99024
		0.7	0.09608	0.87336	1.53586	-1.22270
		0.9	0.07499	0.76822	1.59081	-1.38280

for active control of nanoparticles is observed when value of Brownian parameter Nb is increasing. Meanwhile, magnitude of the reduced Nusselt number in passive control remains stagnant even though the value of Brownian parameter Nb is increased. This pattern can be explained by the zero mass flux condition at the surface. It can also be suggested that with the absence of nanoparticles, there is no Brownian motion.

4.4 Concluding Remarks

The problem of a two-dimensional steady viscous flow of an incompressible Maxwell fluid saturated with nanoparticles near a stagnation point over a slipped stretching surface is introduced. A hydrodynamic slip velocity is proposed as a partial expression in the general surface stretching velocity. The active control condition of nanoparticles is combined together with a realistic passive boundary condition to assume zero nanoparticles flux at the surface while taking into account the effects of both Brownian motion and thermophoresis. The model is further solved numerically using a classical shooting technique with Newton's method by utilizing MATLAB $bvp4c$ function. The effects of active and passive controls of nanoparticles with emerging parameters are sketched and tabulated accordingly. The main results of the present analysis are listed below:

- Temperature and nanoparticle volume fraction are decreasing functions of stagnation flow parameter.
- Temperature distribution in passive control model is lower than the active control model.
- Both temperature and nanoparticle volume fraction show identical behavior in reaction to increasing non-Newtonian elasticity parameter and hydrodynamic slip parameter.
- The reduced skin friction coefficient, heat transfer rate and mass transfer rate decrease as the slip parameter increases.
- The Brownian motion parameter has negligible effect on the reduced heat transfer rate when nanoparticles are passively controlled at the surface.
- Increasing value of Brownian motion and thermophoresis parameter causes the heat transfer rate of the fluid to decline.
- The heat transfer performance of Newtonian fluid (in the absence of elasticity

parameter) is better than the non-Newtonian Maxwell fluid.

- The stagnation parameter contributes towards better heat transfer performance for both active and passive controls on normal mass flux.
- The heat transfer rate under passive control recorded a much higher reading compared to those under active control.

CHAPTER 5: ACTIVE AND PASSIVE CONTROLS OF THE WILLIAMSON STAGNATION NANOFLUID FLOW OVER A STRETCHING/SHRINKING SURFACE

5.1 Introduction

This chapter presented the model of a stagnation-point flow of a Williamson nanofluid. It covers both stretching and shrinking surface and is studied under both active and passive control of nanoparticles. The work has been published in Neural Computing and Applications (Halim, Sivasankaran, & Noor, 2017)

5.2 Problem Formulation

Consider a two-dimensional steady stagnation-point flow of an incompressible Williamson nanofluid towards a horizontal linearly stretching/shrinking sheet which coincides with the plane $y = 0$. The flow is assumed to be confined to $y > 0$ with stretching/shrinking velocity $u_w(x) = \pm cx$ while the ambient fluid is moving with a velocity $u_e(x) = ax$, where a and c are positive constants. It is also assumed that the stretching/shrinking surface has constant value of temperature defined as T_w. Nanoparticle volume fraction takes the value C_w at the surface for actively controlled mass flux while the ambient temperature and concentration are denoted by T_∞ and C_∞. The nanoparticle volume fraction for passively controlled mass flux is defined separately by the temperature gradient resulting with zero nanoparticles normal flux. The above problem can be formulate using the continuity equation (3.2), energy equation (3.6) and nanoparticle volume concentration equation (3.8) with the momentum equation given as (Nadeem & Hussain, 2014a):

$$u\frac{\partial u}{\partial x} + v\frac{\partial u}{\partial y} = u_e\frac{du_e}{dx} + \nu\frac{\partial^2 u}{\partial y^2} + \sqrt{2}\nu\Upsilon_0\frac{\partial u}{\partial y}\frac{\partial^2 u}{\partial y^2}, \tag{5.1}$$

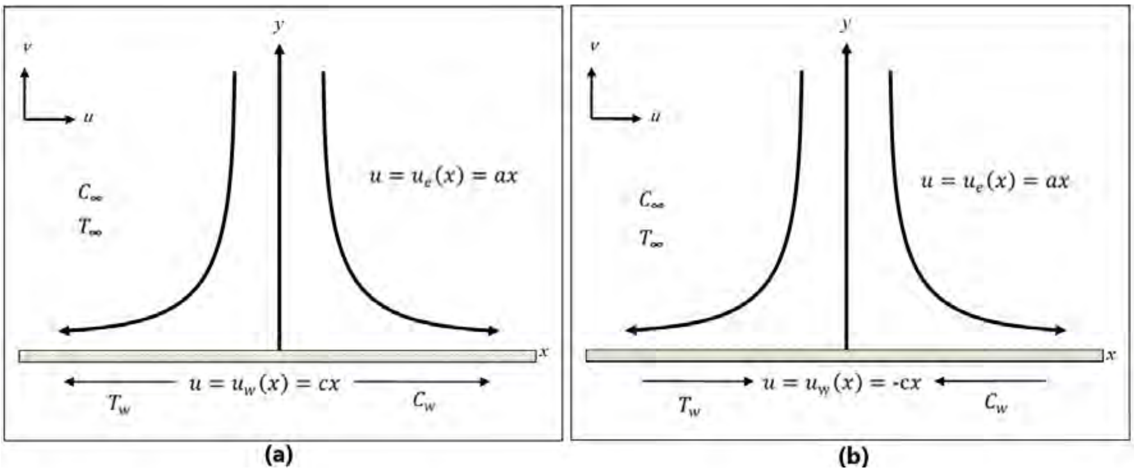

Figure 5.1: Geometry of the flow over a) stretching surface and b) shrinking surface in Cartesian coordinate.

subject to velocity boundary condition (3.37, 3.39), temperature boundary condition (3.40, 3.42) and the active and passive control of nanoparticle condition (3.43, 3.44). In the momentum equation above, u and v are the velocity components in the x, y directions respectively, ν is the kinematic viscosity, $\Upsilon_x = \Upsilon/x > 0$ is a local time constant and $x \neq 0$. Applying the set of non-dimensional variables for steady flow (3.48), the above model can then be transformed into a simplified non-linear ordinary differential equation below:

$$\begin{aligned}
&f''' - (f')^2 + ff'' + r^2 + \lambda f'' f''' = 0,\\
&\theta'' + \Pr f\theta' + \frac{N_c}{Le}\theta'\phi' + \frac{N_c}{LeN_{bt}}(\theta')^2 = 0,\\
&\phi'' + Scf\phi' + \frac{1}{N_{bt}}\theta'' = 0,
\end{aligned} \tag{5.2}$$

subject to the corresponding boundary conditions:

$$
\begin{aligned}
& f(0)=0, \qquad f'(0)=S, \qquad \theta(0)=1,\\
& \qquad \begin{cases} N_c\,\phi'(0)+\frac{N_c}{N_{bt}}\,\theta'(0)=0, & \text{for passive control of } \phi,\\[2ex] \phi(0)=1, & \text{for active control of } \phi,\end{cases} \qquad (5.3)\\
& f'(\infty)=r, \qquad \theta(\infty)=0, \qquad \phi(\infty)=0,
\end{aligned}
$$

where primes denote differentiation with respect to η. Here, $r = a/c$ is the stagnation parameter, S is the stretching/shrinking parameter that can take a positive value for a stretching sheet or a negative value for a shrinking sheet, Pr is the Prandtl number, Le is the Lewis number, Sc is the Schmidt number, N_c is the heat capacity ratio (3.60) and N_{bt} is the diffusivity ratio (3.61). The following non-dimensional parameter are introduced by Nadeem and Hussain (2014a):

$$\lambda = \Upsilon\sqrt{\frac{2c^3}{\nu}}, \qquad (5.4)$$

where λ is the non-Newtonian Williamson parameter. It is important to note that we have redefined the Williamson parameter λ by introducing the term $\Upsilon_x = \Upsilon/x > 0$ (refer (5.1)) to eliminate the x.

The physical quantities of interest are the local skin friction coefficient (3.62), the wall heat transfer coefficient or the local Nusselt number (3.68) and the wall deposition flux or the local Sherwood number (3.70). These expressions can be reduced into the dimensionless form below:

$$
\begin{aligned}
&Cf_x Re_x^{1/2} = f''(0) + \frac{\lambda}{2} f''(0)^2,\\
&Nu_x Re_x^{-1/2} = -\theta'(0),\\
&\begin{cases}
Sh_x Re_x^{-1/2} = -\phi'(0), & \text{for active control of } \phi\\[2ex]
Sh_x Re_x^{-1/2} = \frac{Nt}{Nb}\theta'(0), & \text{for passive control of } \phi
\end{cases}
\end{aligned}
\tag{5.5}
$$

where Re_x stands for local Reynolds number.

To solve the model, the system of differential equations (5.2) are first converted into a first-order system as below:

$$
\begin{aligned}
{x_3}' &= \frac{1}{1+\lambda x_3}\left[{x_2}^2 - x_1 x_3 - r^2\right],\\
{x_5}' &= -\left[\Pr x_1 x_5 + \frac{N_c}{Le}\left(x_5 x_7 + \frac{1}{N_{bt}}{x_5}^2\right)\right],\\
{x_7}' &= -\left[Sc x_1 x_7 - \frac{1}{N_{bt}}{x_5}'\right],
\end{aligned}
\tag{5.6}
$$

subject to boundary conditions:

$$
\begin{aligned}
&x_1(0) = 0, \qquad x_2(0) = S, \qquad x_4(0) = 1,\\
&\begin{cases}
N_c\, x_7(0) + \frac{N_c}{N_{bt}}\, x_5(0) = 0, & \text{for passive control of } \phi\\[2ex]
x_6(0) = 1, & \text{for active control of } \phi
\end{cases}\\
&x_2(\infty) = r, \qquad , x_4(\infty) = 0, \qquad x_6(\infty) = 0.
\end{aligned}
\tag{5.7}
$$

The desired solution for the system of ordinary differential equations (5.6) requires an initial guess that should satisfy the boundary conditions (5.7). Determining an initial guess for the solution using *bvp4c* is not difficult as for this specific problem, the solution will converge to the first solution even with poor guesses. The mesh selection and error control are based on the residual of the continuous solution. The relative error tolerance has been set to 10^{-10} and a suitable finite value of $\eta \rightarrow \infty$ are chosen as $\eta = \eta_\infty = 10$. Unless otherwise specified, the parameter values used throughout this chapter are as follows: $r = 1, Pr = 10, N_{bt} = 2, N_c = 0.5, Le = 4, \lambda = 0.2, Sc = 2$ and $S = 1$.

5.3 Results and Discussion

To ensure the accuracy of our results, comparisons between present and available published results are presented in Table 5.1 to Table 5.3. Table 5.1 shows the comparison of results of $f''(0)$ for various values of r obtained by Ishak et al. (2007) using Keller-box method and Mustafa et al. (2011) who used the homotopy analysis method (HAM). In Table 5.2 and Table 5.3, values for skin friction coefficient $f''(0)$, reduced Nusselt number, $-\theta'(0)$ and reduced Sherwood number, $-\phi'(0)$ for different parameters are compared with the results published by Mustafa et al. (2011) and Nadeem and Hussain (2014a) using HAM. From the comparison tables, it can be seen that all the results are in a very good agreement.

Table 5.1: Comparison of results of $f''(0)$ for various values of r when $Le = \mathrm{Pr} = N_{bt} = N_c = Sc = \lambda = 0$.

$r = a/c$	$f''(0)$		
	Ishak et al. (2007)	**Mustafa et al. (2011)**	**Present Work**
0.01	0.9980	0.99823	0.99803
0.10	0.9694	0.96954	0.96939
0.20	0.9181	0.91813	0.91811
0.50	0.6673	0.66735	0.66726
2.00	2.0175	2.01767	2.01750
3.00	4.7294	4.72964	4.72928

Computations have been made to see the influence of various emerging parameters such as stagnation parameter r, shrinking/stretching parameter S, the Lewis number Le, the Prandtl number Pr, the Schmidt number Sc, the diffusivity ratio N_{bt} and the heat capacity ratio, N_c under both active and passive control environments. The results are presented

Table 5.2: Comparison of results for the physical quantity of interest when $\Pr = N_c = 0.5, Sc = N_{bt} = 2, r = 0, Le = 4, Sc = 2, \lambda = 0.2$.

	$Cf_xRe_x^{1/2}$	$Nu_xRe_x^{-1/2}$	$Sh_xRe_x^{-1/2}$
Nadeem and Hussain (2014a) (30th HAM approx.)	1.076	0.308	0.824
Present Work	1.076	0.311	0.825

Table 5.3: Comparison of results for the physical quantity of interest when $Le = \Pr = N_{bt} = Sc = 1, N_c = 0.2, r = 0.1, \lambda = 0$.

	$Cf_xRe_x^{1/2}$	$Nu_xRe_x^{-1/2}$	$Sh_xRe_x^{-1/2}$
Mustafa et al. (2011) (40th HAM approx.)	0.969386	0.555204	0.257129
Present Work	0.969386	0.511275	0.293838

in Fig. 5.2 to Fig. 5.10. Numerical values of reduced skin friction coefficient $Re_x^{1/2}C_f$, reduced Nusselt number $Re_x^{1/2}Nu_x$ and reduced Sherwood number $Re_x^{1/2}Sh_x$ for various parameters are tabulated for both active and passive controls of mass transfer.

Figure 5.2 and Fig. 5.3 show the effects of stagnation parameter r towards velocity, temperature and nanoparticle volume fraction profiles. The stagnation parameter is the ratio of the free stream rate, a over the stretching/shrinking rate, c. It is observed that velocity increases as r increases. Oppositely, it turns out that both temperature and nanoparticle volume fraction are decreasing functions of r in both active and passive controls. As the external velocity increases, heat is dispersed more quickly to the surrounding hence reducing the fluid temperature. The stronger external stream also causes the nanoparticle concentration to thin out and reduced the volume fraction.

In Fig. 5.4, effect of the stretching/shrinking parameter S is observed. The negative value of S represents a shrinking surface while the positive value of S represents a stretching surface. Increasing the values of S will results in increasing velocity. Although temperature behaves similarly as a decreasing function of S in both active and passive controls, the nanoparticle volume fractions react in the opposite manner in both cases. In active control,

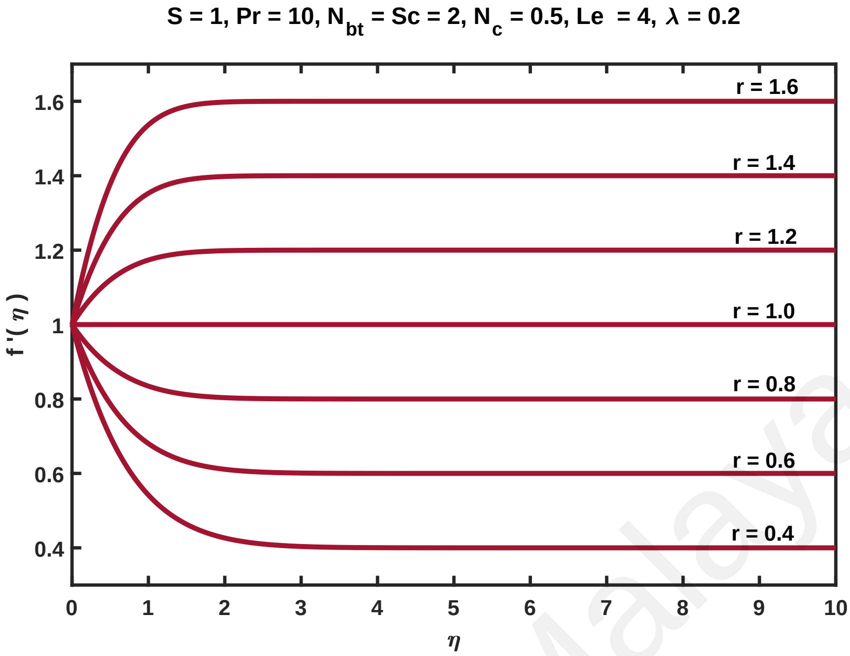

Figure 5.2: Velocity profiles for different values of the stagnation parameter r.

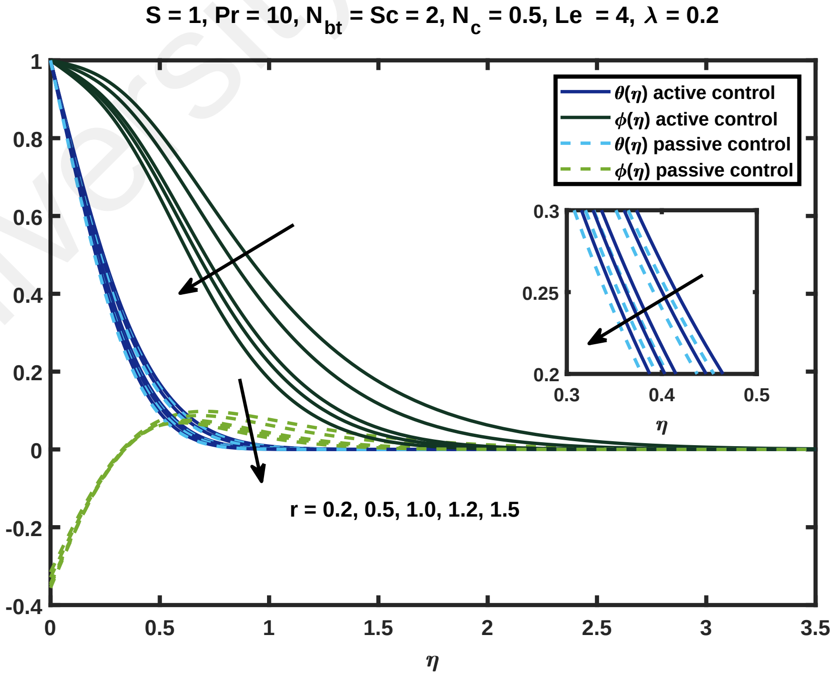

Figure 5.3: Temperature and nanoparticle volume fraction profiles for both active and passive controls for different stagnation parameter r.

$\phi(\eta)$ decreases as S increases and in passive control, $\phi(\eta)$ increases with S.

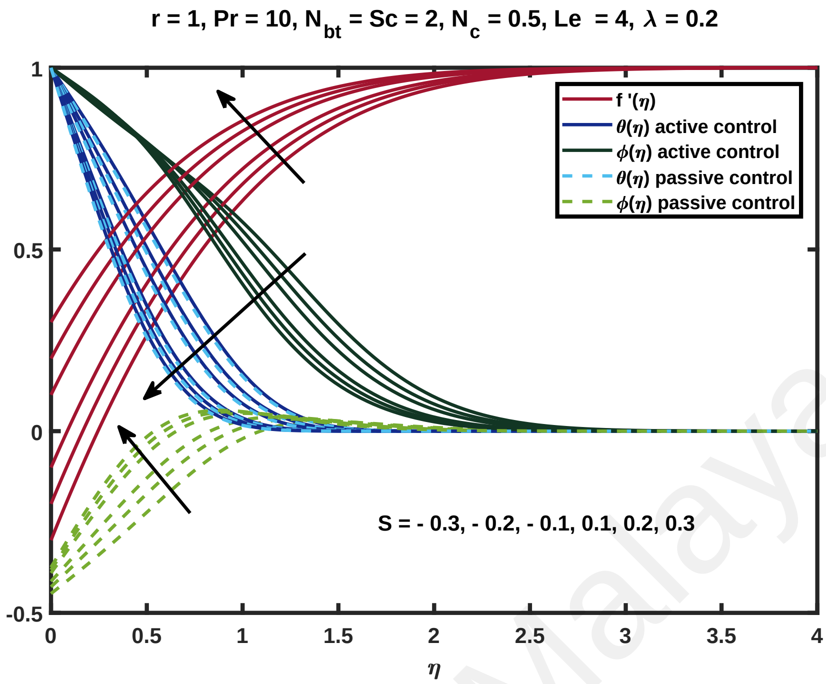

Figure 5.4: Velocity, temperature and nanoparticle volume fraction profiles for both active and passive controls for different stretching/shrinking parameter, S.

The effects of varied Prandtl number towards temperature and nanoparticle volume fraction are displayed in Fig. 5.5. Temperature is a decreasing function of Pr in both active and passive controls environment. Nanoparticle volume fraction seems to be quite sensitive with Prandtl number. It appears that for each Pr value the trend for ϕ flips to opposite direction at different critical points, from decreasing to increasing manner in active control and vice versa in passive control respectively.

Referring to Fig. 5.6 and Fig. 5.7, Sc and N_{bt} show the same effects towards temperature and nanoparticle volume fraction. They have almost negligible effects on temperature in both active and passive controls. $\phi(\eta)$ is a decreasing function for active control and it overshoots when Sc and N_{bt} values are less than 0.8. When the Brownian diffusivity is stronger ($Sc < 1$), the nanoparticles are spread out more due to frequent collisions between the particles and hence increasing the nanoparticles volume fraction. Thermophoresis

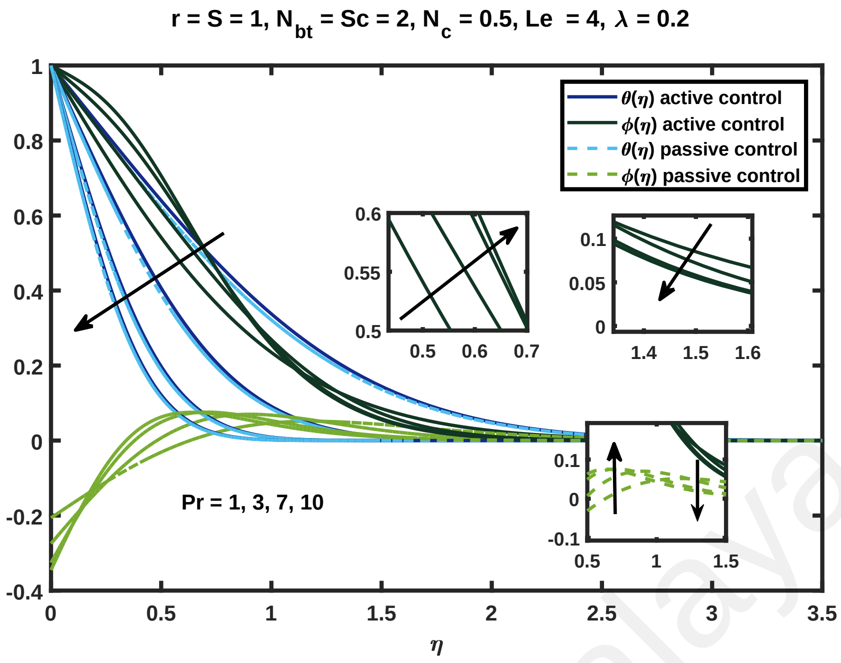

Figure 5.5: Temperature and nanoparticle volume fraction profiles for both active and passive controls for different Prandtl number, Pr.

controls the migration of nanoparticles that arises due to temperature difference. With higher temperature gradient, the nanoparticles are dispersed more while increasing the volume fraction. In passive control, $\phi(\eta)$ increases before flips to decrease with increasing values of Sc and N_{bt}.

It is shown in Fig. 5.8 and Fig. 5.9 that N_c and Le have a similar but opposite behaviours towards temperature and nanoparticle volume fraction in active control. Both parameters have little effect on temperature in active control and almost insignificant effect in passive control. Temperature shows increment with increasing N_c and a decrement with increasing Le. $\phi(\eta)$ seems to decrease with increasing N_c but increases with Le in the region near the surface before it converges as the flow moves away from the surface. In passive control, both parameter have insignificant effects towards $\phi(\eta)$.

Figure 5.10 shows the effect of increasing value of the non-Newtonian Williamson parameter λ towards skin friction at different rate of stretching and shrinking parameter S.

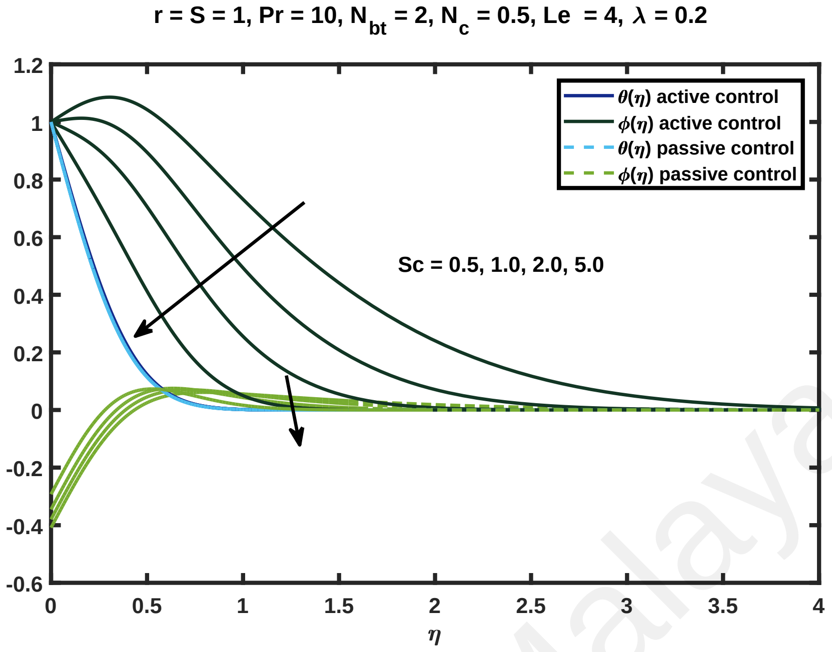

Figure 5.6: Temperature and nanoparticle volume fraction profiles for both active and passive controls for different Schmidt number, Sc.

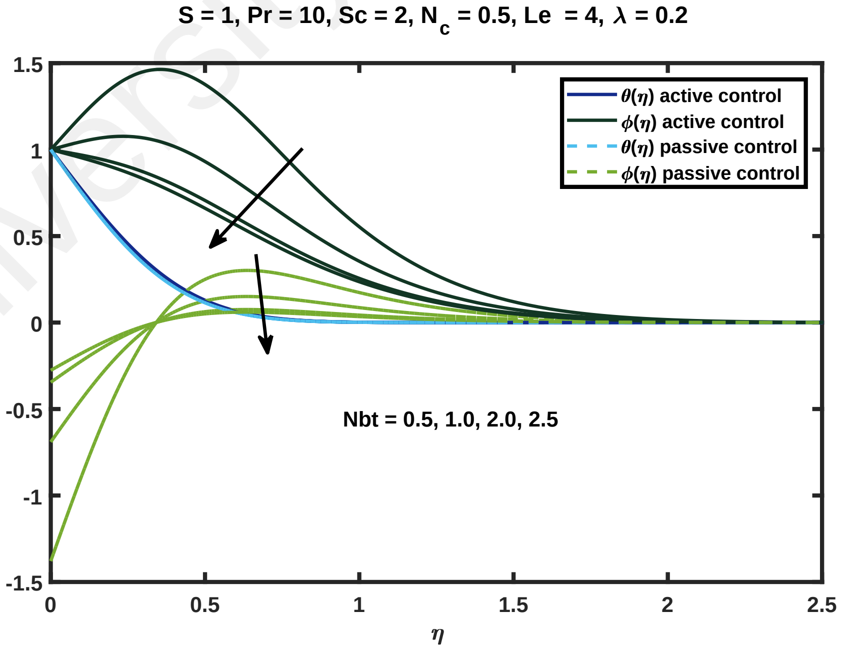

Figure 5.7: Temperature and nanoparticle volume fraction profiles for both active and passive controls for different diffusivity ratio, N_{bt}.

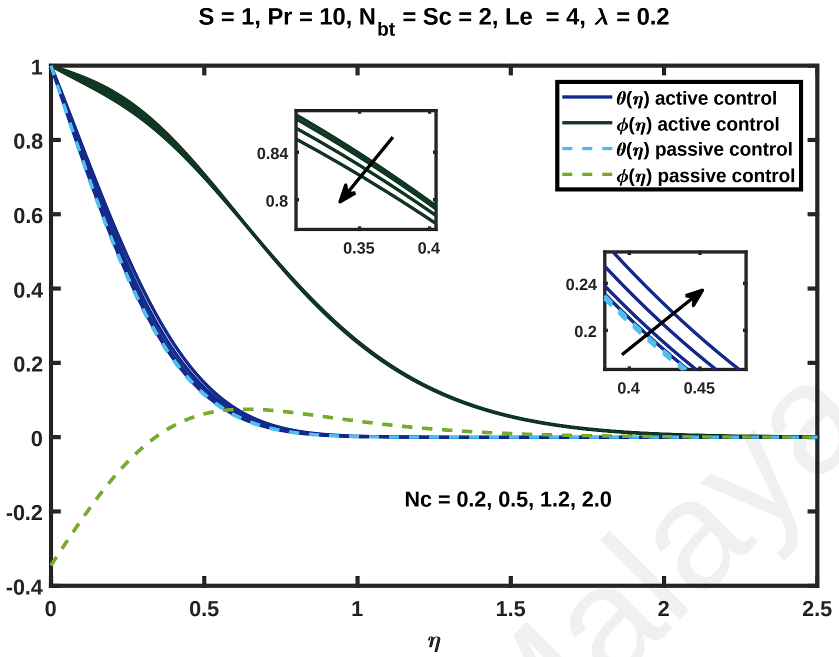

Figure 5.8: Temperature and nanoparticle volume fraction profiles for both active and passive controls for different heat capacity ratio, N_c.

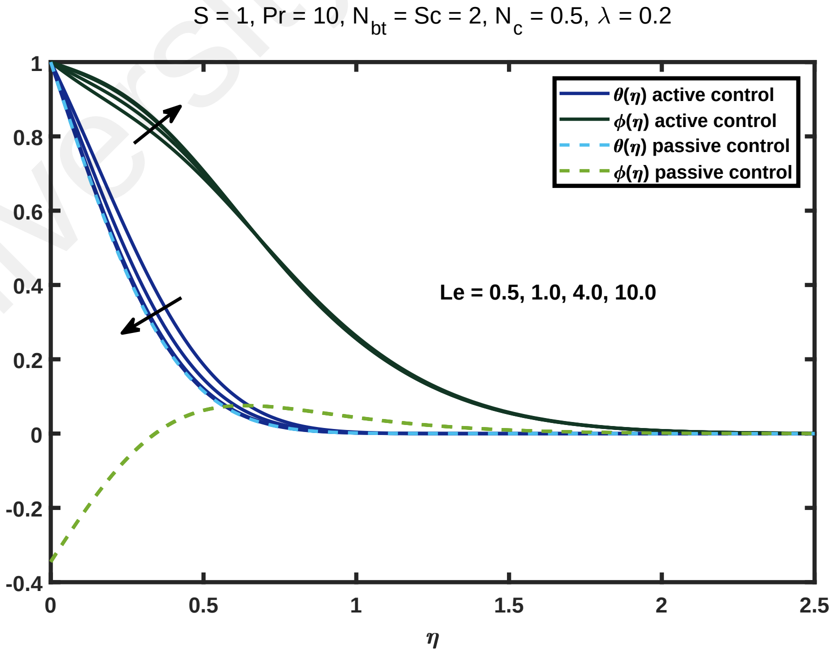

Figure 5.9: Temperature and nanoparticle volume fraction profiles for both active and passive controls for different Lewis number, Le.

Here, $\lambda = 0$ represents the special case of Newtonian fluid. It is observed that the reduced skin friction $Cf_x Re_x^{1/2}$ increases when λ increases. The results agree with equation (5.5). It can also be seen that skin friction is larger on the shrinking surface than on the stretching surface.

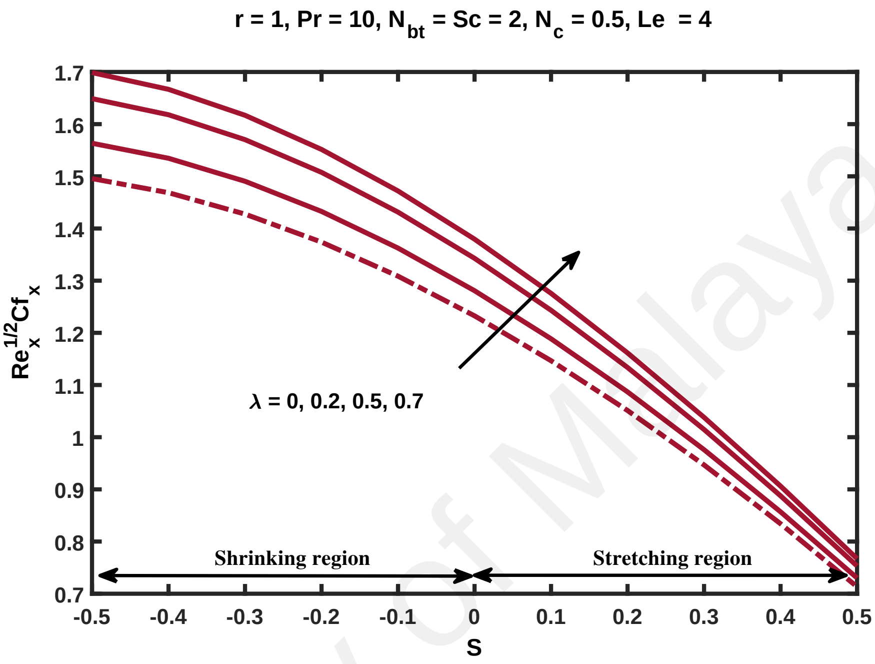

Figure 5.10: Variation of reduced skin friction for different value of Williamson parameter λ at different stretching/shrinking rate, S.

In Fig. 5.11 and Fig. 5.12, the effects of increasing heat capacity ratio N_c towards the reduced Nusselt number, $Nu_x Re_x^{-1/2}$ are presented. The rate of heat transfer is decreasing but the effect as N_c increases in passive control is reduced to minimum compared to its effect in active control. This is due to the disappearance of N_c in the boundary condition for passive control of $\phi(\eta)$. Heat transfer on shrinking surface is less than heat transfer on stretching surface and the diffusivity ratio N_{bt} does not seem to have much influence on the rate of heat transfer in passive control.

From Fig. 5.3 to Fig. 5.9, it can be seen that the variable $\phi(\eta)$ in passive control overshoots and attains negative values in the neighborhood of the surface. This behaviour

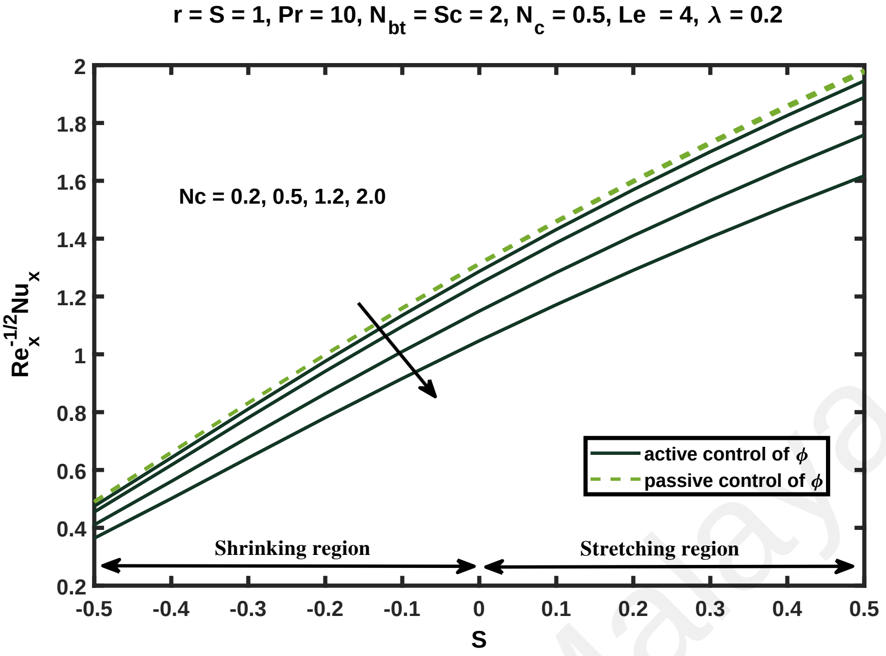

Figure 5.11: Variation of reduced Nusselt number for both active and passive controls for different capacity ratio, N_c at different stretching/shringking rate, S.

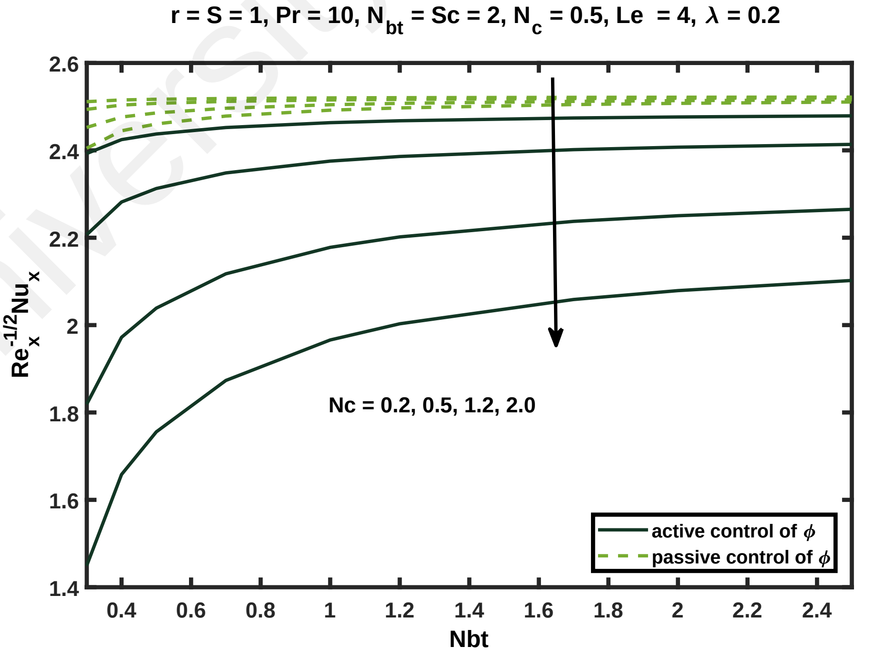

Figure 5.12: Variation of reduced Nusselt number for both active and passive controls for different heat capacity ratio, N_c and diffusivity ratio, N_{bt}.

illustrates that the nanoparticle flux at the surface is being suppressed due to the zero nanoparticle flux condition at the surface (Ishfaq et al., 2016). Note also that the temperature for passive control model is always less or equal to the temperature in active control model.

Table 5.4 to Table 5.6 list the values of reduced skin friction, reduced Nusselt number and reduced Sherwood number for different parameters. It is observed that the values of $Re_x^{-1/2}Sh_x$ in passive controls are all negative. The mass is being transferred to surroundings due to the zero mass flux condition at the surface that prevents nanoparticle deposition. Increasing values of the stagnation parameter r will increase the magnitude of all the physical quantities. Shrinking/stretching parameter S has a mixed effect on skin friction, heat flux and mass flux. Values of $Re_x^{1/2}Cf_x$ and $Re_x^{-1/2}Sh_x$ in active control seem to fluctuate with increasing S. Critical point of S for skin friction is at $S_{C_f} = -0.59$. The skin friction is increasing before it turns to decrease at the critical point. The same manner is observed for $Re_x^{-1/2}Sh_x$ in active control at the critical point $S_{Sh} = -0.54$. Meanwhile, increasing values of Schmidt number, Lewis number and the heat capacity ratio have opposite effects towards the reduced Nusselt number and reduced Sherwood number. $Re_x^{-1/2}Nu_x$ is a decreasing function of Sc and N_c but an increasing function of Le. The opposite is true for $Re_x^{-1/2}Sh_x$ number. Moreover, N_bt has increasing effect to both $Re_x^{-1/2}Nu_x$ and $Re_x^{-1/2}Sh_x$.

Table 5.4: Values of $Re_x^{1/2}Cf_x, Re_x^{-1/2}Nu_x$ and $Re_x^{-1/2}Sh_x$ for both active and passive controls when r varies.

r	$Re_x^{1/2}Cf_x$	$Re_x^{-1/2}Nu_x$		$Re_x^{-1/2}Sh_x$	
		active	**passive**	**active**	**passive**
0.2	-0.885587	2.223107	2.316252	0.118880	-1.158126
0.5	-0.650677	2.282267	2.382625	0.196667	-1.191313
1.0	0.000000	2.407227	2.519242	0.311215	-1.259621
1.2	0.341642	2.459335	2.575648	0.350948	-1.287824
1.5	0.936789	2.536589	2.658957	0.405215	-1.329478

Table 5.5: Values of $Re_x^{1/2}Cf_x, Re_x^{-1/2}Nu_x$ and $Re_x^{-1/2}Sh_x$ for both active and passive controls when S varies.

S	$Re_x^{1/2}Cf_x$	$Re_x^{-1/2}Nu_x$		$Re_x^{-1/2}Sh_x$	
		active	passive	active	passive
-1.0	1.377493	0.004139	0.004615	2.519242	-0.002308
-0.5	1.563384	0.454633	0.489208	0.478660	-0.244604
-0.3	1.490488	0.780779	0.831684	0.452715	-0.415842
0.3	0.976010	1.648791	1.733553	0.363877	-0.866777
0.5	0.730184	1.888375	1.981760	0.344411	-0.990880
1.0	0.000000	2.407227	2.519242	0.311215	-1.259621

Table 5.6: Values of $Re_x^{-1/2}Nu_x$ and $Re_x^{-1/2}Sh_x$ for both active and passive controls with various parameters.

Sc	Le	N_c	N_{bt}	$Re_x^{-1/2}Nu_x$		$Re_x^{-1/2}Sh_x$	
				active	passive	active	passive
0.5	4.0	0.5	2.0	2.460264	2.522084	-0.436034	-1.261042
1.0				2.437035	2.521089	-0.119055	-1.260545
2.0				2.407227	2.519242	0.311215	-1.259621
5.0				2.358554	2.514594	1.118822	-1.257297
2.0	0.5			1.687442	2.491917	0.646164	-1.245959
	1.0			2.078924	2.507551	0.464904	-1.253776
	4.0			2.407227	2.519242	0.311215	-1.259621
	10.0			2.476387	2.521577	0.278678	-1.260788
2.0	4.0	0.2		2.476387	2.521577	0.278678	-1.260788
		0.5		2.407227	2.519242	0.311215	-1.259621
		1.2		2.250364	2.513790	0.384812	-1.256895
		2.0		2.078924	2.507551	0.464904	-1.253776
2.0	4.0	0.5	0.5	2.312640	2.507551	-1.963494	-5.015102
			1.0	2.375364	2.515348	-0.476146	-2.515348
			2.0	2.407227	2.519242	0.311215	-1.259621
			2.5	2.413640	2.520020	0.472247	-1.008008

5.4 Concluding Remarks

The problem of a two-dimensional steady stagnation-point flow of an incompressible Williamson nanofluid is solved numerically on both shrinking and stretching surfaces. Both conditions of zero and nonzero normal fluxes are introduced at the surface while taking into account the effects of both Brownian motion and thermophoresis. The numerical results are produced by converting the boundary value problem into an initial value problem. The main results of the present analysis are listed below:

- Temperature and nanoparticle volume fraction are decreasing functions of the stagnation parameter, r.
- Temperature distribution in passive control model is always less or equal to the temperature distribution in active control model.
- Both temperature and nanoparticle volume fraction show identical behaviours in reaction to increasing Schmidt number (Sc) and diffusivity ratio (N_{bt}) effects.
- $Cf_x Re_x^{1/2}$ increases when value of λ increases.
- The stagnation parameter contributes towards better heat transfer performance for both active and passive controls on normal mass flux.
- Heat transfer rate is more susceptible to changes in parameter $Sc, Le, N_c, N_b t$ under active control.
- Heat transfer rate on shrinking surface is lower than heat transfer rate on stretching surface.
- Heat transfer rate under passive control is higher than those under active control.

CHAPTER 6: ACTIVE AND PASSIVE CONTROLS OF NANOPARTICLES IN STAGNATION-POINT FLOW OF SECOND GRADE NANOFLUID OVER A STRETCHED SURFACE

6.1 Introduction

This chapter presented the model of stagnation-point flow of a second grade nanofluid. The model incorporates the augmented boundary condition to cover for the insufficient boundary condition and is studied under active and passive control of nanoparticles. The work are being solved using BVPh 2.0; a Mathematica package software based on HAM developed by Zhao and Liao (2013).

6.2 Problem Formulation

A boundary layer flow of an incompressible second grade nanofluid near a stagnation point is examined on a permeable stretching surface parallel to the plane $y = 0$. The flow is presumed to be limited to $y > 0$ and u and v are the velocity components in the x, y directions. The free stream velocity and the stretching velocity are defined as $u_e(x) = ax$ and $u_w(x) = cx$ respectively with a and c as positive constants. Temperature near the wall surface is kept at a constant T_w. The surrounding temperature and concentration are identified as T_∞ and C_∞ respectively. The nanoparticle volume fraction for actively controlled nanoparticle is assumed to be constant and takes the value C_w near the wall while nanoparticle volume fraction for passively controlled nanoparticle is defined by the temperature gradient accordingly. Brownian diffusion coefficient, D_B and thermophoretic diffusion coefficient, D_T is incorporated in the model following the Buongiorno's model (Buongiorno, 2006). The governing equations are defined as The above problem can be formulate using the continuity equation (3.2), energy equation (3.6) and nanoparticle

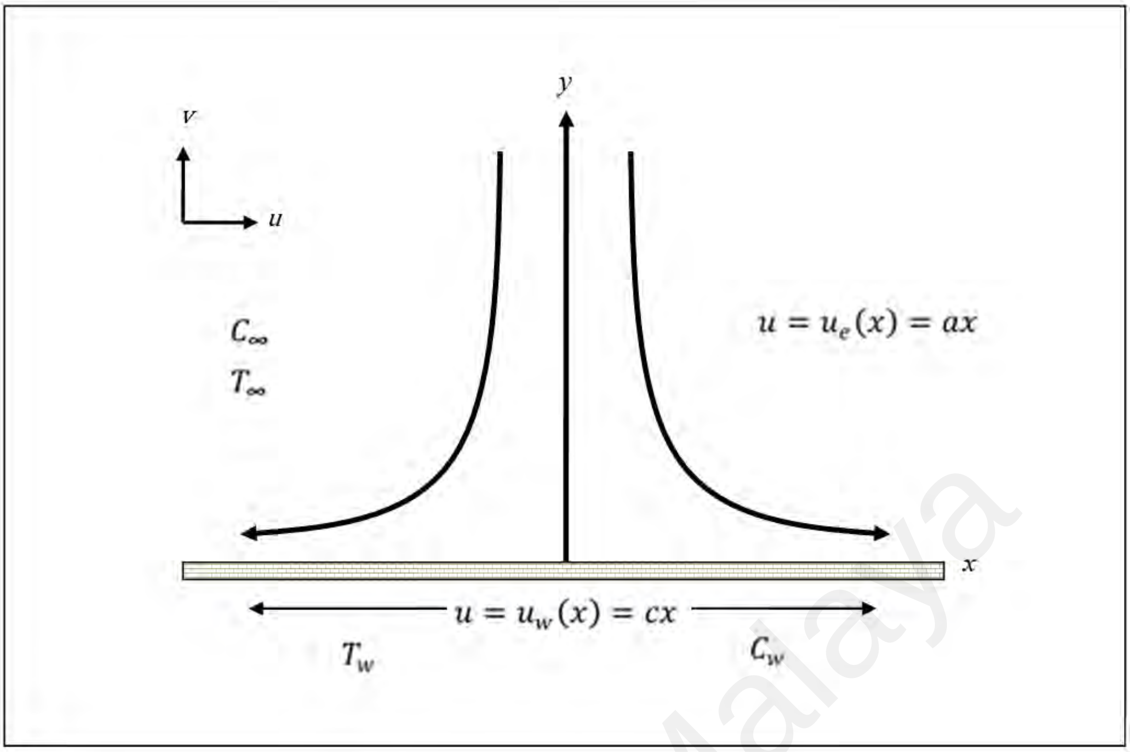

Figure 6.1: Geometry of the flow in Cartesian coordinate.

volume concentration equation (3.8) with the momentum equation given as:

$$u\frac{\partial u}{\partial x} + v\frac{\partial u}{\partial y} = u_e\frac{du_e}{dx} + \nu\frac{\partial^2 u}{\partial y^2} + \frac{\omega}{\rho}\left[u\frac{\partial^3 u}{\partial x\partial y^2} + \frac{\partial u}{\partial x}\frac{\partial^2 u}{\partial y^2} + v\frac{\partial^3 u}{\partial y^3} + \frac{\partial u}{\partial y}\frac{\partial^2 v}{\partial y^2},\right] \tag{6.1}$$

subject to velocity boundary condition (3.35), temperature boundary condition (3.40, 3.42), the active and passive control of nanoparticle condition (3.43, 3.44) and also the augmented boundary condition (3.46). In the momentum equation above, u and v are the velocity components in the x, y directions respectively, ν is the kinematic viscosity, ω is the material fluid parameter and ρ is the fluid density. By utilizing the set of non-dimensional variables for steady flow (3.48), the above model can then be transformed into a third order non-linear ordinary differential equation below:

$$\begin{aligned}
&f''' - (f')^2 + ff'' + r^2 + \lambda\left[2f'f''' - (f'')^2 - ff^{(iv)}\right] = 0,\\
&\theta'' + \Pr\left[f\theta' + Nb\,\theta'\phi' + Nt\,(\theta')^2\right] = 0,\\
&\phi'' + LePrf\phi' + \frac{Nt}{Nb}\theta'' = 0.
\end{aligned} \tag{6.2}$$

The associated boundary conditions can be written as:

$$\begin{aligned}
&f(0) = 0, \qquad f'(0) = 1, \qquad \theta(0) = 1,\\
&\quad\begin{cases} Nb\,\phi'(0) + Nt\,\theta'(0) = 0, & \text{for passive control of } \phi\\ \phi(0) = 1, & \text{for active control of } \phi \end{cases},\\
&f'(\infty) = r, \qquad f''(\infty) = 0, \qquad \theta(\infty) = 0, \qquad \phi(\infty) = 0,
\end{aligned} \tag{6.3}$$

where primes indicate the differentiation with respect to η. In the above equations, $r = a/c$ represent the stagnation parameter, $\lambda = \omega c/\mu$ is the viscoelastic parameter, Pr is the Prandtl number and Le is the Lewis number. Brownian motion parameter Nb and thermophoresis parameter Nt are defined in (3.58) and (3.59) respectively. The local skin friction coefficient Cf_x (3.62), the local Nusselt number Nu_x (3.68) and the local Sherwood number Sh_x (3.70) can be define in dimensionless form as:

$$\begin{aligned}
&Cf_x Re_x^{1/2} = f''(0) + \lambda\left[3f'(0)f''(0) - f(0)f'''(0)\right],\\
&Nu_x Re_x^{-1/2} = -\theta'(0),\\
&\quad\begin{cases} Sh_x Re_x^{-1/2} = -\phi'(0), & \text{for active control of } \phi\\ Sh_x Re_x^{-1/2} = \frac{Nt}{Nb}\theta'(0), & \text{for passive control of } \phi. \end{cases}
\end{aligned} \tag{6.4}$$

where Re_x stands for local Reynolds number.

The model are solved using HAM-based package BVPh 2.0; an open-source software written in Mathematica for boundary value problems (Zhao & Liao, 2013). The input needed to solve the problem by BVPh 2.0 includes the governing nonlinear ordinary differential equations (6.2) with the boundary conditions (6.3), initial guesses and convergence-control parameters. The accuracy of the approximate solutions is measured by computing the squared residual error over the corresponding solution interval. As the boundary conditions (6.3) are established in a semi-infinite interval, there is a need to truncate the infinite interval to a finite interval to save the computation time. In this case, the integral interval are defined as $[0, 10]$.

The auxiliary linear operators for the model are selected as follow:

$$\begin{aligned}\mathbb{L}_f &= \frac{\partial^3 f}{\partial \eta^3} + \frac{\partial^2 f}{\partial \eta^2},\\ \mathbb{L}_\theta &= \frac{\partial^2 \theta}{\partial \eta^2} - \theta,\\ \mathbb{L}_\phi &= \frac{\partial^2 \phi}{\partial \eta^2} - \phi,\end{aligned} \tag{6.5}$$

with the properties

$$\begin{aligned}&\mathbb{L}_f[C_1 + C_2 e^{\eta} + C_3 e^{-\eta}] = 0,\\ &\mathbb{L}_\theta[C_4 e^{\eta} + C_5 e^{-\eta}] = 0,\\ &\mathbb{L}_\phi[C_6 e^{\eta} + C_7 e^{-\eta}] = 0,\end{aligned} \tag{6.6}$$

where $C_j (j = 1, ..., 7)$ are the arbitrary constants to be resolved by the boundary conditions. By employing the rule of solution expressions and using the corresponding boundary

Table 6.1: Optimal values of convergence control parameters of different orders of approximation with $r = \lambda = 0.2, Pr = 2, Le = 1, Nt = Nb = 0.5$.

Order of approx., m	**Minimum total error at m-th order**	**Active control**			**CPU time (s)**
		Convergence control parameter			
		c_o^f	c_o^θ	c_o^ϕ	
2	4.48×10^{-3}	-0.44817	-0.64750	-0.23974	4.87
4	1.63×10^{-3}	-0.42605	-0.64272	-0.81381	31.14
6	8.54×10^{-4}	-0.38091	-0.50385	-0.66990	103.84
8	4.82×10^{-4}	-0.34946	-0.42493	-0.57484	341.27
10	2.90×10^{-4}	-0.32791	-0.37268	-0.50772	1099.71
12	1.83×10^{-4}	-0.30756	-0.33626	-0.45612	3270.44
14	1.18×10^{-4}	-0.26290	-0.30894	-0.41742	8707.95

constraints, the initial guesses f_o, θ_o and ϕ_o of $f(\eta), \theta(\eta)$ and $\phi(\eta)$ are specified as follows:

$$f_o(\eta) = r\eta + (1-r)[1-e^{-\eta}], \qquad \theta_o(\eta) = e^{-\eta},$$
$$\begin{cases} \phi_o(\eta) = -\frac{Nt}{Nb}e^{-\eta}, & \text{for passive control of } \phi \\ \phi_o(\eta) = e^{-\eta}, & \text{for active control of } \phi. \end{cases} \tag{6.7}$$

The optimal values of the convergence-control parameters $c_o^f, c_o^\theta, c_o^\phi$ are achieved by minimizing the averaged squared residual error. The convergence-control parameter can regulate and control the convergence region and ratio of the approximation series. Table 6.1 shows the optimal values of the convergence control parameters together with the minimum squared residual error of the m-th order approximation and its CPU time. It can be seen that the optimal values of the convergence-control parameters are not unique but stays within a certain range of values. Higher order of approximation will require more CPU time. Table 6.2 displays the error for each ODE in the system at increasing orders of HAM approximation, k. The values are obtained using values of c_o^f, c_o^θ and c_o^ϕ from the 14th order of approximation in Table 6.1. Furthermore, the BVPh 2.0 convergence can also be easily seen via the converging values of coefficient of skin friction, heat flux and mass flux in Table 6.3.

Table 6.2: Individual average squared residual errors at increasing orders of HAM approximation, k with $r = \lambda = 0.2, Pr = 2, Le = 1, Nt = Nb = 0.5$.

k	ε_k^f	ε_k^θ	ε_k^ϕ	**CPU time (s)**
2	2.30×10^{-5}	2.02×10^{-2}	8.10×10^{-4}	0.97
4	2.87×10^{-6}	4.42×10^{-3}	2.09×10^{-3}	3.70
6	2.94×10^{-7}	1.24×10^{-4}	1.58×10^{-3}	9.56
8	2.82×10^{-8}	3.64×10^{-4}	8.31×10^{-4}	20.17
10	2.61×10^{-9}	1.16×10^{-4}	3.72×10^{-4}	38.11
12	2.22×10^{-10}	4.82×10^{-5}	1.66×10^{-5}	67.95
14	6.68×10^{-11}	2.63×10^{-5}	9.20×10^{-5}	112.2
16	5.65×10^{-10}	1.93×10^{-5}	7.96×10^{-5}	174.06

Table 6.3: Convergence of HAM on the basis of the coefficient of skin friction $f''(0)$, heat flux $-\theta'(0)$ and mass flux $-\phi'(0)$ under active control of nanoparticles with $r = \lambda = 0.2, Pr = 2, Le = 1, Nt = Nb = 0.5$

k	$f''(0)$	$-\theta'(0)$	$-\phi'(0)$
1	-0.825	0.753	0.736
5	-0.822	0.466	0.728
10	-0.821	0.410	0.832
12	-0.821	0.404	0.846
14	-0.821	0.402	0.853
16	-0.821	0.401	0.857
17	-0.821	0.401	0.858
18	-0.821	0.401	0.858
19	-0.821	0.401	0.859
20	-0.821	0.401	0.859

Similarly, Fig. 6.2 shows the combined curve plot of the total residual error against the order of approximation for a specific set of physical parameters at different Nt values. It can be seen that the errors are converging to zero at different rates as the order of iteration increases.

6.3 Results and Discussion

Under this section, the effect of various influential parameters such as stagnation parameter r, viscoelastic parameter λ, Lewis number Le, Brownian motion parameter Nb, thermophoresis parameter Nt and Prandtl number Pr in active and passive control conditions are discussed. Figure 6.3 and Fig. 6.4 illustrate the effect of stagnation parameter

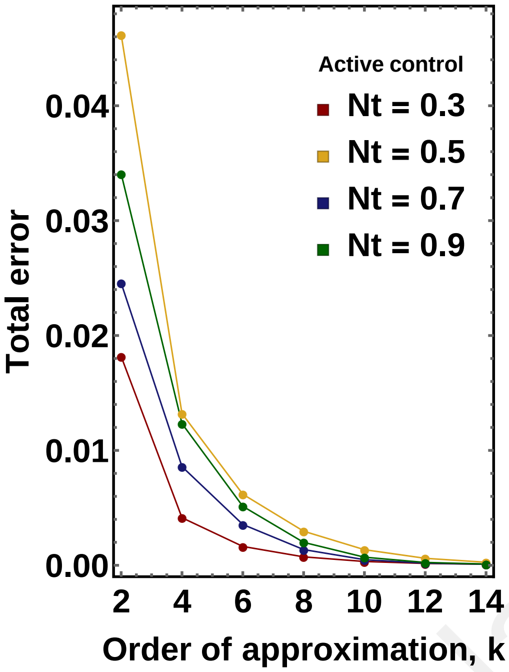

Figure 6.2: Total residual error vs. order of approximation when Nt varies under active control.

r and viscoelastic parameter λ on velocity, temperature and nanoparticle volume fraction profiles respectively. It is discovered that both parameters react similarly under active and passive controls. As r and λ increase, $f'(\eta)$ will increase but temperature and nanoparticle volume fraction will decrease. Note that $f'(\eta)$ will converge asymptotically towards the value of r, obeying the defined boundary conditions (6.3). Here, the value $\lambda = 0$ represents the special case of Newtonian fluid. In terms of velocity, the Newtonian fluid has lower velocity compared to non-Newtonian fluids. Higher velocity helps to spread the heat and nanoparticles to the surrounding faster and further, thus lowering the temperature and concentration of the fluid. Relatively, stagnation parameter r has a bigger impact towards the fluid profile as compared to the viscoelastic parameter, λ.

In Fig. 6.5, it shows that temperature and also nanoparticle volume fraction will follow the increasing trend profile as thermophoresis parameter Nt increases. The increasing temperature difference leads the nanoparticles to migrate in search of a cooler environment causing the increment of the nanoparticle volume fraction. Observed that there is almost no change in nanoparticle volume fraction near the wall under active control where it

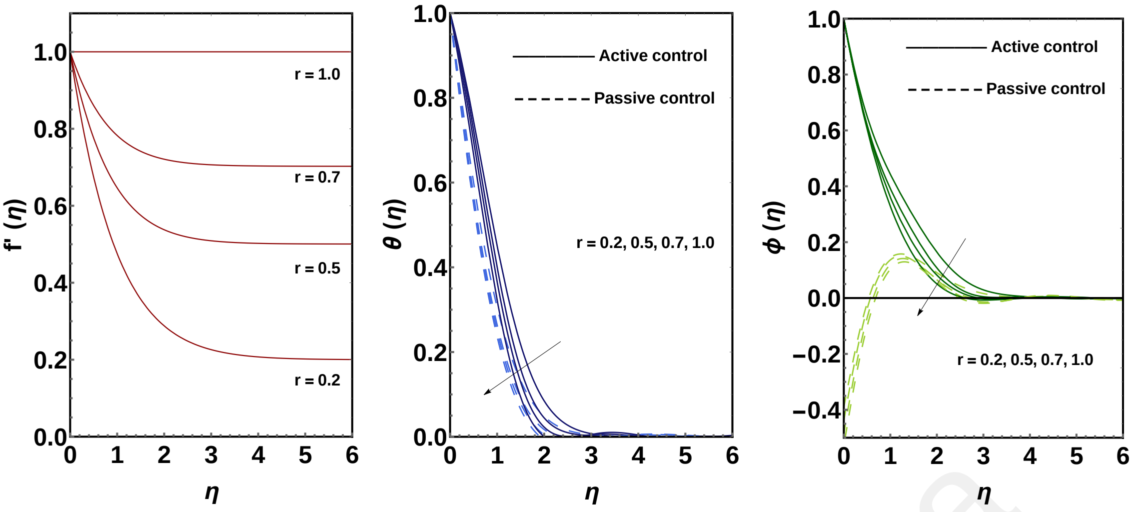

Figure 6.3: Effect of stagnation parameter r on fluid profiles profiles when $\lambda = 0.2, Pr = 2, Le = 1, Nb = Nt = 0.5$.

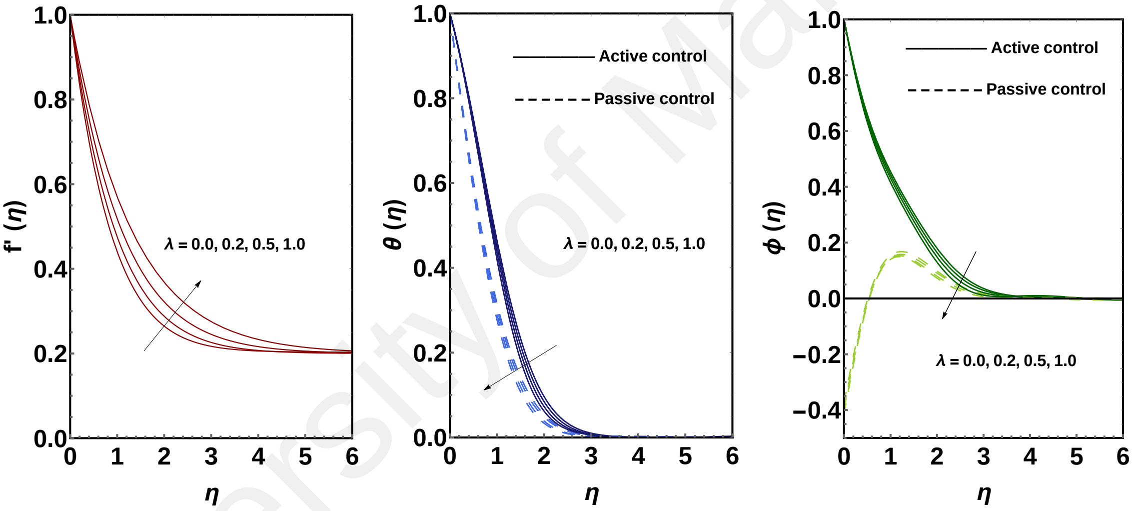

Figure 6.4: Effect of viscoelastic parameter λ on fluid profiles when $r = 0.2, Pr = 2, Le = 1, Nb = Nt = 0.5$.

is assumed to be constant. Figure 6.6 shows the impact of increasing Brownian motion Nb parameter towards temperature and nanoparticle volume fraction. Note that it has barely any effect on temperature under passive control but contributes toward increment in temperature under active control. However, increasing Nb will lower the magnitude of nanoparticle volume fraction in active control as well as in passive control. From Fig. 6.5 and Fig. 6.6, it shows that thermophoresis is of more important slip mechanism than the Brownian motion since it has more influence especially towards temperature under passive

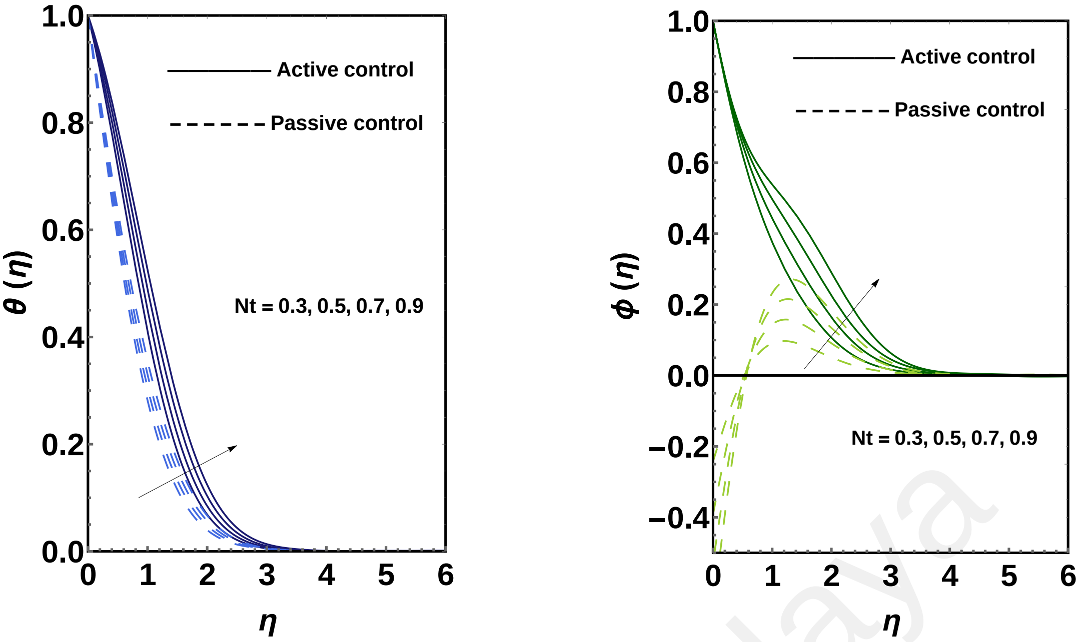

Figure 6.5: Effect of thermophoresis parameter Nt on fluid profiles when $r = \lambda = 0.2, Pr = 2, Le = 1, Nb = 0.5$.

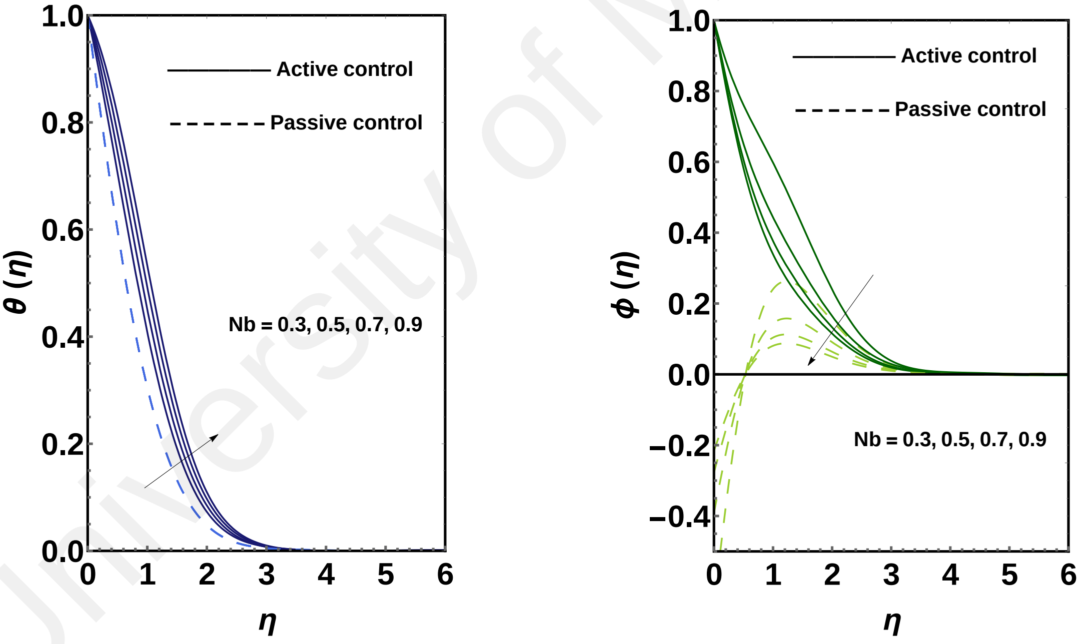

Figure 6.6: Effect of Brownian parameter Nb on fluid profiles when $r = \lambda = 0.2, Pr = 2, Le = 1, Nt = 0.5$.

control environment.

Result of increasing Lewis number Le towards temperature and nanoparticle volume fraction can be seen in Fig. 6.7. Near the wall, temperature seems to be increasing in active control and also in passive control. However, the temperature in active control environment

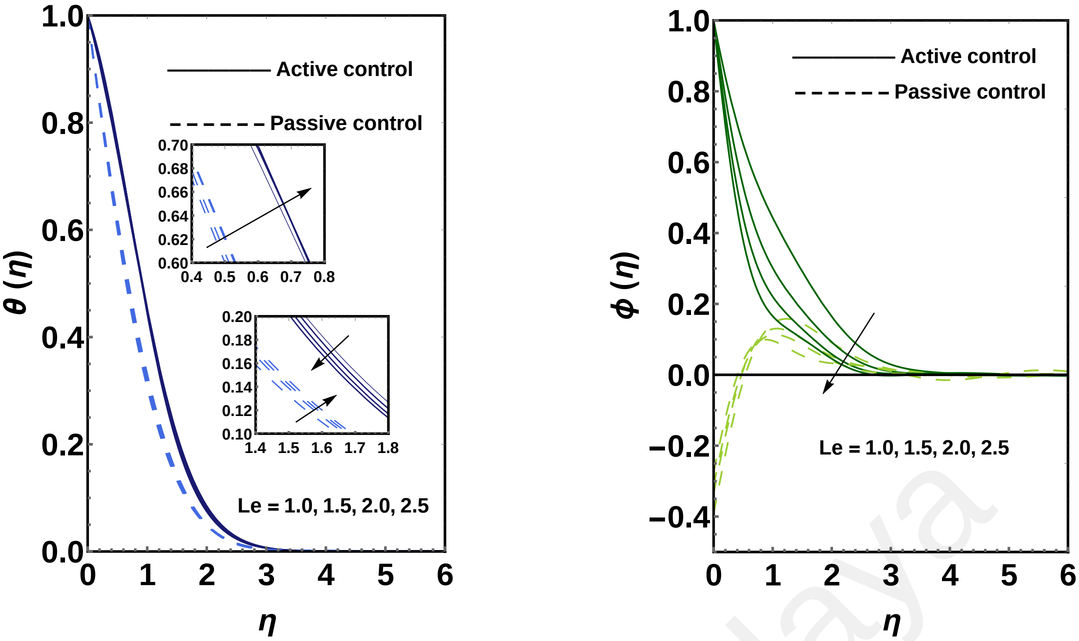

Figure 6.7: Effect of Lewis number Le on fluid profiles when $r = \lambda = 0.2, Pr = 2, Nb = Nt = 0.5$.

starts to decline midway as the fluid moves further from the wall. Nanoparticle volume fraction, on the other hand, turns out to be a decreasing function of Le. Comparatively, the impact of Le towards temperature profile is minimal and the nanoparticle volume fraction are found to be more susceptible towards changes in Le. Figure 6.8 shows the effect of Prandtl number on temperature and nanoparticle volume fraction. Both are showing a decreasing trend as value of Pr increases. From the results above, lower temperature is recorded in passive control environment as compared to in active control environment (Figs. 6.3b, 6.4b, 6.5a, 6.6a, 6.7a, 6.8a). Also, due to the passive control of mass transfer, the variable $\phi(\eta)$ attains negative values near the surface illustrating the suppressed nanoparticle flux (Figs. 6.3c, 6.4c, 6.5b, 6.6b, 6.7b, 6.8b).

Table 6.4 lists the values of the coefficient of reduced skin friction $f''(0)$, reduced Nusselt number Nu and reduced Sherwood number Sh for different parameter variations. The magnitude of $f''(0)$ are the same for active control as well as passive control. It is only affected by the increment of two parameters r and λ and remain stagnant with other parameters' variation. The active and passive control conditions of the model are

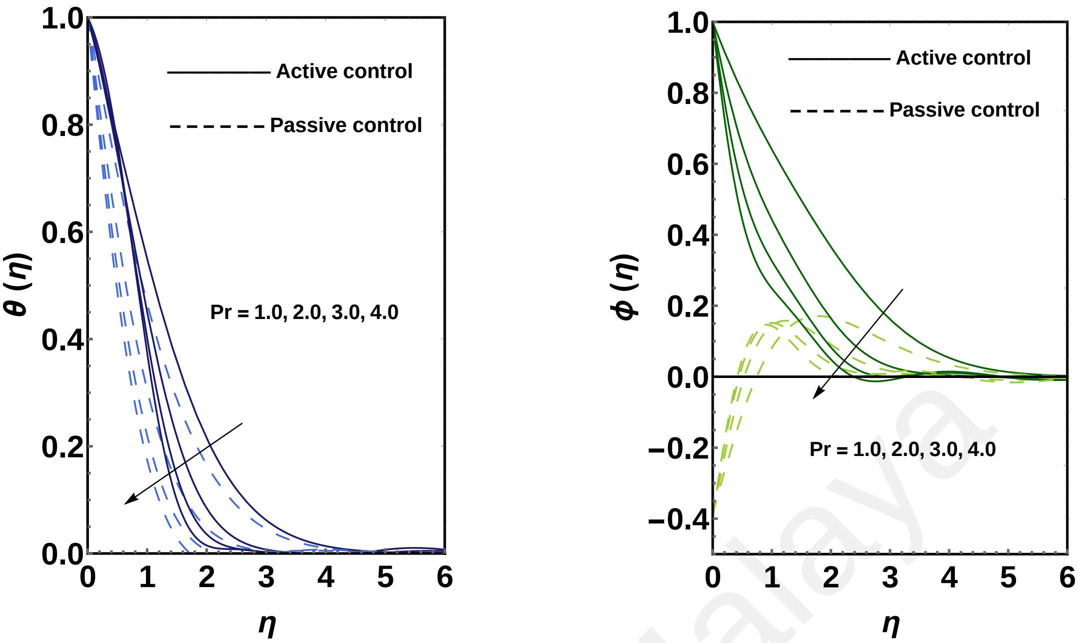

Figure 6.8: Effect of Prandtl number Pr on fluid profiles when $r = \lambda = 0.2, Le = 1, Nb = Nt = 0.5$.

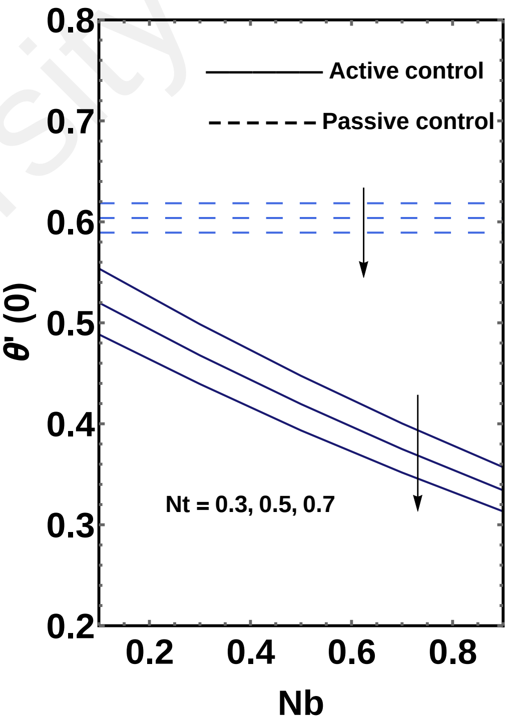

Figure 6.9: Effect of thermophoresis parameter Nt and Brownian motion parameter Nb on heat transfer rate when $r = \lambda = 0.2, Pr = 2, Le = 1$.

Table 6.4: Values of $f''(0), -\theta'(0)$ and $-\phi'(0)$ for both active and passive control.

r	λ	Nt	Nb	Le	Pr	$f''(0)$	$Re_x^{-1/2}Nu_x$		$Re_x^{-1/2}Sh_x$	
							active	passive	active	passive
0.2	0.2	0.5	0.5	1.0	1.0	-0.821	0.420	0.604	0.439	-0.604
0.5						-0.576	0.459	0.670	0.520	-0.670
0.7						-0.367	0.482	0.708	0.568	-0.708
0.2	0.2					-0.821	0.420	0.604	0.439	-0.604
	1.0					-0.608	0.443	0.641	0.479	-0.641
	2.5					-0.445	0.461	0.671	0.515	-0.671
0.2	0.2	0.3				-0.821	0.447	0.618	0.507	-0.371
		0.5				-0.821	0.420	0.604	0.439	-0.604
		0.7				-0.821	0.393	0.589	0.387	-0.825
0.2	0.2	0.5	0.3			-0.821	0.468	0.604	0.239	-1.006
			0.5			-0.821	0.420	0.604	0.439	-0.604
			0.7			-0.821	0.375	0.604	0.523	-0.431
0.2	0.2	0.5	0.5	1.0		-0.821	0.420	0.604	0.439	-0.604
				1.5		-0.821	0.397	0.594	0.659	-0.594
				2.0		-0.821	0.383	0.587	0.838	-0.587
0.2	0.2	0.5	0.5	1.0	1.0	-0.821	0.420	0.604	0.439	-0.604
					2.0	-0.821	0.401	0.859	0.859	-0.859
					3.0	-0.821	0.313	1.049	1.212	-1.049

controlled by the value of both Nb and Nt. Its effect towards the heat transfer rate is highlighted in Fig. 6.9. It is noted that heat transfer rate for active control is lower than the heat transfer rate in passive control. Under active control environment, Nu is a decreasing function of Nb. However, Nu remains stagnant despite the increasing value of Nb under passive control environment. This agrees with previous observation (Fig. 6.6a) where increment in Nb does not affect the temperature under passive control environment. On the other hand, increasing Nt will reduce the heat transfer in active control and also in passive control.

6.4 Concluding Remarks

The model of a two-dimensional second grade nanofluid flow near a stagnation point is examined. The main findings of the examination are listed below:

- Velocity is an increasing function of the stagnation parameter r and viscoelastic parameter λ.

- Increasing stagnation parameter will decrease both fluid temperature and concentration in active and passive controls of nanoparticles.
- Temperature is an increasing function of the thermophoresis parameter Nt and also Brownian motion parameter Nb.
- Nanoparticle volume fraction is an increasing function of Nt but a decreasing function of other parameters, r, λ, Le, Nb and Pr.
- Newtonian fluid has lower velocity compared to non-Newtonian second grade fluid but higher temperature and nanoparticle volume concentration.
- Increasing Nb and Nt will cause a decline in the heat transfer rate of the flow.
- The fluid behaves in the same trend when the parameters are varied under active and passive controls except for when Le is varied and the temperature behaves in opposite trend.
- The heat transfer rate is unaffected by variation of the Brownian motion parameter Nb under passive control environment.
- The heat transfer performance is better in magnitude wise under passive control environment.

CHAPTER 7: STAGNATION-POINT FLOW OF MHD CARREAU NANOFLUID UNDER ACTIVE AND PASSIVE CONTROLS OF NANOPARTICLES OVER A STRETCHING SURFACE WITH THERMAL RADIATION

7.1 Introduction

This chapter presented the model of an unsteady stagnation-point flow of Carreau nanofluid. The model took into consideration the effects of magnetohydrodynamic as well as thermal radiation towards the flow. It was solved under active and passive control of nanoparticles. It is believed that there is no work published on unsteady stagnation point flow of Carreau nanofluid yet.

7.2 Problem Formulation

An unsteady two-dimensional magnetohydrodynamic (MHD) flow of an incompressible Carreau nanofluid towards a stagnation point is examined on a permeable stretching surface which coincides with the plane $y = 0$. Velocity of the stretching surface is assumed to be $u_w(x,t) = cx/(1 - bt)$ and the velocity outside the boundary layer is defined as $u_e(x,t) = ax/(1 - bt)$ where a, b and c are positive constants. A time dependent magnetic field $B(t) = B_0/\sqrt{1 - bt}$ is applied normally to the surface, where B_0 is the initial strength of the magnetic field. The Reynolds number for the flow is assumed to be very small making the induced magnetic field negligible. Temperature at the surface is defined as $T_w(x,t)$ for both cases of active and passive controls. On the other hand, nanoparticle volume fraction for actively controlled mass flux takes the value $C_w(x,t)$ at the surface while the nanoparticle volume fraction for passively controlled mass flux is determined by the temperature gradient that results in zero normal flux of nanoparticles. The ambient temperature and concentration are denoted by T_∞ and C_∞ respectively. Taking into consideration the effect of thermal radiation, Brownian motion and thermophoresis, along with the above assumptions, the governing equations consists of the continuity equation

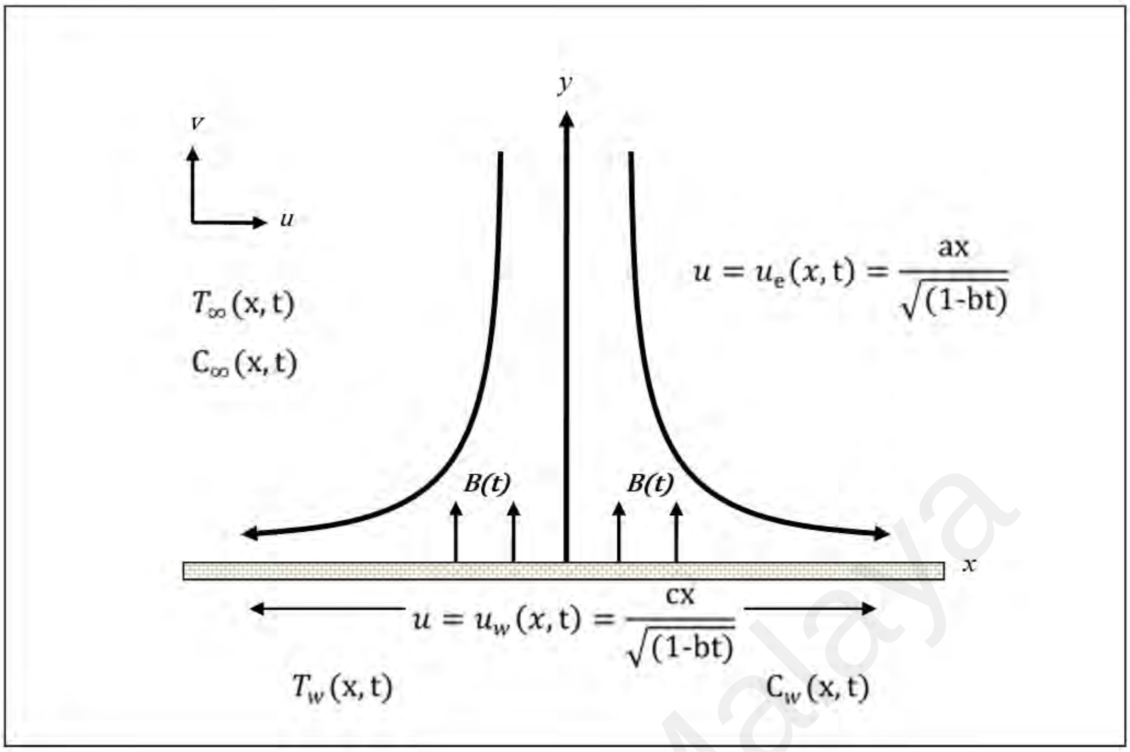

Figure 7.1: Geometry of the flow in Cartesian coordinate.

(3.2), momentum (M. Khan, Azam, & Munir, 2017), energy and nanoparticle volume fraction equations are given as follows:

$$\begin{aligned}
\frac{\partial u}{\partial t} + u\frac{\partial u}{\partial x} + v\frac{\partial u}{\partial y} &= u_e\frac{du_e}{dx} + \nu\frac{\partial^2 u}{\partial y^2}\left[1 + \Gamma^2\left(\frac{\partial u}{\partial y}\right)^2\right]^{\frac{n-1}{2}} \\
&\quad + \nu(n-1)\Gamma^2\frac{\partial^2 u}{\partial y^2}\left(\frac{\partial u}{\partial y}\right)^2\left[1 + \Gamma^2\left(\frac{\partial u}{\partial y}\right)^2\right]^{\frac{n-3}{2}} - \frac{\sigma B^2(t)}{\rho}u, \\
\frac{\partial T}{\partial t} + u\frac{\partial T}{\partial x} + v\frac{\partial T}{\partial y} &= \mathring{\alpha}\frac{\partial^2 T}{\partial y^2} - \frac{1}{\rho c_p}\frac{\partial q_r}{\partial y} + \tau D_B\frac{\partial C}{\partial y}\frac{\partial T}{\partial y} + \tau\frac{D_T}{T_\infty}\left(\frac{\partial T}{\partial y}\right)^2, \\
\frac{\partial C}{\partial t} + u\frac{\partial C}{\partial x} + v\frac{\partial C}{\partial y} &= D_B\frac{\partial^2 C}{\partial y^2} + \frac{D_T}{T_\infty}\frac{\partial^2 T}{\partial y^2},
\end{aligned} \tag{7.1}$$

subject to velocity boundary condition (3.36), temperature boundary condition (3.41, 3.42), the active and passive control of nanoparticle condition (3.43, 3.44). In the above equations, u and v are the velocity components in the x, y directions respectively, ν is the kinematic viscosity, Γ is the material constant, n is the power law index, σ is the electrical conductivity, ρ is the fluid density, $\mathring{\alpha}$ is the thermal diffusivity, c_p is the specific heat, τ

is the ratio of effective heat capacity between the nanoparticles material and the fluid, q_r is the radiative heat flux (3.33), D_B is the Brownian diffusion coefficient and D_T is the thermophoretic diffusion coefficient . Here, T and C represent the fluid temperature and the nanoparticle volume fraction respectively.

By making use of the set of non-dimensional variables for an unsteady flow (3.49), the above model can then be transformed into non-linear ordinary differential equation below:

$$\begin{aligned}
&\left[1 + We^2(f'')^2\right]\left[1 + We^2(f'')^2\right]^{\frac{n-3}{2}} f''' + f f''' - A(f' + \frac{\eta}{2}f'') \\
&\qquad\qquad\qquad\qquad - (f')^2 + r^2 - M^2 f' = 0, \\
&(1 + \frac{4}{3}Rd)\theta'' + \Pr\left[f\theta' - f'\theta + Nb\,\theta'\phi' + Nt\,(\theta')^2\right] - \Pr\frac{A}{2}(\eta\theta' + 4\theta) = 0, \\
&\text{For passive control of } \phi : \\
&\phi'' + LePr(f\phi' - \frac{A}{2}\eta\phi') + \frac{Nt}{Nb}\theta'' = 0, \\
&\text{For active control of } \phi : \\
&\phi'' + LePr(f\phi' - f'\phi) - Le\Pr\frac{A}{2}(\eta\phi' + 4\phi) + \frac{Nt}{Nb}\theta'' = 0,
\end{aligned} \tag{7.2}$$

subject to the corresponding boundary conditions:

$$\begin{aligned}
&f(0) = 0, \qquad f'(0) = 1, \qquad \theta(0) = 1, \\
&\qquad\left\{\begin{array}{ll} Nb\,\phi'(0) + Nt\,\theta'(0) = 0, & \text{for passive control of } \phi \\ \phi(0) = 1, & \text{for active control of } \phi \end{array}\right. , \\
&f'(\infty) = r, \qquad \theta(\infty) = 0, \qquad \phi(\infty) = 0,
\end{aligned} \tag{7.3}$$

where primes denote the differentiation with respect to η. Here, $A = b/c$ is the unsteadiness parameter, $r = a/c$ is the stagnation parameter, Pr is the Prandtl number, Le is the Lewis number, Nb and Nt is the parameters of Brownian motion and thermophoresis. The local

Weissenberg number We, magnetic parameter M and thermal radiation parameter Rd are defined as:

$$We = \sqrt{\frac{\Gamma^2 c^3 x^2}{\nu}}, \qquad M = \frac{\sigma B_o^2}{\rho c}, \qquad Rd = \frac{4\sigma^*}{\kappa k^*} T_\infty^3, \tag{7.4}$$

where σ is the electrical conductivity parameter, σ^* is the Stefan-Boltzmann constant, κ is the thermal conductivity and k^* is the Rosseland mean absorption coefficient. The local skin friction coefficient Cf_x (3.62), the local Nusselt number Nu_x (3.68) and the local Sherwood number Sh_x (3.70) can be reduce into the dimensionless form below:

$$\begin{aligned}
&Cf_x Re_x^{1/2} = f''(0) + \left[1 + We^2 (f''(0))^2\right]^{\frac{n-1}{2}}, \\
&Nu_x Re_x^{-1/2} = -\theta'(0), \\
&\begin{cases}
Sh_x Re_x^{-1/2} = -\phi'(0), & \text{for active control of } \phi \\
Sh_x Re_x^{-1/2} = \frac{Nt}{Nb}\theta'(0), & \text{for passive control of } \phi
\end{cases}
\end{aligned} \tag{7.5}$$

where Re_x stands for local Reynolds number.

The solution for the problem is obtained using the *bvp*4*c* package in MATLAB that provides fourth-order accurate continuous solution. First, the governing nonlinear ordinary differential equations (7.2) with the boundary conditions (7.3) are written as a system of seven first-order ODEs:

$$
\begin{aligned}
x_1' &= x_2, \\
x_2' &= x_3, \\
x_3' &= \frac{A(x_2 + \frac{\eta}{2}x_3) - ff'' + (x_2)^2 - r^2 + M^2 x_2}{[1 + nWe^2(x_3)^2][1 + We^2(x_3)^2]^{\frac{n-3}{2}}}, \\
x_4' &= x_5, \\
x_5' &= \frac{\Pr \frac{A}{2}(\eta x_5 + 4x_4) - \Pr(x_1 x_5 - x_2 x_4 + Nb x_5 x_7 + Nt(x_5)^2}{1 + \frac{4}{3}Rd}, \\
x_6' &= x_7, \\
&\text{For passive control of } \phi : \\
x_7' &= Le \Pr\left(\frac{A}{2}\eta x_7 - x_1 x_7\right) - \frac{Nt}{Nb}x_5', \\
&\text{For active control of } \phi : \\
x_7' &= Le \Pr \frac{A}{2}(\eta x_7 + 4x_6) - Le \Pr(x_1 x_7 - x_2 x_6) - \frac{Nt}{Nb}x_5',
\end{aligned}
\tag{7.6}
$$

with the boundary conditions

$$
\begin{aligned}
& x_1(0) = 0, \qquad x_2(0) = 1, \qquad x_4(0) = 1, \\
& \begin{cases} Nbx_7(0) + Ntx_5(0) = 0, & \text{for passive control of } \phi \\ x_6(0) = 1, & \text{for active control of } \phi \end{cases} , \\
& x_2(\infty) = r, \qquad x_4(\infty) = 0, \qquad x_6(\infty) = 0.
\end{aligned}
\tag{7.7}
$$

For calculation purpose, $\eta \to \infty$ in this problem are set to $\eta_\infty = 10$ and the numerical solutions are evaluate at 100 equally spaced points with suitable initial guesses. The relative tolerance are set to 1×10^{-10}. To ensure the accuracy of our calculation and method of choice, present results are compared with published results of others who used different methods. Table 7.1 lists the compared values of $f''(0)$ for various values of

Table 7.1: Comparison of results for $f''(0)$ of various valued of stagnation parameter, r when $We = Nb = Nt = Rd = A = M = 0, Pr = Le = 1$.

r	Ishak et al. (2007) Keller Box	Mabood and Khan (2016) HAM	Current Study $bvp4c$
0.01	- 0.9980	-	- 0.99803
0.1	- 0.9694	- 0.96938	- 0.96939
0.2	- 0.9181	- 0.91811	- 0.91811
0.5	- 0.6673	- 0.66726	- 0.66726
2.0	2.0175	2.01750	2.01750
3.0	4.7294	4.72928	4.72928
10.0	36.2603	-	36.25733

stagnation parameter r. From the table, it is evident that the present results are consistent with existing studies.

7.3 Results and Discussion

In this section, the effect of different instrumental parameters such as local Weissenberg number We, power law index n, unsteadiness parameter A, stagnation parameter r, magnetic parameter M, thermal radiation parameter Rd, Lewis number Le, Prandtl number Pr, Brownian motion parameter Nb and thermophoresis parameter Nt in both active and passive controls of nanoparticles are presented and discussed. These parameters influence towards velocity $f'(\eta)$, temperature $\theta(\eta)$ and nanoparticle volume fraction $\phi(\eta)$ are displayed in Fig. 7.2 to Fig. 7.11, while their effects towards skin friction coefficient $f''(0)$, local Nusselt number $-\theta(0)$ and local Sherwood number $-\phi(0)$ are tabulated in Table 7.2 and Table 7.3. Interesting results towards heat transfer rate and mass transfer rate are highlighted in Fig. 7.12 to Fig. 7.14.

Figure 7.2 depicts the impact that stagnation parameter r had on the fluid profiles. As value of r increases, velocity of the fluid too increases but both temperature and nanoparticle volume fraction decrease. Assuming that the stream velocity is constant, increasing value of r also implies decreasing stretching velocity. The existence of two

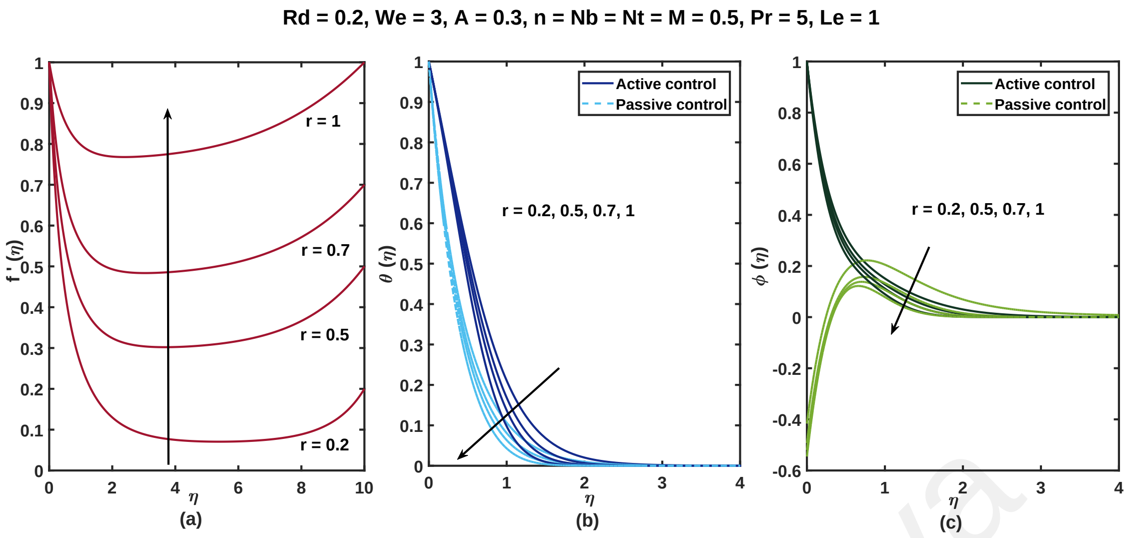

Figure 7.2: Effect of stagnation parameter r on a) velocity, b) temperature and c) nanoparticle volume fraction profiles.

different velocities give rise to skin friction which lowers the velocity in general. Lower stretching velocity means lower skin friction and hence higher velocity. The same pattern

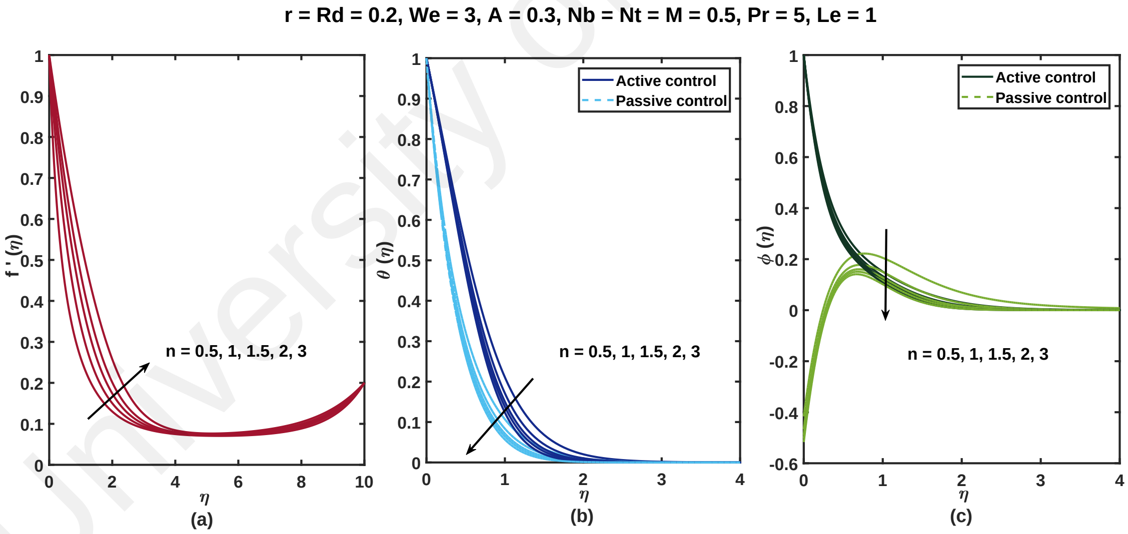

Figure 7.3: Effect of power law index n on a) velocity, b) temperature and c) nanoparticle volume fraction profiles.

is observed in Fig. 7.3 where the power law index n is concerned. The nonlinearity of the fluid depends on the value of n. The fluid is called pseudoplastic or shear-thinning fluid when $n < 1$, a dilatant or shear-thickening fluid when $n > 1$ and Newtonian fluid when $n = 1$. Velocity of the fluid increases with increasing value of n. Opposite behaviours are recorded when the local Weissenberg number We and magnetic parameter M are varied (Figs. 7.4, 7.5). When values of both parameters are increased, the velocity will decrease resulting in increasing temperature and nanoparticle volume fraction. The We number is the product of a characteristic time of the fluid and a characteristic rate of deformation that is used to describe the degree of exhibited nonlinearity of the fluid (Dealy, 2010). Meanwhile, applied magnetic field onto the fluid creates a drag force called Lorentz force causing the velocity to decrease. As the velocity increases, the surrounding

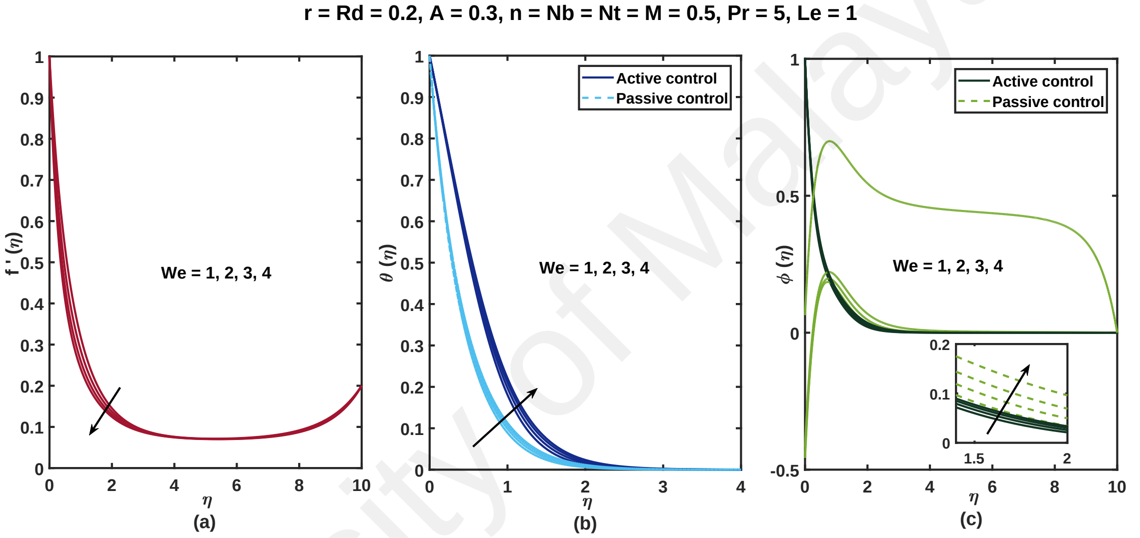

Figure 7.4: Effect of local Weissenberg number We on a) velocity, b) temperature and c) nanoparticle volume fraction profiles.

heat gets swiftly distributed together with the nanoparticles and both the temperature and nanoparticle volume fraction will decrease accordingly (Figs.7.2, 7.3). The opposite applies when the velocity decreases (Figs. 7.4, 7.6). However, a different reaction is noted when the unsteadiness parameter A is varied. It is found that increasing A has decreasing effect towards velocity and temperature profiles. It is interesting to highlight that the trend for nanoparticle volume fraction profile is different between active and passive controls. The profile decreases with increasing value of A under active control but increases when passive control is applied.

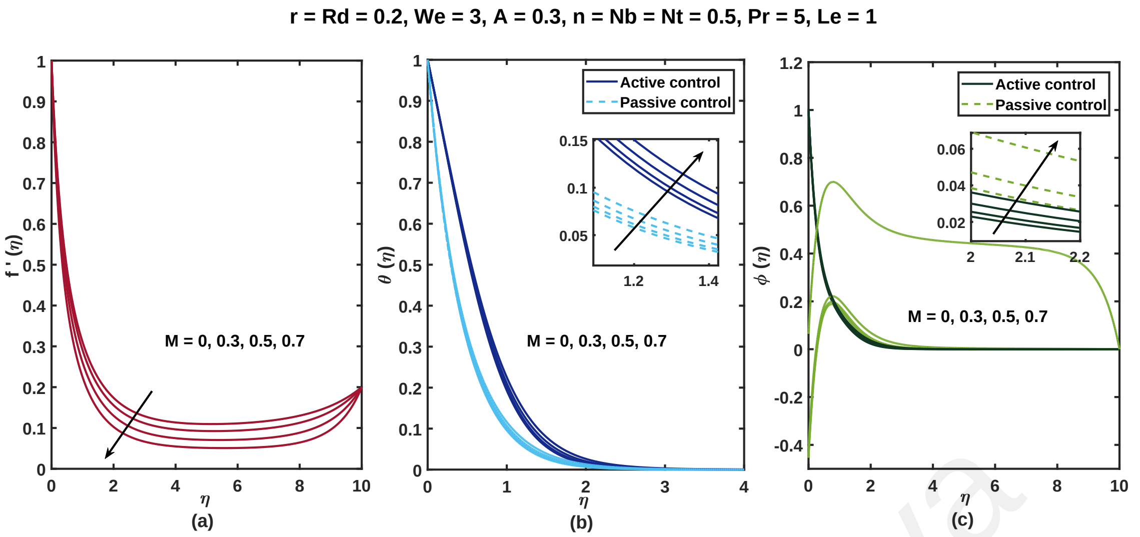

Figure 7.5: Effect of magnetic parameter M on a) velocity, b) temperature and c) nanoparticle volume fraction profiles.

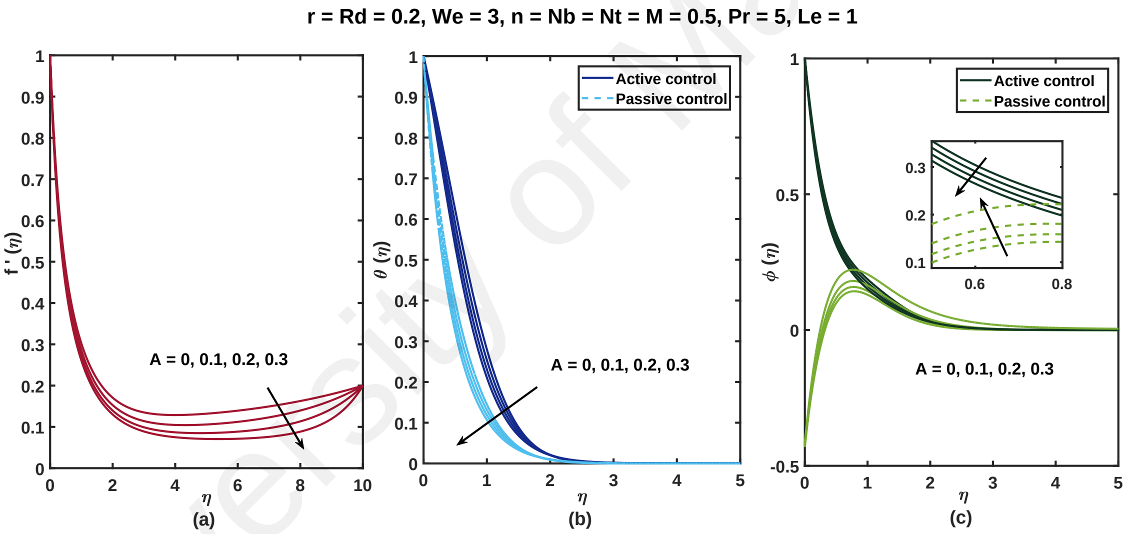

Figure 7.6: Effect of unsteadiness parameter A on a) velocity, b) temperature and c) nanoparticle volume fraction profiles.

From Fig. 7.2 to Fig. 7.6, it is observed that near the wall, velocity seems to decrease sharply before steadily increases and converges towards the particular value of r following the defined boundary condition, resulting in a convex-like profile. Due to the chosen value of $r < 1$ where the surface stretching velocity rate is higher than the external fluid velocity, the resulting surface friction reacting in the opposite direction of the flow is stronger near the wall hence it pulls down the velocity of the fluid as a whole. Combining the opposing force from other parameters involved, the velocity becomes even more slower before it slowly recovers its speed as it moves away from the surface and weakens the opposing force. In Fig. 7.7, the effects of thermal radiation parameter Rd towards temperature and nanoparticle volume fraction are displayed. Increasing the value of Rd will increase the temperature as more heat is being emitted by the fluid. Interesting trends of profiles in nanoparticle volume fraction can be seen between active control and passive control. As value of Rd increases, nanoparticle volume fraction under active control decreases near the surface but will eventually increases as it moves away from the wall. In case of passive control of nanoparticles, the nanoparticle volume fraction will increase together with the increasing value Rd. Fig. 7.8 illustrates the temperature and nanoparticle volume fraction reactions towards increasing Prandtl number, Pr. It can be seen that both profiles are a decreasing function of Pr as larger Pr renders the thermal diffusivity to be secondary to momentum diffusivity. On the other hand, both temperature and nanoparticle volume

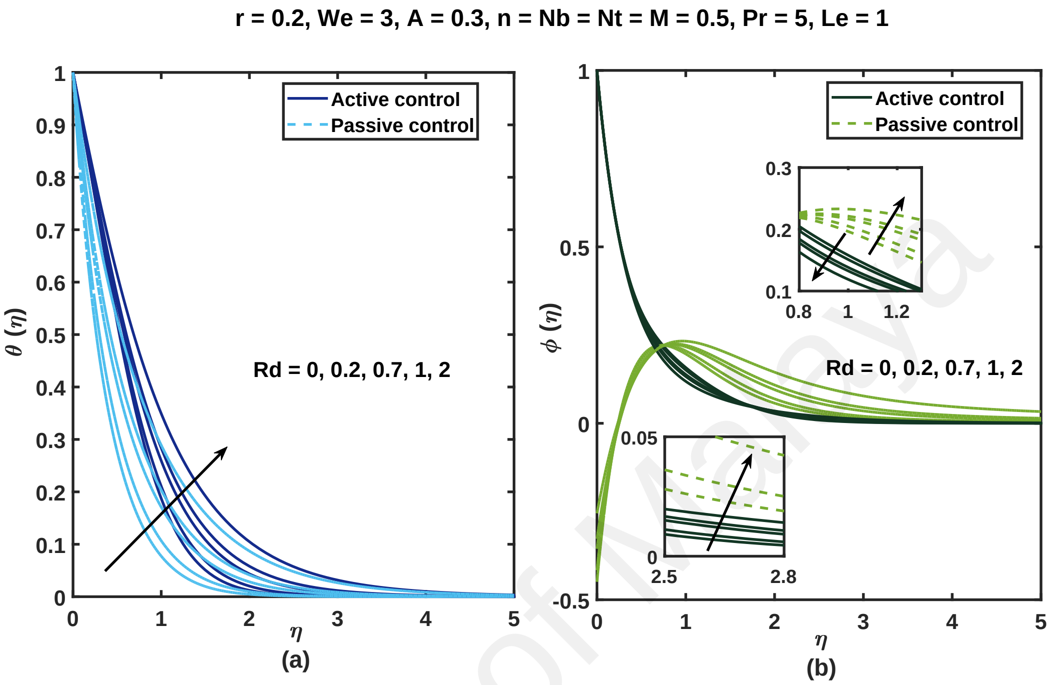

Figure 7.7: Effect of thermal radiation parameter Rd on a) temperature and b) nanoparticle volume fraction profiles.

fraction turn out to be increasing functions of thermophoresis parameter, Nt (Fig. 7.9). Higher Nt corresponds to higher temperature gradient which causes the nanoparticles to be spread further in an attempt to escape to a cooler environment.

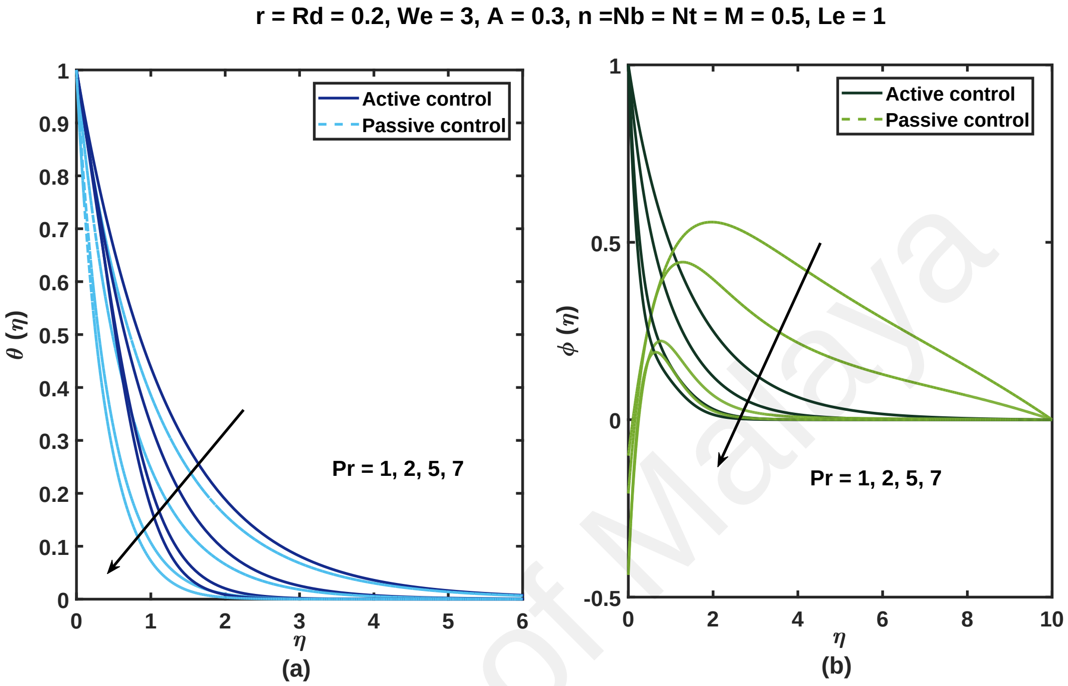

Figure 7.8: Effect of Prandtl number Pr on a) temperature and b) nanoparticle volume fraction profiles.

Temperature and nanoparticle volume fraction respond in opposite trend when Brownian motion parameter, Nb is varied as shown in Fig.7.10. As Nb increases, temperature too will increase but nanoparticle volume fraction will decrease. Increasing Nb leads to more frequent clashing between the fluid particles and nanoparticles, producing heat that subsequently gives rise to the temperature. At the same time, distance between particles will increase thus it lowers the concentration of nanoparticles in the area. Notice that, under passive control of nanoparticle, the temperatures are unaffected by the increasing Nb making Nt a significant contributor towards temperature increment in the presence of nanoparticle. In Fig.7.11, the effects of Lewis number, Le towards temperature and nanoparticle volume fraction are displayed. Increasing Le will result in

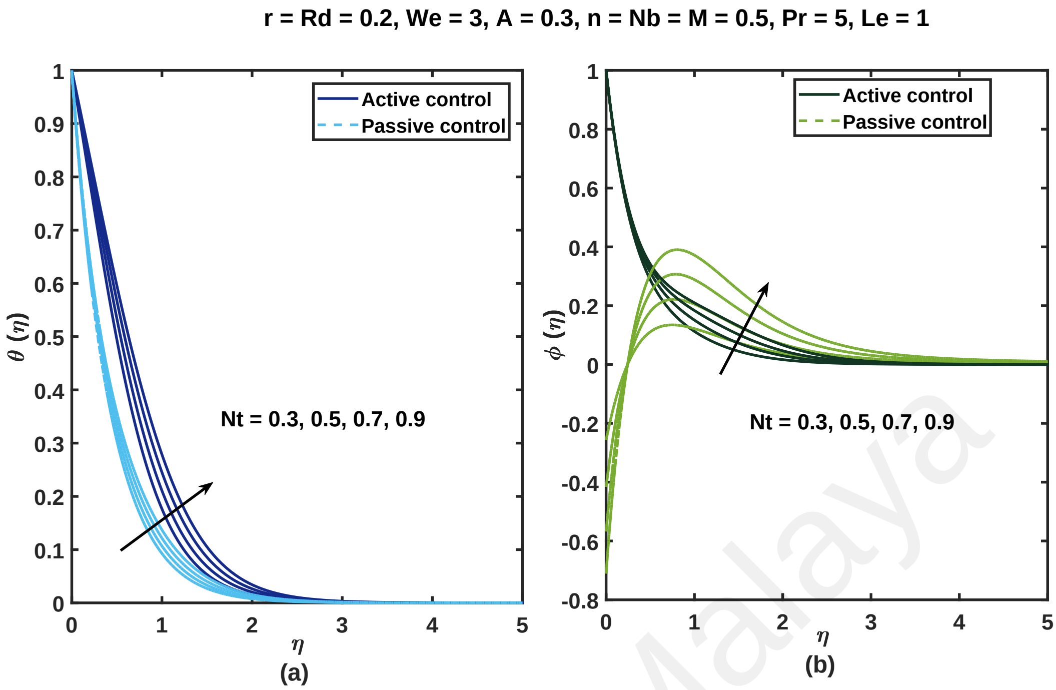

Figure 7.9: Effect of thermophoresis parameter Nt on a) temperature and b) nanoparticle volume fraction profiles.

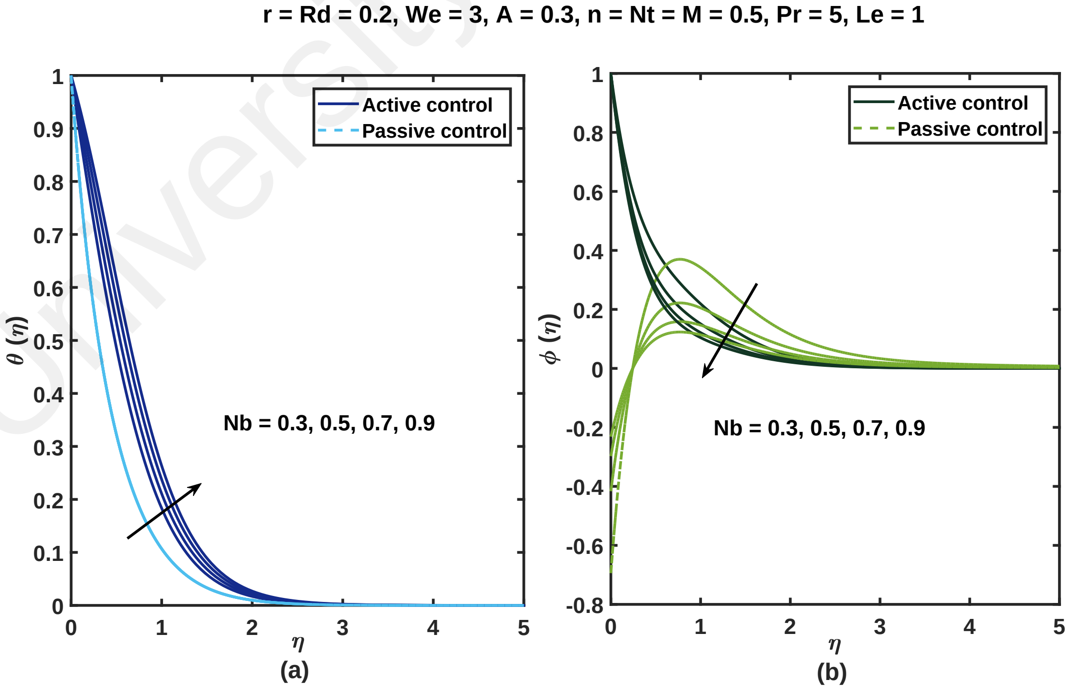

Figure 7.10: Effect of Brownian motion parameter Nb on a) temperature and b) nanoparticle volume fraction profiles.

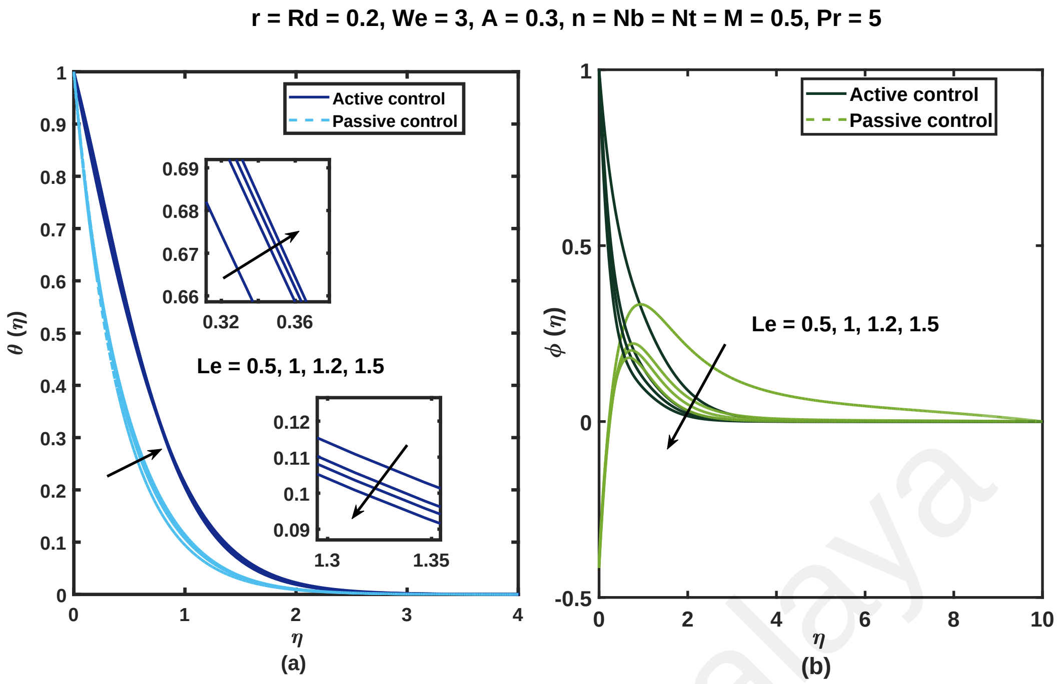

Figure 7.11: Effect of Lewis number *Le* on a) temperature and b) nanoparticle volume fraction profiles.

decreasing temperature in passive control but shows a swaping trend under active control of nanoparticles. Temperature is in increasing pattern near the surface but converts into a decreasing pattern in the midway of distribution. Nanoparticle volume fraction on the other hand is a decreasing function of *Le* in both active and passive controls of nanoparticle. From the graphs, *Le* seems to have a bigger impact on nanoparticle volume fraction as compared to the very minimal changes in temperature.

Comparing the results from Fig.7.2 to Fig.7.11 with the values from Table 7.2, it is found that increasing velocity is paired with decreasing magnitude of skin friction coefficient $f''(0)$ and vice versa. The temperature under active control too is notably higher than temperature under passive control. This finding is supported by the record in Table 7.2 and Table 7.3, that show higher heat transfer rate under passive control of nanoparticles in which heat are distributed more quickly to the neighbouring areas causing drops in the temperature under passive control. It is also noted that the nanoparticle volume fraction under passive control is in negative region near the wall. Similarly, the mass transfer rates are also in negative values for passive control. This is due to the boundary condition defined in (7.7) in which, according to Ishfaq et al. (2016) is a statement that translates to the normal flux of nanoparticles being zero at the boundary when thermophoresis is taken into account. Some other outcomes on the local Nusselt numbers and local Sherwood numbers are highlighted in Fig.7.12 to Fig.7.14. As Nb is increasing, heat transfer rate seems to be declining in active control but appears constant in passive control (Fig. 7.12). On the other hand, a curve pattern is observed on Nu under active control with increasing values of Pr in Fig.7.13. Heat transfer rate increases till it reaches a critical point of Pr where it starts declining. Similarly in opposite trend, as Rd increases, Sh will decrease first before it reaches a point where it starts increasing together with the increasing Rd as seen in Fig.7.14.

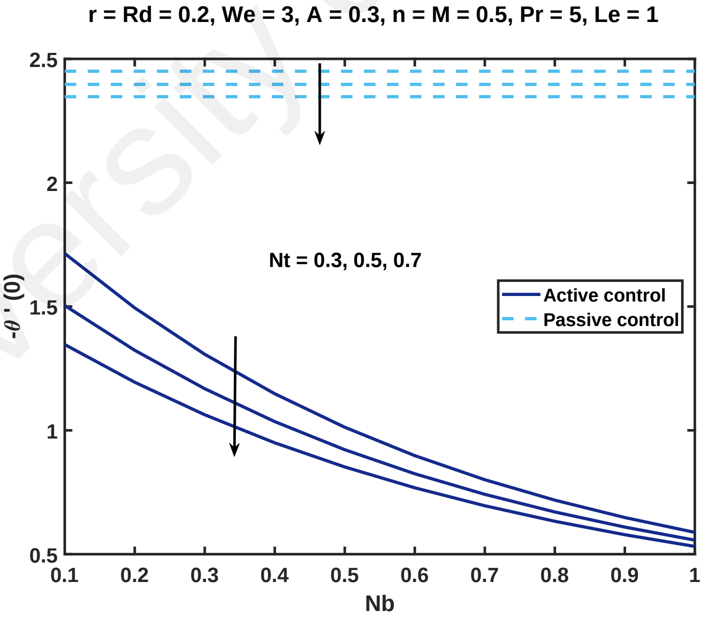

Figure 7.12: Effect of Brownian motion parameter Nb with varied thermophoresis parameter Nt on heat transfer rate $-\theta'(0)$.

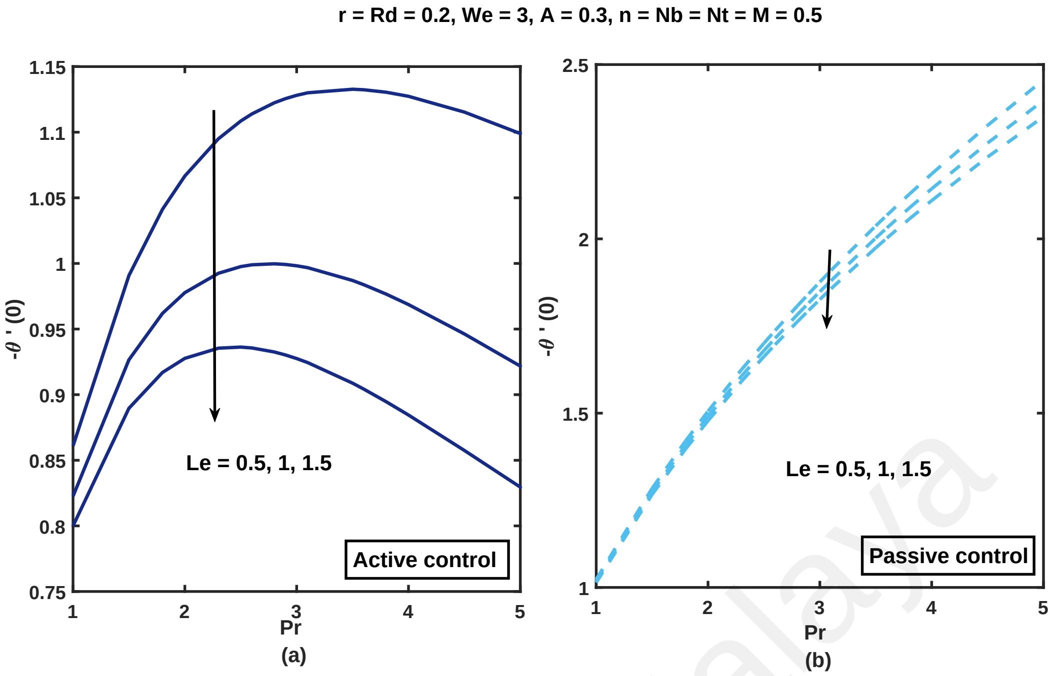

Figure 7.13: Effect of Prandtl number Pr with varied Lewis number Le on heat transfer rate $-\theta'(0)$ under a) active control and b) passive control.

Table 7.2: Values of $f''(0)$, $-\theta'(0)$ and $-\phi'(0)$ for both active and passive controls.

r	We	n	A	M	$f''(0)$	$-\theta'(0)$		$-\phi'(0)$	
						active	passive	active	passive
0.2	3.0	0.5	0.3	0.5	-2.19033	0.92176	2.39707	2.74201	-2.39707
0.5					-1.70397	0.92262	2.47324	2.87255	-2.47324
0.7					-1.23263	0.92522	2.53856	2.98124	-2.53856
1.0					-0.47035	0.93072	2.63589	3.14052	-2.63589
0.2	1.0				-1.42960	0.93015	2.47432	2.85994	-2.47432
	2.0				-1.85975	0.92540	2.43107	2.79398	-2.43107
	3.0				-2.19033	0.92176	2.39707	2.74201	-2.39707
	4.0				-2.44601	0.91896	2.37124	2.70254	-2.37124
0.2	3.0	0.5			-2.19033	0.92176	2.39707	2.74201	-2.39707
		1.0			-1.17062	0.93295	2.50027	2.89960	-2.50027
		1.5			-0.85404	0.93494	2.54598	2.97456	-2.54598
		2.0			-0.69777	0.93533	2.57156	3.01811	-2.57156
		3.0			-0.53880	0.93528	2.59949	3.06689	-2.59949
0.2	3.0	0.5	0.0		-1.88777	0.69973	1.89715	2.28052	-1.89715
			0.1		-1.99378	0.78130	2.07403	2.43939	-2.07403
			0.2		-2.09415	0.85461	2.24034	2.59381	-2.24034
			0.3		-2.19033	0.92176	2.39707	2.74201	-2.39707
0.2	3.0	0.5	0.3	0.0	-1.88446	0.92393	2.43420	2.80228	-2.43420
				0.3	-1.99768	0.92316	2.42017	2.77940	-2.42017
				0.5	-2.19033	0.92176	2.39707	2.74201	-2.39707
				0.7	-2.46311	0.91957	2.36592	2.69213	-2.36592
				1.0	-2.99685	0.91475	2.30578	2.60384	-2.30578

Table 7.3: Values of $Re_x^{-1/2}Nu_x$ and $Re_x^{-1/2}Sh_x$ for both active and passive controls.

Rd	Pr	Nb	Nt	Le	$Re_x^{-1/2}Nu_x$ active	$Re_x^{-1/2}Nu_x$ passive	$Re_x^{-1/2}Sh_x$ active	$Re_x^{-1/2}Sh_x$ passive
0.0	5.0	0.5	0.5	1.0	0.91624	2.72070	2.76051	-2.72070
0.2					0.92176	2.39707	2.74201	-2.39707
0.7					0.91497	1.90846	2.71444	-1.90846
1.0					0.90249	1.72341	2.70679	-1.72341
2.0					0.84625	1.34648	2.70341	-1.34648
3.0					0.78887	1.13510	2.71250	-1.13510
0.2	1.0				0.82258	1.01825	0.78481	-1.01825
	3.0				0.99821	1.84862	1.86516	-1.84862
	5.0				0.92176	2.81916	2.74201	-2.81916
	7.0				0.82278	2.78608	3.45626	-2.78608
0.2	5.0	0.3			1.16812	2.39707	2.36554	-3.99512
		0.5			0.92176	2.39707	2.74201	-2.39707
		0.7			0.74163	2.39707	2.86424	-1.71219
		0.9			0.60933	2.39707	2.91110	-1.33171
0.2	5.0	0.5	0.3		1.01254	2.45016	2.77696	-1.47010
			0.5		0.92176	2.39707	2.74201	-2.39707
			0.7		0.85212	2.34732	2.71862	-3.28625
			0.9		0.79725	2.30090	2.69986	-4.14162
0.2	5.0	0.5	0.5	0.5	1.09897	2.45620	1.58049	-2.45620
				1.0	0.92176	2.39707	2.74201	-2.39707
				1.2	0.87922	2.37728	3.09904	-2.37728
				1.5	0.82953	2.35069	3.57176	-2.35069

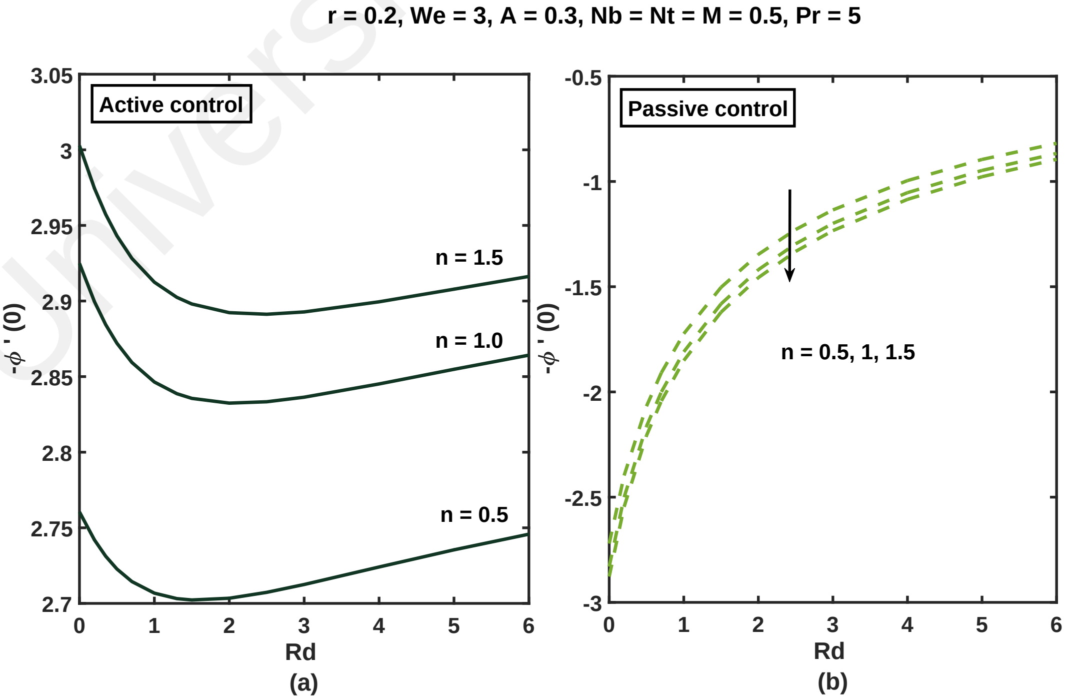

Figure 7.14: Effect of thermal radiation parameter Rd with varied power law index n on mass transfer rate $-\phi'(0)$ under a) active control and b) passive control.

7.4 Concluding Remarks

The problem of a two-dimensional unsteady stagnation point flow of a MHD Carreau nanofluid with thermal radiation is examined. The main observations of the study are given below:

- Stagnation parameter r and power law index n increase the fluid velocity while reducing the magnitude of skin friction coefficient at the same time.
- Both temperature and nanoparticle volume fraction are increasing function of the local Weissenberg number We, magnetic parameter M and thermophoresis parameter Nt.
- Unsteadiness parameter A has an opposite effect on active and passive controls for nanoparticle volume fraction.
- Increasing values of Brownian motion Nb and thermophoresis Nt parameter will reduce the heat transfer rate of the flow.
- Stagnation parameter r increases the heat transfer rate of the fluid.
- Magnetic parameter M decreases the heat transfer rate of the fluid.
- Thermal radiation Rd raises the fluid temperature and lowers the heat transfer rate.
- The heat transfer rate is higher under passive control of nanoparticles than the heat transfer rate under active control of nanoparticles.

CHAPTER 8: MIXED CONVECTION FLOW OF POWELL-EYRING NANOFLUID NEAR A STAGNATION POINT ALONG A VERTICAL STRETCHING SHEET WITH ACTIVE AND PASSIVE CONTROLS OF NANOPARTICLES

8.1 Introduction

This chapter presented the model of a stagnation-point flow of Powell-Eyring nanofluid flow. The model incorporated the effect of buoyancy forces towards the fluid flow on a vertical surface as well as the effects of active and passive controls of nanoparticles.

8.2 Problem Formulation

Take into account a steady two-dimensional mixed convection stagnation point flow of an incompressible Powell-Eyring nanofluid towards a vertical stretching surface. The Cartesian coordinate system is chosen in such a way that the $x-$axis is along the vertical linearly stretching surface at $y = 0$ and the fluid occupies the area $y > 0$. Near the surface, velocity is assumed to be $u_w(x) = cx$ with temperature $T = T_w$. Depending on the fluid environment setting, the fluid concentration is assumed to be constant $C = C_w$ when under active control surrounding but it will be depending on the temperature gradient when it is put under passive control of nanoparticles. Velocity of the free stream flow is defined as $u_e(x) = ax$ with ambient temperature and concentration of T_∞ and C_∞ respectively. With the above premises, the governing equations of the boundary layer flow can be formulate with the continuity equation (3.2), energy equation (3.6) and nanoparticle volume concentration equation (3.8) with the momentum equation given as (Hayat et al., 2013):

$$\begin{aligned} u\frac{\partial u}{\partial x} + v\frac{\partial u}{\partial y} = u_e\frac{du_e}{dx} + \left(\nu + \frac{1}{\rho\beta\grave{e}}\right)\frac{\partial^2 u}{\partial y^2} - \frac{1}{2\rho\beta\grave{e}^3}\left(\frac{\partial u}{\partial y}\right)^2\frac{\partial^2 u}{\partial y^2} \\ +g\left[\beta_T(T - T_\infty) + \beta_C(C - C_\infty)\right] \end{aligned} \tag{8.1}$$

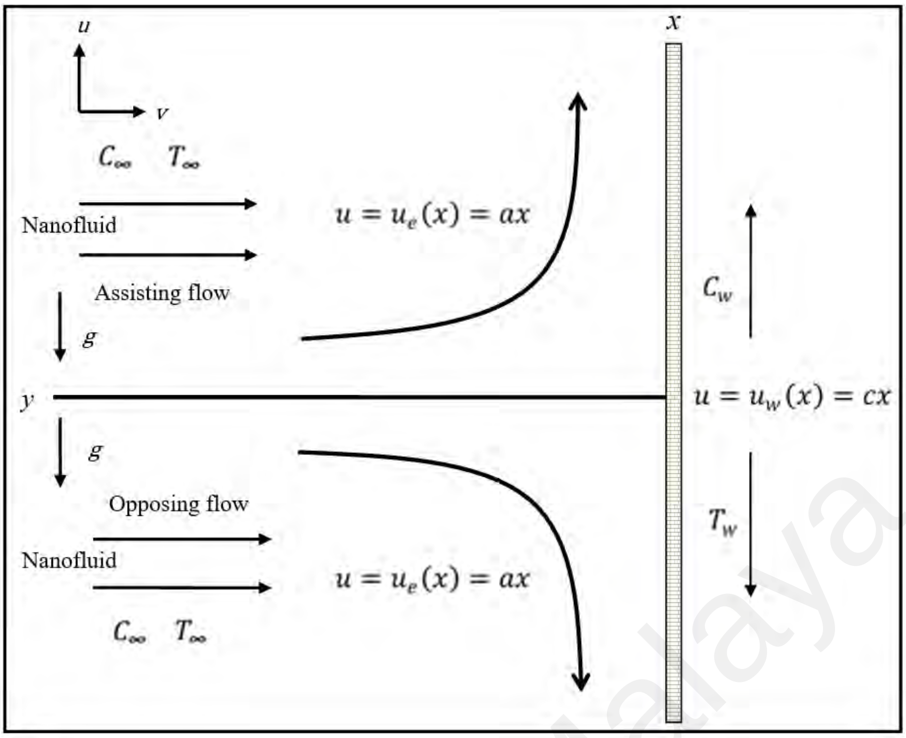

Figure 8.1: Geometry of the flow in Cartesian coordinate.

subject to velocity boundary conditions (3.37, 3.39), temperature boundary conditions (3.40, 3.42) and the active and passive control of nanoparticle conditions (3.43, 3.44). In the equation above, u and v are the velocity components along $x-$ and $y-$ axes respectively. Here, a and c are positive constants, $\nu = \mu/\rho$ is the kinematic viscosity, ρ si the fluid density, β and è are the fluid parameters, g is the acceleration due to gravity, β_T is the thermal expansion coefficient, β_C is the nanoparticle volumetric coefficient, T and C are the fluid temperature and concentration. Applying the set of non-dimensional variables for steady flow (3.48), the above model can then be transformed into a simplified non-linear ordinary differential equation below: The resulting ordinary differential equations are:

$$
\begin{aligned}
&(1+\epsilon)f''' - (f')^2 + f f''' + r^2 - \epsilon\delta(f'')^2 f''' + \gamma[\theta + N\phi],\\
&\theta'' + \Pr\left[f\theta' + Nb\,\theta'\phi' + Nt\,(\theta')^2\right] = 0, \qquad (8.2)\\
&\phi'' + LePr\,f\phi' + \frac{Nt}{Nb}\theta'' = 0,
\end{aligned}
$$

subject to the corresponding boundary conditions:

$$\begin{aligned} &f(0)=0, \qquad f'(0)=1, \qquad \theta(0)=1,\\ &\qquad \begin{cases} Nb\,\phi'(0)+Nt\,\theta'(0)=0, & \text{for passive control of } \phi,\\ \phi(0)=1, & \text{for active control of } \phi, \end{cases} ,\\ &f'(\infty)=r, \qquad \theta(\infty)=0, \qquad \phi(\infty)=0, \end{aligned} \tag{8.3}$$

where primes denote differentiation with respect to η. Here, $r = a/c$ is the stagnation parameter, Pr is the Prandtl number and Le is the Lewis number. Brownian motion parameter Nb and thermophoresis parameter Nt are defined in (3.58) and (3.59) respectively. The fluid parameters ϵ and δ, buoyancy parameter γ and buoyancy force ratio N are defined as

$$\begin{aligned} \epsilon &= \frac{1}{\mu\beta\grave{e}}, \qquad\qquad \delta = \frac{c^3x^2}{2\grave{e}^2\nu},\\ N &= \frac{\beta_C(C-C_\infty)}{\beta_T(T-T_\infty)},\\ \gamma &= \frac{(Gr)_x}{(Re_x)^2} = \frac{g\beta_T(T-T_\infty)x^3/\nu^2}{(u_w(x)x/\nu)^2}, \end{aligned} \tag{8.4}$$

where $(Gr)_x$ is the local Grashoff number and Re_x is the local Reynolds number.

The physical quantities of practical interest are the local skin friction coefficient Cf_x (3.62), the heat transfer rate or the local Nusselt number Nu_x (3.68) and the mass transfer rate also known as local Sherwood number Sh_x (3.70), which can be simplified into the dimensionless form below:

$$
\begin{aligned}
&Cf_x Re_x^{1/2} = (1+\epsilon) f''(0) - \frac{\epsilon\delta}{3}\left(f''(0)\right)^3, \\
&Nu_x Re_x^{-1/2} = -\theta'(0), \\
&\begin{cases}
Sh_x Re_x^{-1/2} = -\phi'(0), & \text{for active control of } \phi \\[2ex]
Sh_x Re_x^{-1/2} = \frac{Nt}{Nb}\theta'(0), & \text{for passive control of } \phi
\end{cases}
\end{aligned}
\tag{8.5}
$$

The *bvp4c* function in MATLAB is utilized in solving the problem. First, the governing nonlinear ODEs (8.2) with the boundary conditions (8.3) are rewritten as a system of seven first-order ODEs:

$$
\begin{aligned}
x_1' &= x_2, \\
x_2' &= x_3, \\
x_3' &= \frac{(x_2)^2 - x_1 x_3 - r^2 - \gamma[x_4 + N x_6]}{1 + \epsilon - \epsilon\delta(x_3)^2}, \\
x_4' &= x_5, \\
x_5' &= -\Pr(x_1 x_5 + Nb x_5 x_7 + Nt(x_5)^2, \\
x_6' &= x_7, \\
x_7' &= -Le \Pr x_1 x_7 - \frac{Nt}{Nb} x_5',
\end{aligned}
\tag{8.6}
$$

with the boundary conditions

$$
\begin{aligned}
&x_1(0) = 0, \qquad x_2(0) = 1, \qquad x_4(0) = 1 \\
&\qquad\begin{cases}
Nb x_7(0) + Nt x_5(0) = 0, & \text{for passive control of } \phi. \\[2ex]
x_6(0) = 1, & \text{for active control of } \phi
\end{cases} \\
&x_2(\infty) = r, \qquad x_4(\infty) = 0, \qquad x_6(\infty) = 0
\end{aligned}
\tag{8.7}
$$

Table 8.1: Comparison of results of Nusselt number, Nu for variation of thermophoresis parameter Nt, when $r = \epsilon = \delta = \gamma = N = 0, Pr = 3.97, Nb = 0.1$ and $Le = 10/Pr$.

Nt	**Ishfaq et al. (2016)** $RK4$	**Current study** $bvp4c$
0.1	1.2764	1.27637
0.2	1.1836	1.18362
0.3	1.0957	1.09571
0.4	1.0131	1.01309
0.5	0.9361	0.93607

For calculation purpose, $\eta \to \infty$ in this problem are set to $\eta_\infty = 10$ and the numerical solutions are evaluated at 100 equally spaced points with suitable initial guesses. The relative tolerance are set to 1×10^{-12}. To ensure the accuracy of our calculation and method of choice, present results are compared with published results of others. Table 8.1 lists the compared values of $-\theta'(0)$ for various values of thermophoresis parameter Nt. From the table, it is evident that the results are in good agreement with each other thus validating the accuracy of current results.

8.3 Results and Discussion

This section provides analysis and discussion on the impact that parameters $r, \epsilon, \delta, \gamma, N$, Nt, Nb, Le and Pr had on the fluid flow characteristics, specifically the velocity, temperature and nanoparticle volume concentration. Values of particular parameters are varied and the results are presented in graphical forms in Fig. 8.2 to Fig. 8.10. The physical properties of interest; the skin friction coefficient $f''(0)$, the heat transfer rate $-\theta'(0)$ or Nusselt number Nu and the mass transfer rate $-\phi'(0)$ or Sherwood number Sh are calculated numerically and recorded in tabular form (Table 8.2, 8.3). The parameters' values used throughout this section are $r = 0.2, \epsilon = 0.3, \delta = 0.1, \gamma = 1, N = Nt = Nb = 0.5, Le = 1, Pr = 5$ unless stated otherwise.

Figure 8.2 and Fig. 8.3 displayed the fluid profiles when stagnation parameter r and fluid parameter ϵ are varied. Both parameters seem to bring out the same outcome from the fluid flow. The fluid velocity increase when r and ϵ increases. The fluid velocity under active control is higher than the fluid velocity under passive control but both eventually converge to a uniform velocity as the fluid moves away from the surface. As the velocity increases, both fluid temperature and concentration are decreasing. Heat is being dispersed quicker to the surrounding and particles are being spread out farther with the fluid flow. In Fig. 8.5, the effect of another fluid parameter δ is shown. Compared to fluid parameter ϵ, fluid parameter δ does not seem to make significant impact towards the fluid profiles. A very minimal changes can be seen in velocity where the velocity seems to be decreasing with increasing values of δ while changes in temperature and concentration are non-visible.

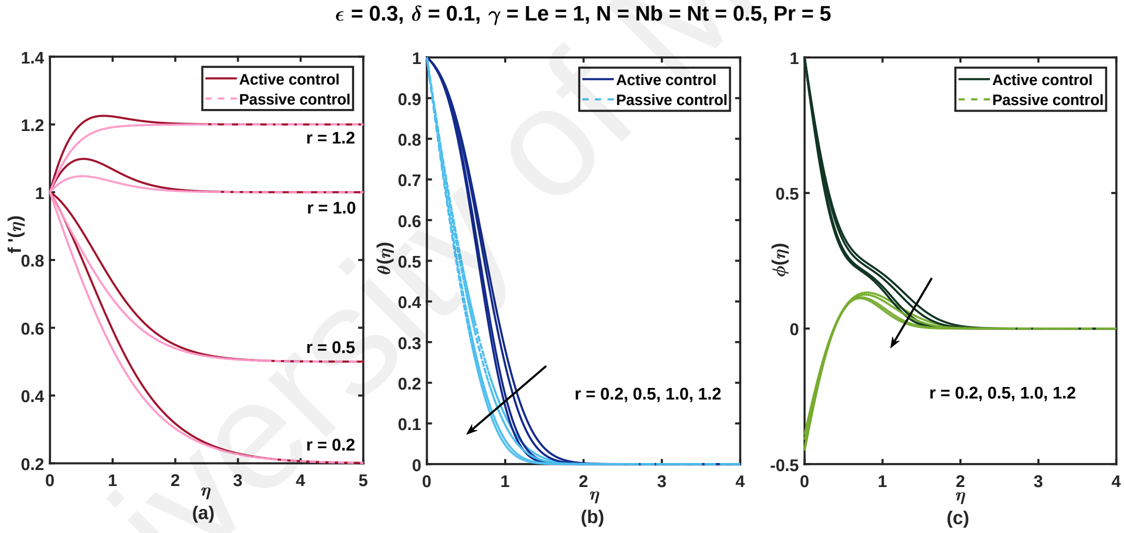

Figure 8.2: Impact of stagnation parameter r on a) velocity, b) temperature and c) nanoparticle volume fraction profiles.

Influences of the mixed convection parameter γ and buoyancy ratio parameter N are presented in Fig. 8.5 and Fig. 8.6. The outcomes are similar to those of varied r and ϵ. Fluid velocity increases while temperature and nanoparticle volume concentration decrease when the values of parameters γ and N increase. Here, $\gamma > 0$ represents assisting flow, $\gamma < 0$ represents opposing flow and $\gamma = 0$ represents the flow when no buoyancy force is present. In assisting flow, fluid velocity is higher in active control than velocity in passive

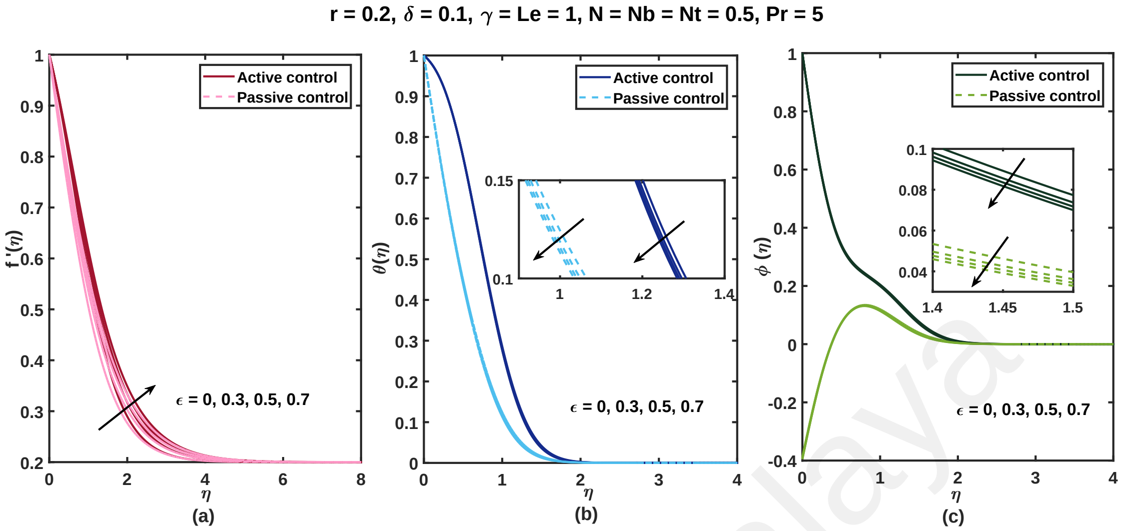

Figure 8.3: Impact of fluid parameter ϵ on a) velocity, b) temperature and c) nanoparticle volume fraction profiles.

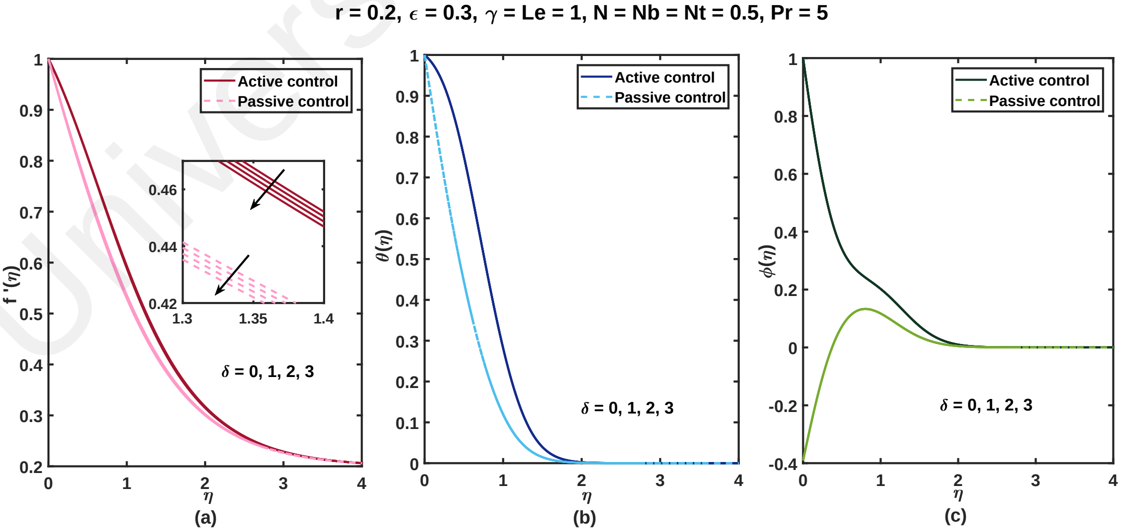

Figure 8.4: Impact of fluid parameter δ on a) velocity, b) temperature and c) nanoparticle volume fraction profiles.

control. The opposite is true for the opposing flow. Relatively, the mixed convection parameter or the buoyancy parameter γ leaves a bigger impact towards the flow profile than N.

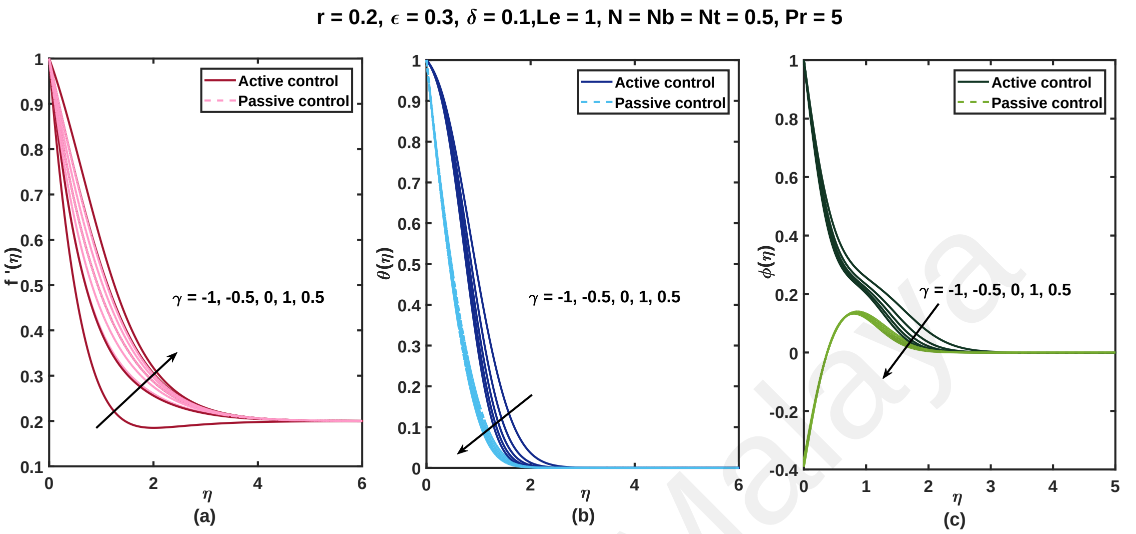

Figure 8.5: Impact of mixed convection parameter γ on a) velocity, b) temperature and c) nanoparticle volume fraction profiles.

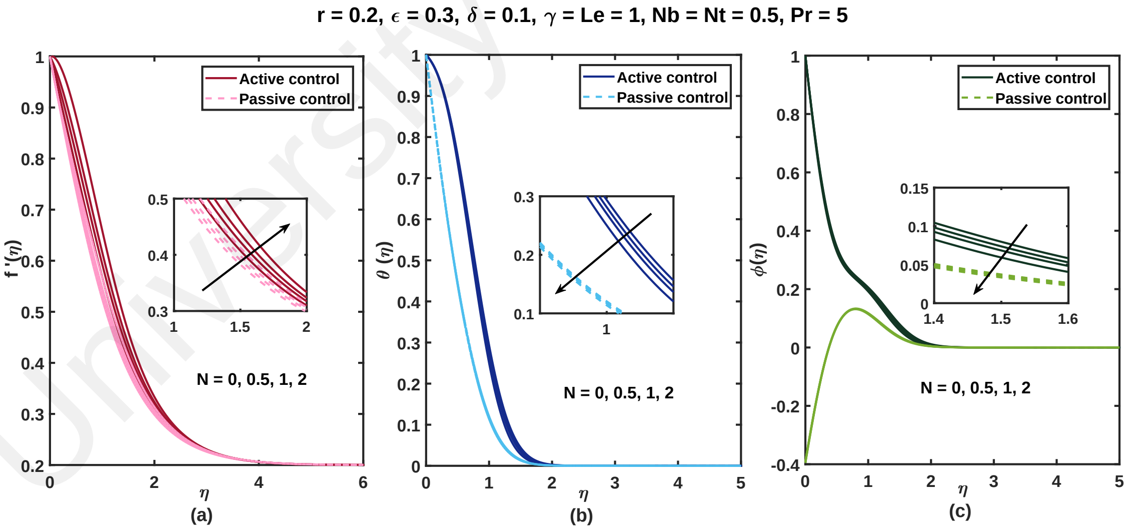

Figure 8.6: Impact of buoyancy ratio parameter N on a) velocity, b) temperature and c) nanoparticle volume fraction profiles.

The effects of nanoparticles can be seen through thermophoresis parameter Nt and Brownian motion parameter Nb in Fig. 8.7 and Fig. 8.8. The parameter Nt has increasing effects towards all the three fluid profiles. Thermophoresis represents the movement of particles due to temperature gradient. Increasing value of Nt means increasing movement due to increasing temperature gradient. Concentration too will increase following the movement of the particles. On the other hand, Brownian motion represents the motion of particles due to their collision to each other. Increasing value of Nb will cause the fluid velocity and nanoparticle volume concentration to decrease but as the collision produces heat, the fluid temperature will increase. However, note that temperature under passive control remains constant and is not affected by the changes in Nb.

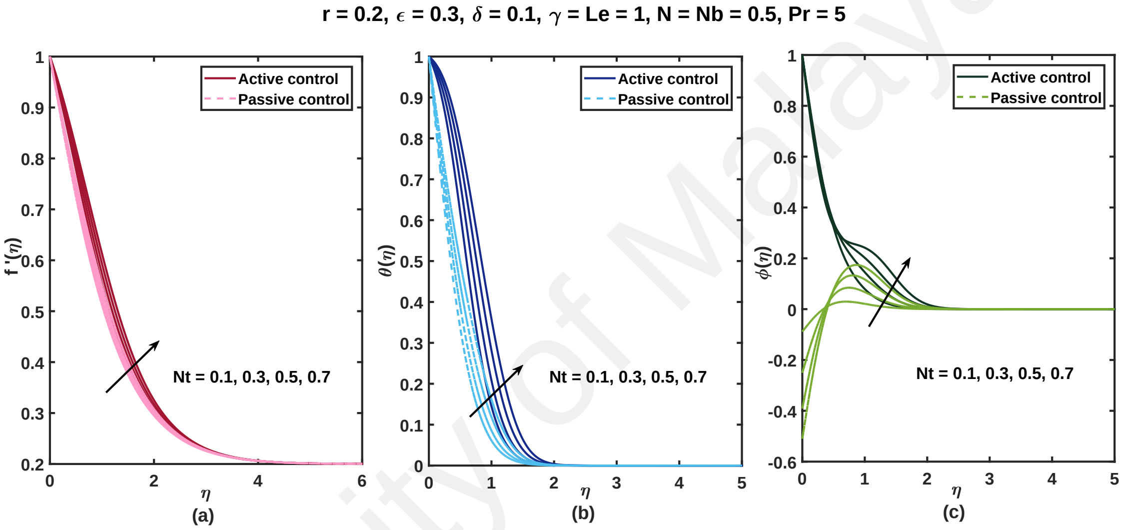

Figure 8.7: Impact of thermophoresis parameter Nt on a) velocity, b) temperature and c) nanoparticle volume fraction profiles.

Last but not least are the influences of Lewis number Le and Pr towards the fluid profiles as shown in Fig. 8.9 and Figure 8.10. Interesting results can be seen in temperature profile between active and passive controls when Le is varied where the trend turns out to be opposite of each other. Increasing Le will cause temperature to rise under passive control but to decline under active control. Other than that, the fluid has a decreasing trend when Le and Pr increases.

Table 8.2 and Table 8.3 listed the values of $f''(0), -\theta'(0)$ and $-\phi'(0)$ under both active and passive controls. Magnitude of skin friction coefficient shows similar trend under active control as well as passive control when γ, Nt and Pr are varied. It will increase

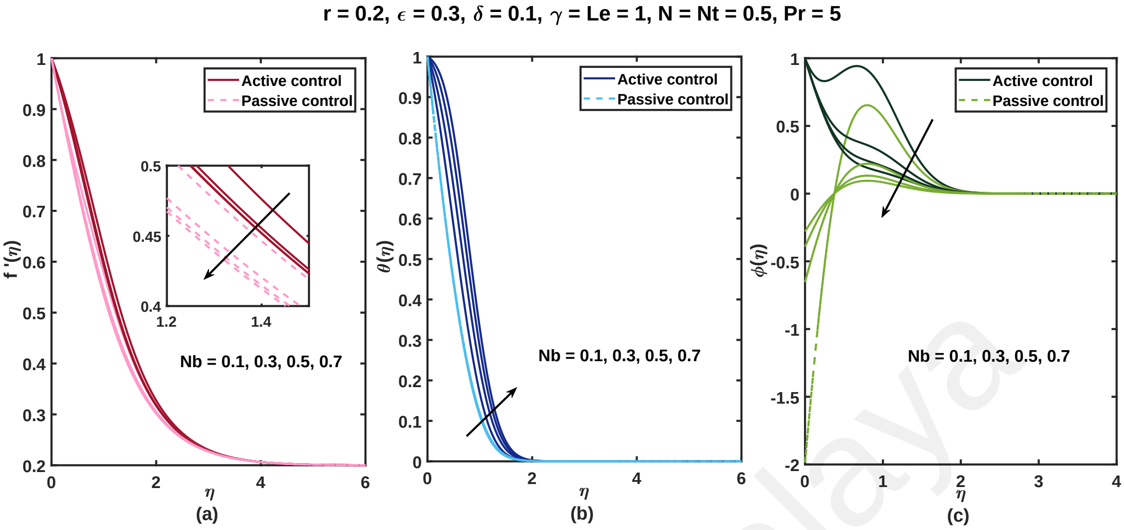

Figure 8.8: Impact of Brownian motion parameter Nb on a) velocity, b) temperature and c) nanoparticle volume fraction profiles.

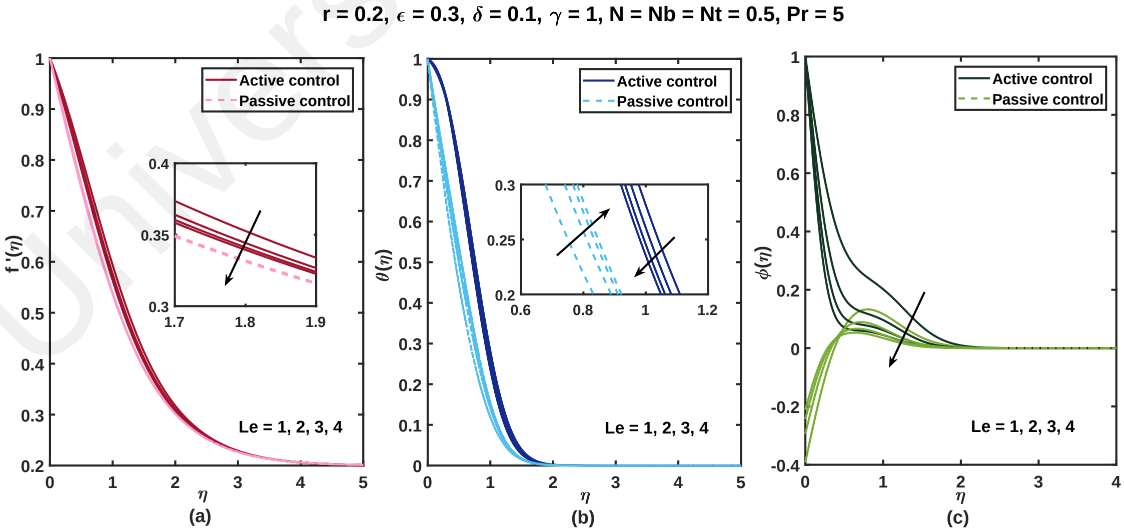

Figure 8.9: Impact of Lewis number Le on a) velocity, b) temperature and c) nanoparticle volume fraction profiles.

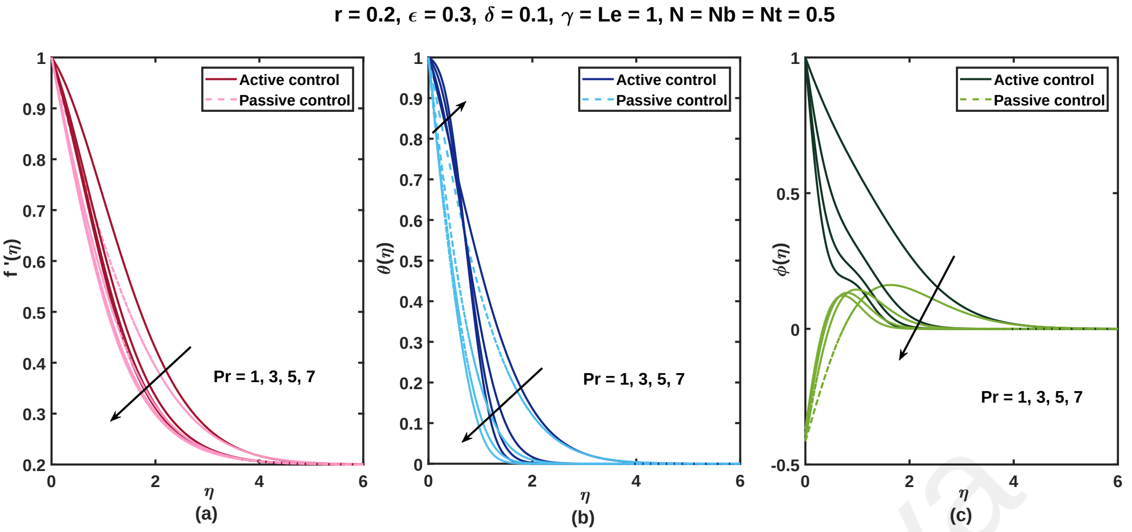

Figure 8.10: Impact of Prandtl number Pr on a) velocity, b) temperature and c) nanoparticle volume fraction profiles.

with increasing γ under opposing flows but will decrease with increasing γ under assisting flow. When there is no buoyancy force, the magnitude of $f''(0)$ will remain the same between active and passive controls. Other parameters will result in opposite trends of $f''(0)$ between active and passive control. Parameter r, γ, N and Pr will help in enhancing the heat transfer rate of the fluid while parameters Nt, Nb and Le do the opposite. Varying the fluid parameter ϵ will decrease the heat transfer under active control but will increase the heat transfer under passive control. Meanwhile, fluid parameter δ has a very minimal influence on heat and mass transfer of the fluid as the magnitude barely changes when δ increases and heat transfer remains stagnant under active control. Increasing value of parameter $r, \epsilon, \gamma, N, Nt$ and Pr will contribute in improving the mass transfer rate of the fluid. Interestingly, parameter Nb shows a more dynamic trend under active control for skin friction coefficient and mass transfer rate. The result is highlighted in Fig. 8.11. With small values of Nb, the trend of $f''(0)$ seems to be increasing but at certain point it starts to decline. On the other hand, $-\phi'(0)$ increases till Nb reaches a large enough number and starts to decrease.

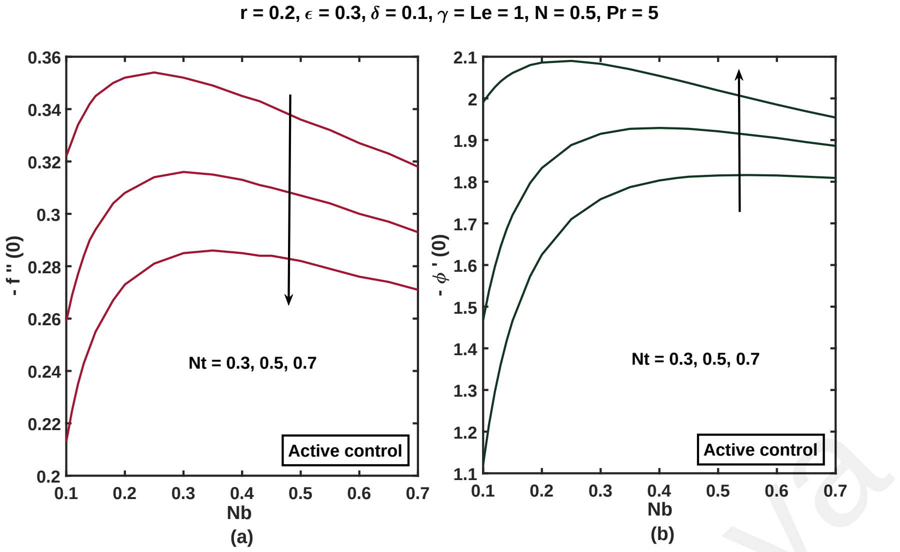

Figure 8.11: Impact of Brownian motion parameter Nb with varied thermophoresis parameter Nt on a) skin friction coefficient $f''(0)$ and b) mass transfer rate $-\phi'(0)$.

Table 8.2: Values of $f''(0), -\theta'(0)$ and $-\phi'(0)$ for parameter $r, \epsilon, \delta, \gamma$ and N under active and passive control.

r	ϵ	δ	γ	N	$f''(0)$ active	$f''(0)$ passive	$-\theta'(0)$ active	$-\theta'(0)$ passive	$-\phi'(0)$ active	$-\phi'(0)$ passive
0.2	0.3	0.1	1	0.5	-0.3071	-0.5445	0.1620	1.2594	1.9210	-1.2594
0.5					-0.1121	-0.3418	0.1628	1.3079	1.9985	-1.3079
1.0					0.4303	0.2151	0.1673	1.4104	2.1538	-1.4104
1.2					0.7128	0.5023	0.1698	1.4540	2.2185	-1.4540
0.2	0				-0.3009	-0.5904	0.1623	1.2478	1.9108	-1.2478
	0.1				-0.3041	-0.5736	0.1622	1.2520	1.9144	-1.2520
	0.3				-0.3071	-0.5445	0.1620	1.2594	1.9210	-1.2594
	0.5				-0.3074	-0.5198	0.1618	1.2656	1.9269	-1.2656
	0.7				-0.3062	-0.4985	0.1617	1.2710	1.9321	-1.2710
0.2	0.3	0			-0.3073	-0.5438	0.1620	1.2595	1.9211	-1.2595
		0.1			-0.3071	-0.5445	0.1620	1.2594	1.9210	-1.2594
		0.3			-0.3068	-0.5457	0.1620	1.2591	1.9209	-1.2591
		0.5			-0.3065	-0.5469	0.1620	1.2589	1.9208	-1.2589
		0.7			-0.3063	-0.5482	0.1620	1.2586	1.9207	-1.2586
0.2	0.3	0.1	-1		-1.4386	-1.1039	0.1479	1.1653	1.5966	-1.1653
			-0.5		-1.0936	-0.9507	0.1524	1.1939	1.7275	-1.1939
			0		-0.8081	-0.8081	0.1561	1.2184	1.8077	-1.2184
			0.5		-0.5493	-0.6733	0.1592	1.2399	1.8695	-1.2399
			1		-0.3071	-0.5445	0.1620	1.2594	1.9210	-1.2594
0.2	0.3	0.1	1	0.0	-0.4274	-0.5383	0.1608	1.2560	1.8975	-1.2560
				0.5	-0.3071	-0.5445	0.1620	1.2594	1.9210	-1.2594
				1	-0.1899	-0.5513	0.1631	1.2625	1.9429	-1.2625
				2	0.0371	-0.5666	0.1652	1.2684	1.9829	-1.2684

Table 8.3: Values of $f''(0), -\theta'(0)$ and $-\phi'(0)$ for parameter Nt, Nb, Le and Pr under active and passive control.

Nt	Nb	Le	Pr	$f''(0)$		$-\theta'(0)$		$-\phi'(0)$	
				active	passive	active	passive	active	passive
0.1	0.5	1	5	-0.3700	-0.5772	0.3120	1.5658	1.7157	-0.3132
0.3				-0.3364	-0.5615	0.2212	1.4090	1.8154	-0.8454
0.5				-0.3071	-0.5445	0.1620	1.2594	1.9210	-1.2594
0.7				-0.2815	-0.5263	0.1225	1.1202	2.0193	-1.5683
0.5	0.1			-0.2593	-0.5750	0.5876	1.2712	1.4680	-6.3558
	0.3			-0.3156	-0.5489	0.3172	1.2615	1.9149	-2.1025
	0.5			-0.3071	-0.5445	0.1620	1.2594	1.9210	-1.2594
	0.7			-0.2931	-0.5426	0.0785	1.2584	1.8860	-0.8989
0.5	0.5	1		-0.3071	-0.5445	0.1620	1.2594	1.9210	-1.2594
		2		-0.3449	-0.5255	0.1135	1.1013	2.7166	-1.1013
		3		-0.3653	-0.5162	0.0963	1.0159	3.3040	-1.0159
		4		-0.3788	-0.5107	0.0873	0.9614	3.7925	-0.9614
0.5	0.5	1	1	-0.1451	-0.4212	0.4777	0.6640	0.5283	-0.6640
			3	-0.2693	-0.5142	0.3335	1.0731	1.3429	-1.0731
			5	-0.3071	-0.5445	0.1620	1.2594	1.9210	-1.2594
			7	-0.3258	-0.5567	0.0697	1.3396	2.3250	-1.3396

8.4 Concluding Remarks

The model of a steady two-dimensional stagnation point flow of a Powell-Eyring nanofluid with mixed convection under actively and passively controlled nanoparticles is examined. The main observations of the study are listed below:

- Stagnation parameter r has bigger impact towards heat transfer rate under passive control of nanoparticle.
- The effect of fluid parameter ϵ is higher than δ towards the flow.
- Assisting flow has a higher rate of heat and mass transfer compared to opposing flow.
- Both Brownian parameter, Nb and thermophoresis parameter Nt lower the heat transfer rate of the fluid.
- The heat transfer rate is higher under passive control of nanoparticles than the heat transfer rate under active control of nanoparticles.

CHAPTER 9: SUMMARY AND FUTURE RESEARCH

9.1 Summary and Contribution

The aim of this thesis is to provide a better understanding of the stagnation-point flow of some non-Newtonian nanofluids under various stream conditions. The research emphasizes on the study of flow and heat mass transfer of nanofluids under active and passive controls of nanoparticles. For the purpose of this study, existing model of some non-Newtonian nanofluid are extended to incorporate stagnation-point flow and other various stream and boundary conditions. The extended model of considered non-Newtonian nanofluids are as follows:

- A steady stagnation-point flow of Maxwell nanofluid with slip velocity.
- A steady stagnation-point flow of Williamson nanofluid over a stretching/shrinking surface.
- A steady stagnation-point flow of second grade nanofluid with augmented boundary condition.
- An unsteady stagnation-point flow of MHD Carreau nanofluid with thermal radiation.
- A steady mixed convection stagnation-point flow of Powell-Eyring nanofluid over a vertical stretching surface.

The governing partial differential equations for all the models are simplified into systems of ordinary differential equations (ODEs) using similarity transformation. The Maxwell, Williamson, Carreau and Powell-Eyring models are then solved using *bvp*4*c* function by MATLAB. Their system of ODEs are first reduced into nonlinear first order ODEs subject to their corresponding boundary conditions. Shooting method is employed to obtain the initial conditions for each model. Due to the nature of the second grade fluid model, the

$BVPh2.0$ package in Mathematica is used to solve the problem instead. It is based on homotopy analysis method for boundary value problems. All numerical calculations are first validated either by comparing results with other published papers or by performing a convergence analysis. The obtained results are then presented in graphical and tabular forms.

The main findings of the research are listed according to chapters as below:

In Chapter 4, the effect of slip velocity in stagnation point flow of Maxwell nanofluid is studied. It is found that the slip parameter causes the reduced skin friction coefficient, heat and mass transfer to decline. In the absence of elasticity parameter Maxwell (i.e Newtonian fluid), the heat transfer performance is better than those of Maxwell fluid. Both slip and elasticity parameter increase the fluid temperature and nanoparticle volume concentration with the slip parameter showing a bigger influence towards the fluid compared to the Maxwell parameter.

In Chapter 5, the flow characteristic of stagnation point flow of Williamson nanofluid is studied over a stretching and shrinking surface. The Schmidt number, Sc and diffusivity ratio, N_{bt} are proven to have major influence on nanoparticle volume concentration while at the same time having little to no effect on the fluid temperature. The heat transfer rate of Williamson is found to be more susceptible to parameter value changes when under active control of nanoparticles. Also, shrinking surface have higher skin friction coefficient and lower heat transfer rate if compared to stretching surface.

In Chapter 6, the stagnation point flow of second-grade nanofluid is studied using an augmented boundary condition. The results show that second-grade nanofluid flow has a higher velocity but lower temperature and nanoparticle volume concentration when compared to a Newtonian fluid. The fluid behaves in the same trend under active and passive controls except for Lewis number when it is varied and the temperature behaves in opposite trend midway. It can also be seen that the nanoparticle volume fraction only increases when parameter Nt is varied and decreases with other parameters' variation.

In Chapter 7, the unsteady flow of MHD Carreau nanofluid near a stagnation point is studied while taking into consideration the effect of thermal radiation. The unsteadiness parameter will cause the Carreau nanoparticle volume concentration to decrease under active control but to increase under passive control. Higher values of power law index give a better heat transfer performance. It is also found that both magnetic parameter and thermal radiation help to increase the fluid temperature but will decrease the heat and mass transfer rate of the fluid.

In Chapter 8, the mixed convection stagnation point flow of Powell-Eyring nanofluid is studied. The existence of buoyancy forces affects the skin friction coefficient of the flow. The flow under passive control of nanoparticle possess a higher skin friction coefficient as compared to those under active control of nanoparticle. When there is no buoyancy, the skin friction coefficient will remain the same under both active and passive controls. Meanwhile, assisting flow is found to have a higher rate of heat and mass transfer if compared to opposing flow in Powell-Eyring nanofluid.

Common results are found from these different models. First, the stagnation parameter increases the heat transfer rate of all the non-Newtonian nanofluids flows studied, regardless of the different conditions the flows are in. In some cases, the stagnation parameter has a bigger impact towards the heat transfer rate when under passive control of nanoparticles. Secondly, it is recorded that the heat transfer performance is better in magnitude wise under passive control environment. Subsequently, it is shown that the temperature distribution in passive control model is lower or equal than the temperature distribution in active control model.

Heat transfer rate under passive control of nanoparticle remains stagnant when Brownian motion parameter is varied. This can be seen in the model of Maxwell, second grade fluid and Carreau model. However, this is not true in Powell-Eyring model due to the effect of combined buoyancy forces. It is also important to note that increasing the value of Brownian motion parameter and thermophoresis parameter decreases the heat transfer rate in both active and passive environment. Zargartalebi et al. (2015) mention in their work that the dispersion of nanoparticles in a base fluid leads to augmentation of the thermal conductivity and the dynamic viscosity of the mixture. At the same time, it also alters the other thermo-physical properties of the nanofluids and thus may cause an increase or a decrease in the heat transfer coefficient of a nanofluid with respect to the base fluid. In the Williamson model, the Brownian and thermophoresis diffusivity ratio are defined instead and these parameters help to increase the heat transfer.

9.2 Future Research

It is believed that the research on nanofluids will continue to mount researchers' interest due to its many applications in various industries that appear very promising. The current research presented the models of some stagnation-point flows of non-Newtonian nanofluids based on Buongiorno's model (Buongiorno, 2006). From the results, there are some outcomes that called for further investigations and improvements.

In this thesis, it is found that the stagnation parameter increases the heat transfer rate for all the non-Newtonian nanofluids flows studied. However, the value of stagnation parameter r considered throughout the thesis is $r < 1$ where the velocity near the wall is bigger than the ambient velocity. It would be appropriate to study for the cases when $r = 1$ where the stretching velocity is equal to the uniform velocity of the fluid stream and $r > 1$ where the velocity of the fluid away from the surface is much higher than the velocity in the boundary layer.

Results also show that the representative term for nanoparticles, that is the Brownian motion parameter Nb and thermophoresis Nt decrease the heat transfer rate of the studied nanofluid models. However, in Williamson model where Brownian and thermophoresis diffusivity ratio are defined, enhancement of the heat transfer are recorded. This shows how important the combination of model and parameters used defined as this will affect the outcome. Zargartalebi et al. (2015) mention that in most studies, the Brownian motion parameter and thermophoresis parameter are assumed much larger than their practical values where most researchers adopted the values in order of 10^{-1} while they should be in the order of 10^{-6} and lower. With such values, the contribution of nanoparticles in the heat transfer equation may be disrupted but the ratio of thermophoresis and Brownian motion parameters may remain significant.

It is also important to note that the non-Newtonian models used in the thesis might be more more suitable in investigating the flows of the nanofluids as it focused on the slip mechanism, Brownian motion and thermophoresis. A different model that emphasizes on the fluid dynamic viscosity and thermal conductivity are better suited to study the heat and mass transfer characteristics. For comparison purpose, it will be interesting to apply other nanofluid model instead of Buongiornos' such as the model proposed by Tiwari and Das (2007) and Khanafer, Vafai, and Lightstone (2003) that highlights the volumetric fraction of nanoparticles. In whichever case, modelling of nanofluids still has enough room for much more improvements. A better representation of the flow and the nanofluid characteristics will definitely helps to maximize the use of nanofluids in practical applications.

REFERENCES

Abbas, Z., Wang, Y., Hayat, T., & Oberlack, M. (2010). Mixed convection in the stagnation-point flow of a Maxwell fluid towards a vertical stretching surface. *Nonlinear Analysis: Real World Applications*, *11*(4), 3218-3228.

Abbasbandy, S., Naz, R., Hayat, T., & Alsaedi, A. (2014). Numerical and analytical solutions for Falkner-Skan flow of MHD Maxwell fluid. *Applied Mathematics and Computation*, *242*, 569-575.

Abbasi, F. M., Shehzad, S. A., Hayat, T., & Alhuthali, M. S. (2016). Mixed convection flow of Jeffrey nanofluid with thermal radiation and double stratification. *Journal of Hydrodynamics, Ser. B*, *28*(5), 840-849.

Acrivos, A., Shah, M. J., & Petersen, E. E. (1960). Momentum and heat transfer in laminar boundary layer flows of non-Newtonian fluids past external surfaces. *AIChE Journal*, *6*(2), 312-317.

Akbar, N. S., Hayat, T., Nadeem, S., & Obaidat, S. (2012). Peristaltic flow of a Williamson fluid in an inclined asymmetric channel with partial slip and heat transfer. *International Journal of Heat and Mass Transfer*, *55*(7-8), 1855–1862.

Akbar, N. S., Khan, Z. H., & Nadeem, S. (2014). The combined effects of slip and convective boundary conditions on stagnation-point flow of CNT suspended nanofluid over a stretching sheet. *Journal of Molecular Liquids*, *196*, 21-25.

Alsaedi, A., Awais, M., & Hayat, T. (2012). Effects of heat generation/absorption on stagnation point flow of nanofluid over a surface with convective boundary conditions. *Communications in Nonlinear Science and Numerical Simulation*, *17*(11), 4210-4223.

Aman, F., Ishak, A., & Pop, I. (2011). Mixed convection boundary layer flow near stagnation-point on vertical surface with slip. *Applied Mathematics and Mechanics*, *32*(12), 1599-1606.

Amani, M., Amani, P., Kasaeian, A., Mahian, O., & Yan, W.-M. (2017). Two-phase mixture model for nanofluid turbulent flow and heat transfer: Effect of heterogeneous distribution of nanoparticles. *Chemical Engineering Science*, *167*, 135-144.

Anderson, J. D. (2005). Ludwig Prandtl's boundary layer. *Physics Today*, *58*(12), 42-48.

Awais, M., Hayat, T., Alsaedi, A., & Asghar, S. (2014). Time-dependent three-dimensional boundary layer flow of a Maxwell fluid. *Computers & Fluids*, *91*, 21-27.

Bachok, N., Ishak, A., & Pop, I. (2010). Boundary-layer flow of nanofluids over a moving surface in a flowing fluid. *International Journal of Thermal Sciences*, *49*(9), 1663-1668.

Bachok, N., Ishak, A., & Pop, I. (2012). The boundary layers of an unsteady stagnation-point flow in a nanofluid. *International Journal of Heat and Mass Transfer*, *55*(23-24), 6499-6505.

Bariş, S. (2002). Steady three-dimensional flow of a second grade fluid towards a stagnation point at a moving flat plate. *Turkish Journal of Engineering and Environmental Sciences*, *27*(1), 21-30.

Bhargava, R., & Goyal, M. (2014). MHD non-Newtonian nanofluid flow over a permeable stretching sheet with heat generation and velocity slip. *International Journal of Mathematical, Computational, Physical, Electrical and Computer Engineering*, *8*(6), 910-916.

Bhatti, M. M., Abbas, T., Rashidi, M. M., Ali, M. E.-S., & Yang, Z. (2016). Entropy generation on mhd eyring–powell nanofluid through a permeable stretching surface. *Entropy*, *18*(6), 224.

Brimmo, A. T., & Qasaimeh, M. A. (2017). Stagnation point flows in analytical chemistry and life sciences. *RSC Advances*, *7*(81), 51206-51232.

Buongiorno, J. (2006). Convective transport in nanofluids. *Journal of Heat Transfer*, *128*(3), 240-250.

Bush, M. B. (1989). Applications in non-newtonian fluid mechanics. In C. A. Brebbia (Ed.), *Viscous flow applications* (p. 134-160). Springer Berlin Heidelberg.

Chen, T. S., Sparrow, E. M., & Mucoglu, A. (1977). Mixed convection in boundary layer flow on a horizontal plate. *Journal of Heat Transfer*, *99*(1), 66-71.

Chhabra, R. P. (2010). Non-Newtonian fluids: An introduction. In *Rheology of complex fluids* (pp. 3–34). Springer New York.

Choi, S. U. S., & Eastman, J. A. (1995). Enhancing thermal conductivity of fluids with nanoparticles. *ASME-Publications-Fed*, *231*, 99-106.

Dealy, J. M. (2010). Weissenberg and Deborah numbers – their definition and use. *Rheology Bulletin*, *79*(2), 14-18.

Dhanai, R., Rana, P., & Kumar, L. (2015). Multiple solutions of MHD boundary layer flow and heat transfer behavior of nanofluids induced by a power-law stretching/shrinking permeable sheet with viscous dissipation. *Powder Technology*, *273*, 62-70.

Dinarvand, S., Hosseini, R., Abulhasansari, M., & Pop, I. (2015). Buongiorno's model for double-diffusive mixed convective stagnation-point flow of a nanofluid considering diffusiophoresis effect of binary base fluid. *Advanced Powder Technology*, *26*(5), 1423-1434.

Dinarvand, S., Hosseini, R., & Pop, I. (2017). Axisymmetric mixed convective stagnation-point flow of a nanofluid over a vertical permeable cylinder by Tiwari-Das nanofluid model. *Powder Technology*, *311*, 147-156.

Eldabe, N. T., Elogail, M. A., Elshaboury, S. M., & Hasan, A. A. (2016). Hall effects on the peristaltic transport of Williamson fluid through a porous medium with heat and mass transfer. *Applied Mathematical Modelling*, *40*(1), 315-328.

Ellahi, R., Riaz, A., & Nadeem, S. (2013). Three dimensional peristaltic flow of Williamson fluid in a rectangular duct. *Indian Journal of Physics*, *87*(12), 1275-1281.

Farooq, M., Khan, M. I., Waqas, M., Hayat, T., Alsaedi, A., & Khan, M. I. (2016). MHD stagnation point flow of viscoelastic nanofluid with non-linear radiation effects. *Journal of Molecular Liquids*, *221*, 1097-1103.

Freidoonimehr, N., Rashidi, M. M., & Mahmud, S. (2015). Unsteady MHD free convective flow past a permeable stretching vertical surface in a nano-fluid. *International Journal of Thermal Sciences*, *87*, 136-145.

Garg, V. K., & Rajagopal, K. R. (1990). Stagnation point flow of a non-Newtonian fluid. *Mechanics Research Communications*, *17*(6), 415-421.

Garg, V. K., & Rajagopal, K. R. (1991). Flow of a non-Newtonian fluid past a wedge. *Acta Mechanica*, *88*(1-2), 113-123.

Garoosi, F., Hoseininejad, F., & Rashidi, M. M. (2016a). Numerical study of heat transfer performance of nanofluids in a heat exchanger. *Applied Thermal Engineering*, *105*, 436-455.

Garoosi, F., Hoseininejad, F., & Rashidi, M. M. (2016b). Numerical study of natural convection heat transfer in a heat exchanger filled with nanofluids. *Energy*, *109*, 664-678.

Gorder, R. A. V., & Vajravelu, K. (2010). Hydromagnetic stagnation point flow of a second grade fluid over a stretching sheet. *Mechanics Research Communications*, *37*(1), 113-118.

Gorla, R. S. R., & Gireesha, B. J. (2016). Dual solutions for stagnation-point flow and convective heat transfer of a Williamson nanofluid past a stretching/shrinking sheet. *Heat and Mass Transfer*, *52*(6), 1153-1162.

Goyal, M., & Bhargava, R. (2014). Boundary layer flow and heat transfer of viscoelastic nanofluids past a stretching sheet with partial slip conditions. *Applied Nanoscience*, *4*(6), 761-767.

Halim, N. A., Haq, R. U., & Noor, N. F. M. (2017). Active and passive controls of nanoparticles in Maxwell stagnation point flow over a slipped stretched surface. *Meccanica*, *52*(7), 1527-1539.

Halim, N. A., Sivasankaran, S., & Noor, N. F. M. (2017). Active and passive controls of the Williamson stagnation nanofluid flow over a stretching/shrinking surface. *Neural Computing and Applications*, *28*(1), 1023-1033.

Hamid, R. A., Nazar, R., & Pop, I. (2015). Non-alignment stagnation-point flow of a nanofluid past a permeable stretching/shrinking sheet: Buongiorno's model. *Scientific Reports*, *5*, 14640.

Haq, R. U., Nadeem, S., Khan, Z. H., & Akbar, N. S. (2015). Thermal radiation and slip effects on MHD stagnation point flow of nanofluid over a stretching sheet. *Physica E: Low-dimensional Systems and Nanostructures*, *65*, 17-23.

Hassan, M. U., & Siddiqui, A. M. (2012). A modified approach to exact solutions of a general form of a non-Newtonian second grade fluid. *Computers & Mathematics with Applications*, *63*(1), 94-99.

Hauke, G. (2008). *An introduction to fluid mechanics and transport phenomena* (Vol. 86). Springer Netherlands.

Hayat, T., Abbas, Z., Pop, I., & Asghar, S. (2010). Effects of radiation and magnetic field on the mixed convection stagnation-point flow over a vertical stretching sheet in a porous medium. *International Journal of Heat and Mass Transfer*, *53*(1-3), 466-474.

Hayat, T., Ahmed, N., Sajid, M., & Asghar, S. (2007). On the MHD flow of a second grade fluid in a porous channel. *Computers & Mathematics with Applications*, *54*(3), 407-414.

Hayat, T., Asad, S., Mustafa, M., & Alsaedi, A. (2014). Boundary layer flow of Carreau fluid over a convectively heated stretching sheet. *Applied Mathematics and Computation*, *246*, 12-22.

Hayat, T., Asad, S., Mustafa, M., & Alsaedi, A. (2015). MHD stagnation-point flow of Jeffrey fluid over a convectively heated stretching sheet. *Computers & Fluids*, *108*, 179-185.

Hayat, T., Aziz, A., Muhammad, T., & Ahmad, B. (2016). On magnetohydrodynamic flow of second grade nanofluid over a nonlinear stretching sheet. *Journal of Magnetism and Magnetic Materials*, *408*, 99-106.

Hayat, T., Farooq, M., Alsaedi, A., & Iqbal, Z. (2013). Melting heat transfer in the stagnation point flow of Powell–Eyring fluid. *Journal of Thermophysics and Heat Transfer*, *27*(4), 761-766.

Hayat, T., Hussain, S., Muhammad, T., Alsaedi, A., & Ayub, M. (2017). Radiative flow of Powell–Eyring nanofluid with convective boundary conditions. *Chinese Journal of Physics*, *55*(4), 1523-1538.

Hayat, T., Khan, M., & Ayub, M. (2005). On non-linear flows with slip boundary condition. *Zeitschrift für angewandte Mathematik und Physik ZAMP*, *56*(6), 1012-1029.

Hayat, T., Khan, M. I., Waqas, M., & Alsaedi, A. (2017). Effectiveness of magnetic nanoparticles in radiative flow of Eyring-Powell fluid. *Journal of Molecular Liquids*, *231*, 126-133.

Hayat, T., Muhammad, T., Shehzad, S. A., & Alsaedi, A. (2015). Similarity solution to three dimensional boundary layer flow of second grade nanofluid past a stretching surface with thermal radiation and heat source/sink. *AIP Advances*, *5*(1), 017107.

Hayat, T., Qasim, M., Shehzad, S. A., & Alsaedi, A. (2014). Unsteady stagnation point flow of second grade fluid with variable free stream. *Alexandria Engineering Journal*, *53*(2), 455-461.

Hayat, T., Sajjad, R., Muhammad, T., Alsaedi, A., & Ellahi, R. (2017). On MHD nonlinear stretching flow of Powell–Eyring nanomaterial. *Results in Physics*, *7*, 535-543.

Hayat, T., Shafiq, A., Imtiaz, M., & Alsaedi, A. (2016). Impact of melting phenomenon in the Falkner–Skan wedge flow of second grade nanofluid: A revised model. *Journal of Molecular Liquids*, *215*, 664-670.

Hayat, T., Shehzad, S., Qasim, M., & Obaidat, S. (2011). Flow of a second grade fluid with convective boundary conditions. *Thermal Science*, *15*(suppl. 2), 253-261.

Hayat, T., Shehzad, S. A., Alsaedi, A., & Alhothuali, M. S. (2012). Mixed convection stagnation point flow of Casson fluid with convective boundary conditions. *Chinese Physics Letters*, *29*(11), 114704.

Hsiao, K.-L. (2016). Stagnation electrical MHD nanofluid mixed convection with slip boundary on a stretching sheet. *Applied Thermal Engineering*, *98*, 850-861.

Hussain, T., Hussain, S., & Hayat, T. (2016). Impact of double stratification and magnetic field in mixed convective radiative flow of Maxwell nanofluid. *Journal of Molecular Liquids*, *220*, 870-878.

Ishak, A., Nazar, R., Amin, N., Filip, D., & Pop, I. (2007). Mixed convection of the stagnation-point flow towards a stretching vertical permeable sheet. *Malaysian Journal of Mathematical Sciences*, *1*(2), 217-226.

Ishak, A., Nazar, R., Bachok, N., & Pop, I. (2010). MHD mixed convection flow near the stagnation-point on a vertical permeable surface. *Physica A: Statistical Mechanics* *and its Applications*, *389*(1), 40-46.

Ishfaq, N., Khan, Z. H., Khan, W. A., & Culham, R. J. (2016). Estimation of boundary-layer flow of a nanofluid past a stretching sheet: A revised model. *Journal of Hydrodynamics*, *28*(4), 596-602.

Jahan, S., Sakidin, H., Nazar, R., & Pop, I. (2017). Flow and heat transfer past a permeable nonlinearly stretching/shrinking sheet in a nanofluid: A revised model with stability analysis. *Journal of Molecular Liquids*, *233*, 211-221.

Khan, A. U., Nadeem, S., & Hussain, S. T. (2016). Phase flow study of MHD nanofluid with slip effects on oscillatory oblique stagnation point flow in view of inclined magnetic field. *Journal of Molecular Liquids*, *224*, 1210-1219.

Khan, I., Fatima, S., Malik, M. Y., & Salahuddin, T. (2018). Exponentially varying viscosity of magnetohydrodynamic mixed convection Eyring-Powell nanofluid flow over an inclined surface. *Results in Physics*, *8*, 1194-1203.

Khan, M. (2016). A revised model to analyze the heat and mass transfer mechanisms in the flow of Carreau nanofluids. *International Journal of Heat and Mass Transfer*, *103*, 291-297.

Khan, M., & Azam, M. (2016). Unsteady boundary layer flow of Carreau fluid over a permeable stretching surface. *Results in Physics*, *6*, 1168-1174.

Khan, M., & Azam, M. (2017). Unsteady heat and mass transfer mechanisms in MHD Carreau nanofluid flow. *Journal of Molecular Liquids*, *225*, 554-562.

Khan, M., Azam, M., & Alshomrani, A. (2017a). Effects of melting and heat generation/absorption on unsteady Falkner-Skan flow of Carreau nanofluid over a wedge. *International Journal of Heat and Mass Transfer*, *110*, 437-446.

Khan, M., Azam, M., & Alshomrani, A. S. (2017b). Unsteady slip flow of Carreau nanofluid over a wedge with nonlinear radiation and new mass flux condition. *Results in Physics*, *7*, 2261-2270.

Khan, M., Azam, M., & Munir, A. (2017). On unsteady Falkner-Skan flow of MHD Carreau nanofluid past a static/moving wedge with convective surface condition. *Journal of Molecular Liquids*, *230*, 48-58.

Khan, M., & Hashim. (2015). Boundary layer flow and heat transfer to Carreau fluid over a nonlinear stretching sheet. *AIP Advances*, *5*(10), 107203.

Khan, M., Hashim, & Alshomrani, A. S. (2016, jun). MHD stagnation-point flow of a Carreau fluid and heat transfer in the presence of convective boundary conditions. *PLoS ONE*, *11*(6), e0157180.

Khan, M., Hussain, M., & Azam, M. (2016). Magnetohydrodynamic flow of Carreau fluid over a convectively heated surface in the presence of non-linear radiation. *Journal of Magnetism and Magnetic Materials*, *412*, 63-68.

Khan, N., Mahmood, T., Sajid, M., & Hashmi, M. S. (2016). Heat and mass transfer on MHD mixed convection axisymmetric chemically reactive flow of Maxwell fluid driven by exothermal and isothermal stretching disks. *International Journal of Heat and Mass Transfer*, *92*, 1090-1105.

Khan, N. A., Khan, S., & Riaz, F. (2014). Boundary layer flow of Williamson fluid with chemically reactive species using scaling transformation and homotopy analysis method. *Mathematical Sciences Letters*, *3*(3), 199-205.

Khan, U., Ahmed, N., Khan, S. I. U., & Mohyud-din, S. T. (2014). Thermo-diffusion effects on MHD stagnation point flow towards a stretching sheet in a nanofluid. *Propulsion and Power Research*, *3*(3), 151-158.

Khan, W. A., Makinde, O. D., & Khan, Z. H. (2016). Non-aligned MHD stagnation point flow of variable viscosity nanofluids past a stretching sheet with radiative heat. *International Journal of Heat and Mass Transfer*, *96*, 525-534.

Khan, W. A., & Pop, I. (2010). Boundary-layer flow of a nanofluid past a stretching sheet. *International Journal of Heat and Mass Transfer*, *53*(11-12), 2477-2483.

Khanafer, K., Vafai, K., & Lightstone, M. (2003). Buoyancy-driven heat transfer enhancement in a two-dimensional enclosure utilizing nanofluids. *International Journal of Heat and Mass Transfer*, *46*(19), 3639-3653.

Kierzenka, J., & Shampine, L. F. (2001). A BVP solver based on residual control and the Maltab PSE. *ACM Transactions on Mathematical Software*, *27*(3), 299-316.

Kuznetsov, A. V., & Nield, D. A. (2013). The Cheng-Minkowycz problem for natural convective boundary-layer flow in a porous medium saturated by a nanofluid: A revised model. *International Journal of Heat and Mass Transfer*, *65*, 682-685.

Kuznetsov, A. V., & Nield, D. A. (2014). Natural convective boundary-layer flow of a nanofluid past a vertical plate: A revised model. *International Journal of Thermal Sciences*, *77*, 126-129.

Labropulu, F., & Li, D. (2008). Stagnation-point flow of a second-grade fluid with slip. *International Journal of Non-Linear Mechanics*, *43*(9), 941-947.

Liao, S. (2013). *Advances in the Homotopy Analysis Method.* World Scientific.

Mabood, F., & Khan, W. A. (2016). Analytical study for unsteady nanofluid MHD flow impinging on heated stretching sheet. *Journal of Molecular Liquids*, *219*, 216-223.

Mahapatra, T. R., & Gupta, A. S. (2002). Heat transfer in stagnation-point flow towards a stretching sheet. *Heat and Mass Transfer*, *38*(6), 517-521.

Makinde, O. D., Khan, W. A., & Khan, Z. H. (2013). Buoyancy effects on MHD stagnation point flow and heat transfer of a nanofluid past a convectively heated stretching/shrinking sheet. *International Journal of Heat and Mass Transfer*, *62*, 526-533.

Malik, M. Y., Khan, I., Hussain, A., & Salahuddin, T. (2015). Mixed convection flow of MHD Eyring-Powell nanofluid over a stretching sheet: A numerical study. *AIP Advances*, *5*(11), 117118.

Mehmood, R., Nadeem, S., & Akbar, N. S. (2013). Non-orthogonal stagnation point flow of a micropolar second grade fluid towards a stretching surface with heat transfer. *Journal of the Taiwan Institute of Chemical Engineers*, *44*(4), 586-595.

Mustafa, M., Hayat, T., Pop, I., Asghar, S., & Obaidat, S. (2011). Stagnation-point flow of a nanofluid towards a stretching sheet. *International Journal of Heat and Mass Transfer*, *54*(25-26), 5588-5594.

Mustafa, M., Khan, J. A., Hayat, T., & Alsaedi, A. (2015). Boundary layer flow of nanofluid over a nonlinearly stretching sheet with convective boundary condition. *IEEE Transactions on Nanotechnology*, *14*(1), 159-168.

Mustafa, M., Nawaz, M., Hayat, T., & Alsaedi, A. (2014). MHD boundary layer flow of second-grade nanofluid over a stretching sheet with convective boundary conditions. *Journal of Aerospace Engineering*, *27*(4), 04014006.

Nadeem, S., & Akram, S. (2010). Peristaltic flow of a Williamson fluid in an asymmetric channel. *Communications in Nonlinear Science and Numerical Simulation*, *15*(7), 1705-1716.

Nadeem, S., Haq, R. U., & Khan, Z. H. (2014). Numerical study of MHD boundary layer flow of a Maxwell fluid past a stretching sheet in the presence of nanoparticles. *Journal of the Taiwan Institute of Chemical Engineers*, *45*(1), 121-126.

Nadeem, S., & Hussain, S. T. (2014a). Flow and heat transfer analysis of Williamson nanofluid. *Applied Nanoscience*, *4*(8), 1005-1012.

Nadeem, S., & Hussain, S. T. (2014b). Heat transfer analysis of Williamson fluid over exponentially stretching surface. *Applied Mathematics and Mechanics*, *35*(4), 489-502.

Nadeem, S., Hussain, S. T., & Lee, C. (2013). Flow of a Williamson fluid over a stretching sheet. *Brazilian Journal of Chemical Engineering*, *30*(3), 619-625.

Nadeem, S., Riaz, A., Ellahi, R., & Akbar, N. S. (2014). Series solution of unsteady peristaltic flow of a Carreau fluid in eccentric cylinders. *Ain Shams Engineering Journal*, *5*(1), 293-304.

Nield, D. A., & Kuznetsov, A. V. (2009). The Cheng-Minkowycz problem for natural convective boundary-layer flow in a porous medium saturated by a nanofluid. *International Journal of Heat and Mass Transfer*, *52*(25-26), 5792-5795.

Nield, D. A., & Kuznetsov, A. V. (2010). The onset of convection in a horizontal nanofluid layer of finite depth. *European Journal of Mechanics-B/Fluids*, *29*(3), 217-223.

Nield, D. A., & Kuznetsov, A. V. (2014a). The onset of convection in a horizontal nanofluid layer of finite depth: A revised model. *International Journal of Heat and Mass Transfer*, *77*, 915-918.

Nield, D. A., & Kuznetsov, A. V. (2014b). Thermal instability in a porous medium layer saturated by a nanofluid: A revised model. *International Journal of Heat and Mass*

Transfer, *68*, 211-214.

Noor, N. F. M., Haq, R. U., Nadeem, S., & Hashim, I. (2015). Mixed convection stagnation flow of a micropolar nanofluid along a vertically stretching surface with slip effects. *Meccanica*, *50*(8), 2007-2022.

Othman, N. A., Yacob, N. A., Bachok, N., Ishak, A., & Pop, I. (2017). Mixed convection boundary-layer stagnation point flow past a vertical stretching/shrinking surface in a nanofluid. *Applied Thermal Engineering*, *115*, 1412-1417.

Pakdemirli, M., & Yurusoy, M. (1998). Similarity transformations for partial differential equations. *SIAM Review*, *40*(1), 96-101.

Pal, D., & Mandal, G. (2015). Mixed convection–radiation on stagnation-point flow of nanofluids over a stretching/shrinking sheet in a porous medium with heat generation and viscous dissipation. *Journal of Petroleum Science and Engineering*, *126*, 16-25.

Pal, D., Mandal, G., & Vajravelu, K. (2014). Flow and heat transfer of nanofluids at a stagnation point flow over a stretching/shrinking surface in a porous medium with thermal radiation. *Applied Mathematics and Computation*, *238*, 208-224.

Pearson, J. R. A., & Tardy, P. M. J. (2002). Models for flow of non-Newtonian and complex fluids through porous media. *Journal of Non-Newtonian Fluid Mechanics*, *102*(2), 447-473.

Qayyum, S., Hayat, T., Shehzad, S. A., & Alsaedi, A. (2017). Nonlinear convective flow of Powell-Erying magneto nanofluid with Newtonian heating. *Results in Physics*, *7*, 2933-2940.

Rahimi, J., Ganji, D. D., Khaki, M., & Hosseinzadeh, K. (2017). Solution of the boundary layer flow of an Eyring-Powell non-Newtonian fluid over a linear stretching sheet by collocation method. *Alexandria Engineering Journal*, *56*(4), 621-627.

Rahman, M. M., Roşca, A. V., & Pop, I. (2014). Boundary layer flow of a nanofluid past a permeable exponentially shrinking/stretching surface with second order slip using Buongiorno's model. *International Journal of Heat and Mass Transfer*, *77*, 1133-1143.

Raja, M., Vijayan, R., Dineshkumar, P., & Venkatesan, M. (2016). Review on nanofluids characterization, heat transfer characteristics and applications. *Renewable and Sustainable Energy Reviews*, *64*, 163-173.

Raju, C. S. K., Hoque, M. M., Anika, N. N., Mamatha, S. U., & Sharma, P. (2017). Natural convective heat transfer analysis of MHD unsteady Carreau nanofluid over a cone packed with alloy nanoparticles. *Powder Technology*, *317*, 408-416.

Ramachandran, N., Chen, T. S., & Armaly, B. F. (1988). Mixed convection in stagnation flows adjacent to vertical surfaces. *Journal of Heat Transfer*, *110*(2), 373-377.

Ramesh, G. K., Gireesha, B. J., Hayat, T., & Alsaedi, A. (2016). Stagnation point flow of Maxwell fluid towards a permeable surface in the presence of nanoparticles. *Alexandria Engineering Journal*, *55*(2), 857-865.

Ramzan, M., & Bilal, M. (2015). Time dependent MHD nano-second grade fluid flow induced by permeable vertical sheet with mixed convection and thermal radiation. *PLoS ONE*, *10*(5), e0124929.

Rao, I. J., & Rajagopal, K. R. (1999). The effect of the slip boundary condition on the flow of fluids in a channel. *Acta Mechanica*, *135*(3), 113-126.

Sadeghy, K., Hajibeygi, H., & Taghavi, S.-M. (2006). Stagnation-point flow of upper-convected Maxwell fluids. *International Journal of Non-Linear Mechanics*, *41*(10), 1242-1247.

Sadeghy, K., Najafi, A.-H., & Saffaripour, M. (2005). Sakiadis flow of an upper-convected Maxwell fluid. *International Journal of Non-Linear Mechanics*, *40*(9), 1220-1228.

Safaei, M. R., Jahanbin, A., Kianifar, A., Gharehkhani, S., Kherbeet, A. S., Goodarzi, M., & Dahari, M. (2016). Mathematical modeling for nanofluids simulation: A review of the latest works. In *Modeling and simulation in engineering sciences.* InTech.

Saif, R. S., Hayat, T., Ellahi, R., Muhammad, T., & Alsaedi, A. (2017). Stagnation-point flow of second grade nanofluid towards a nonlinear stretching surface with variable thickness. *Results in Physics*, *7*, 2821-2830.

Sajid, M., Ahmed, B., & Abbas, Z. (2015). Steady mixed convection stagnation point flow of MHD Oldroyd-B fluid over a stretching sheet. *Journal of the Egyptian*

Mathematical Society, *23*(2), 440-444.

Schowalter, W. R. (1960). The application of boundary-layer theory to power-law pseudoplastic fluids: Similar solutions. *AIChE Journal*, *6*(1), 24-28.

Sharma, A. K., Tiwari, A. K., & Dixit, A. R. (2016). Rheological behaviour of nanofluids: A review. *Renewable and Sustainable Energy Reviews*, *53*, 779-791.

Shehzad, S. A., Alsaedi, A., & Hayat, T. (2013). Hydromagnetic steady flow of Maxwell fluid over a bidirectional stretching surface with prescribed surface temperature and prescribed surface heat flux. *PLoS ONE*, *8*(7), e68139.

Sheikholeslami, M., & Sadoughi, M. (2017). Mesoscopic method for MHD nanofluid flow inside a porous cavity considering various shapes of nanoparticles. *International Journal of Heat and Mass Transfer*, *113*, 106-114.

Sithole, H., Mondal, H., & Sibanda, P. (2018). Entropy generation in a second grade magnetohydrodynamic nanofluid flow over a convectively heated stretching sheet with nonlinear thermal radiation and viscous dissipation. *Results in Physics*, *9*, 1077-1085.

Smits, A. J. (2018). *A Physical Introduction to Fluid Mechanics: Second Edition* (2nd ed.). Retrieved on 20 Aug 2018, from http://www.efluids.com/efluids/books/efluids_books.htm

Solangi, K. H., Kazi, S. N., Luhur, M. R., Badarudin, A., Amiri, A., Sadri, R., . . . Teng, K. H. (2015, 9). A comprehensive review of thermo-physical properties and convective heat transfer to nanofluids. *Energy*, *89*, 1065-1086.

Sulochana, C., Ashwinkumar, G. P., & Sandeep, N. (2016). Transpiration effect on stagnation-point flow of a Carreau nanofluid in the presence of thermophoresis and Brownian motion. *Alexandria Engineering Journal*, *55*(2), 1151-1157.

Tiwari, R. K., & Das, M. K. (2007). Heat transfer augmentation in a two-sided lid-driven differentially heated square cavity utilizing nanofluids. *International Journal of Heat and Mass Transfer*, *50*(9), 2002-2018.

Tulapurkara, E. G. (2005). Hundred years of the boundary layer - Some aspects. *Sadhana*, *30*(4), 499-512.

Upadhay, M. S., Mahesha, & Raju, C. S. K. (2017). Cattaneo-Christov on heat and mass transfer of unsteady Eyring Powell dusty nanofluid over sheet with heat and mass flux conditions. *Informatics in Medicine Unlocked*, *9*, 76-85.

Wang, C. Y. (2008). Similarity stagnation point solutions of the Navier–Stokes equations – review and extension. *European Journal of Mechanics - B/Fluids*, *27*(6), 678-683.

Wang, G., & Zhang, J. (2017). Thermal and power performance analysis for heat transfer applications of nanofluids in flows around cylinder. *Applied Thermal Engineering*, *112*, 61-72.

Wang, X. (2009). Solving optimal control problems with matlab: Indirect methods. *North Carolina State University, Raleigh.*

Waqas, M., Khan, M. I., Hayat, T., & Alsaedi, A. (2017). Numerical simulation for magneto Carreau nanofluid model with thermal radiation: A revised model. *Computer Methods in Applied Mechanics and Engineering*, *324*, 640-653.

Weidman, P. D., & Putkaradze, V. (2003). Axisymmetric stagnation flow obliquely impinging on a circular cylinder. *European Journal of Mechanics-B/Fluids*, *22*(2), 123-131.

Williamson, R. V. (1929). The flow of pseudoplastic materials. *Industrial and Engineering Chemistry Research*, *21*(11), 1108-1111.

Xu, H., Liao, S.-J., & Pop, I. (2006). Series solution of unsteady boundary layer flows of non-Newtonian fluids near a forward stagnation point. *Journal of Non-Newtonian Fluid Mechanics*, *139*(1–2), 31-43.

Zaib, A., Rashidi, M. M., Chamkha, A. J., & Mohammad, N. F. (2018). Impact of nonlinear thermal radiation on stagnation-point flow of a Carreau nanofluid past a nonlinear stretching sheet with binary chemical reaction and activation energy. *Proceedings of the Institution of Mechanical Engineers, Part C: Journal of Mechanical Engineering Science*, *232*(6), 962-972.

Zargartalebi, H., Ghalambaz, M., Noghrehabadi, A., & Chamkha, A. (2015). Stagnation-point heat transfer of nanofluids toward stretching sheets with variable thermo-physical properties. *Advanced Powder Technology*, *26*(3), 819-829.

Zehra, I., Yousaf, M. M., & Nadeem, S. (2015). Numerical solutions of Williamson fluid with pressure dependent viscosity. *Results in Physics*, *5*, 20-25.

Zhao, Y. L., & Liao, S. J. (2013). HAM-based Mathematica package BVPh 2.0 for nonlinear boundary value problems. In S. J. Liao (Ed.), *Advances in the homotopy analysis method* (p. 361-417). Singapore: World Scientific.

LIST OF PUBLICATIONS AND PAPERS PRESENTED

Publications

Halim, N. A., Haq, R. U., & Noor, N. F. M. (2017). Active and passive controls of nanoparticles in Maxwell stagnation point flow over a slipped stretched surface. *Meccanica, 52*(7), 1527-1539.

Halim, N. A., Sivasankaran, S., & Noor, N. F. M. (2017). Active and passive controls of the Williamson stagnation nanofluid flow over a stretching/shrinking surface. *Neural Computing and Applications*, *28*(1), 1023-1033.

Halim, N. A., & Noor, N. F. M. (2015). Analytical solution for Maxwell nanofluid boundary layer flow over a stretching surface. *AIP Conference Proceedings*, *1682*(1), 020006.

Paper Presented

Halim, N. A., & Noor, N. F. M. (2014, 25 November). Analytical solution for Maxwell nanofluid boundary layer flow over a stretching surface. Paper presented at the 22nd National Symposium on Mathematical Science, Shah Alam, Selangor.